At what cost? Attempting to quantify cost of resistance in bacterium-phage interactions

Lotta Anni Ingeborg Landor

Thesis for the degree of Philosophiae Doctor (PhD)
University of Bergen, Norway
2023

UNIVERSITY OF BERGEN

At what cost? Attempting to quantify cost of resistance in bacterium-phage interactions

Lotta Anni Ingeborg Landor

Thesis for the degree of Philosophiae Doctor (PhD)
at the University of Bergen

Date of defense: 15.12.2023

Year: 2023

Title: At what cost? Attempting to quantify cost of resistance in bacterium-phage interactions

Name: Lotta Anni Ingeborg Landor

Print: Skipnes Kommunikasjon / University of Bergen

Scientific environment

The Ph.D. project was completed at the Faculty of Mathematics and Natural Sciences at the University of Bergen, at the Department of Biological Sciences in the Marine Microbiology research group. The project was funded as a part of the research project "SIMPLEX" by the Trond Mohn Research Foundation (TMS2018REK02). The Ph.D. project was also partly funded by the University of Bergen.

Acknowledgements

First of all, I would like to thank my supervisors Selina, Aud, Gunnar and Tatiana for guidance and helpful discussion throughout my Ph.D. period. I especially appreciated how you complemented each other in expertise, which helped me view my work from different perspectives.

Thank you to Jesslyn and Karen who helped with taming the test bacteria, and isolating resistant strains.

Completing this work would have been difficult without the assistance from the skilled technicians in the Marine Microbiology Group. Special thanks to Ela for helping me with the unruly flow cytometer, and Hilde & Hilde for all the help around the labs.

Finally, I would like to thank everyone at the Microbiology Group for a welcoming and supportive atmosphere.

Abstract

Microbial communities are remarkably diverse and trade-offs between life history traits are important to explain the existence and generation of this diversity. Bacteriophages (phages, viruses that infect bacteria) promote trade-offs between competition and defense in bacteria, as phage resistance affects bacterial fitness. The cost of resistance can present itself in different traits, making it challenging to quantify in natural systems. As protein synthesis is a fundamental process in all living organisms, it may be a useful target to measure the cost of resistance. *Escherichia coli* makes a simple model system that can unveil consequences of phage resistance that also could be important for phage therapy applications. In the current study, I isolated both fully and partially phage-resistant *E. coli* and assessed their fitness using multiple trait measurements. In attempts to quantify the cost of resistance, I used the single-cell method termed bioorthogonal non-canonical amino acid tagging (BONCAT), which uses selectively stainable synthetic amino acids that bacteria incorporate into newly synthesized proteins that can be tracked using flow cytometry. The synthetic amino acids were found to impact the bacterial metabolism more than anticipated, but the method was optimized and validated to affect bacterial growth as little as possible. Whole genome sequencing of the phage-resistant *E. coli* revealed unique mutations potentially explaining the resistance. Mucoid phenotypes with different phage susceptibility were linked to reduced growth rates and protein synthetic activity. Another phage-resistant isolate showed no change in growth, but an increase in BONCAT fluorescence and a reduction in yield. Thus, the cost of resistance can manifest either as increased or decreased translational activity, indicating that phage resistance impacts both the rate and efficiency of protein synthesis in bacteria. Further investigation is needed to fully understand the fluorescence-protein synthesis relationship of the method as well as how different phage resistance mechanisms affect uptake and incorporation of amino acids in bacteria.

Sammendrag

Biodiversiteten i mikrobielle samfunn er svært stor. Organismene som danner samfunnet må stadig gjøre avveininger mellom ulike karaktertrekk som påvirker deres muligheter for vekst, konkurranse og overlevelse. For å beskrive og forstå hvordan det mikrobielle mangfoldet har oppstått, utviklet seg og blir opprettholdt, må vi forstå disse avveiningene. Bakterier kan utvikle forsvar mot bakteriofager (fag, virus som infiserer bakterier) men slik resistens kan samtidig gå ut over deres konkuranseevne. I naturlige økosystem er det vanskelig å kvantifisere grad av forsvars- og konkurranseevne, og ikke minst avveininger mellom disse. Proteinsyntese er en fundamental prosess i alle levende organismer, og synes derfor å kunne være en brukbar egenskap for å tallfeste kostnaden av resistens hos bakterier. *Escherichia coli* utgjør et enkelt modellsystem som også er egnet til å avsløre viktige konsekvenser av fagresistens i samband med fagterapi. Jeg isolerte både helt og delvis fagresistente *E. coli* og sammenlignet disse med hensyn på proteinsyntese i enkeltceller. Til dette brukte jeg BONCAT (bioorthogonal non-canonical amino acid tagging) metoden, som baserer seg på bakterienes opptak og inkorporering av syntetiske aminosyrer som kan merkes selektivt med fluoriserende fargestoff og detekteres i flowcytometer. De syntetiske aminosyrene hadde effekter på bakterienes metabolisme utover det som var forventet, men metoden ble likevel optimalisert og validert for bruk i de planlagte eksperimentene uten at bakterienes vekstegenskaper ble påvirket. Ved helgenomsekvensering kunne spesifikke mutasjoner knyttes til fagresistens. Slimdannende fenotyper med ulike grad av fagresistens hadde redusert vekst hastighet og lavere næringsopptak, mens en annen fagresistent mutant hadde økt aminosyreopptak, ingen endring i veksthastighet og redusert vektutbytte. Kostnaden av resistens kan med andre ord manifestere seg enten som både økt eller redusert proteinproduksjon, hvilke tyder på at fagresistens kan ha påvirke raten og effektiviteten av proteinsyntese. Videre forskning er nødvendig for å forstå sammenhengen mellom fluorescens og proteinsyntese i metoden og hvordan ulike fagresistensmekanismer kan påvirke opptak og inkorporering av aminosyrer i bakterier.

Abbreviations

AHA – L-azidohomoalanine (synthetic methionine analogue)

BONCAT – Bioorthogonal non-canonical amino acid tagging

CRISPR-Cas – Clustered regular interspaced short palindromic repeats

DNA – deoxyribose nucleic acid

DsbA – thiol disulfide oxidoreductase

HPG – L-homopropargylglycine (synthetic methionine analogue)

IgaA – membrane protein involved in the Rcs system

LPS - lipopolysaccharide

NCAA – non-canonical amino acid analogue

OmpA – outer membrane protein A

OmpC – outer membrane protein C

Rcs – Complex variant of a two-component system first named by its role in regulation of capsular polysaccharide synthesis in *Enterobacterales*

List of Publications

Paper 1:

Pourhasanzade, F., Iver, S., Tjendra, J., Landor, L.A.I. and Våge, S. (2022): **'Individual-based model highlights the importance of trade-offs for virus-host population dynamics and long-term co-existence'** *PLoS Computational Biology* 18(6), e1010228

Paper 2:

Landor, L.A.I., Bratbak, G., Larsen, A., Tjendra, T. and Våge, S. (2023): '**Differential toxicity of bioorthogonal non-canonical amino acids (BONCAT) in *Escherichia coli*'** *Journal of Microbiological Methods* 206, 106679

Paper 3:

Landor, L.A.I., Tjendra, J., Erstad, K., Krabberød, A., Töpper, J. and Våge, S. (manuscript): **'At what cost? Cost of bacteriophage resistance in *Escherichia coli* is mutation-dependent – Characterization of growth kinetics, protein synthesis and whole genome'**

Contents

Introduction

"The existence of so great a diversity of species on Earth remains a mystery, the solution to which may also explain why and how biodiversity influences the functioning of ecosystems. The answer may lie in quantifying the trade-offs that organisms face in dealing with the constraints of their environment."

- Tilman (2000)

Understanding the laws of nature is a central aim of the life sciences, yet the simple rules of biology have remained elusive, likely due to the overwhelming complexity of interactions between biotic and abiotic systems. Microbial communities are especially challenging to explain, as microorganisms, invisible to the naked eye, are driven by molecular processes and constrained by their microenvironment, yet the collective activity of each microbial cells' traits and properties combine into globally important processes such as biochemical cycling (Fuhrman, 1999; Suttle, 2007). The advancements in sequence-based techniques have revealed vast microbial and viral biodiversity (Roossinck et al., 2015; Hug et al., 2016; Thompson et al., 2017; Gregory et al., 2019), and theories point to trade-offs to explain the existence and generation of biological and microbial diversity (Tilman, 2000; Våge et al., 2018).

The characteristics and lifestyles of bacteria are extraordinarily diverse, ranging from heterotrophy to autotrophy, aerobic to anaerobic (and facultative lifestyles in between), symbiotic to parasitic, susceptible to resistant to wide variety of antimicrobial compounds, but only scratching the surface of possible characteristics and the combinations thereof. The traits that any given bacterial cell can possess are constrained by trade-offs between different life history traits (Litchman et al., 2015; Ferenci, 2016). Bacteria-infecting viruses, bacteriophages (phages), are identified as key drivers shaping diversity in bacterial populations by infecting specific susceptible bacterial strains (Weinbauer and Rassoulzadegan, 2003; Brockhurst et al., 2005; Middelboe et al., 2009; Storesund et al., 2015), which in turn readily develop resistance to the phage. Due to pleiotropy between phage receptor sites and cellular

function (Burmeister et al., 2020), phage resistance promotes trade-offs between bacterial competitive ability – through changes in bacterial fitness and metabolic function – and phage defense (Bohannan et al., 2002; Brockhurst et al., 2006; Lennon et al., 2007; Abedon, 2022; Thingstad, 2022). This trade-off between competition and defense is termed cost of resistance and has theoretically been shown to promote diversification in microbial communities (**Paper 1**; Thingstad, 2000; Våge et al., 2013). Cost of resistance also controls abundance of phages in marine microbial food web models (Våge et al 2013, Thingstad et al 2014), indicating that it is important for the partitioning of bacterial production between the viral shunt and transfer to higher trophic levels (Våge et al 2016). The important consequences for biogeochemical function and production in marine ecosystems motivate a better understanding of the cost of resistance in microbial interactions.

Sequence-based methods show that different resistant genotypes can arise within the same bacterium-phage system (**Paper 3**; Cairns et al., 2017; Sørensen et al., 2021), with potentially different levels of resistance and cost thereof, but the functional trade-off resulting from the genotype cannot be measured in genetic data alone. Experimental testing of trade-offs in phage-resistant and susceptible laboratory cultures have shown reduction of growth rate (**Paper 3**; Brockhurst et al., 2005; Avrani and Lindell, 2015; Sørensen et al., 2021), change in virulence (Jørgensen et al., 2023), biofilm-forming ability (Wannasrichan et al., 2022; Zulk et al., 2022) and change ability to utilize organic substrates (Middelboe et al., 2009; Korf et al., 2020; Jørgensen et al., 2023) in phage-resistant bacteria. However, trade-offs have not observed in all phage-resistant bacteria (Brockhurst et al., 2005; McGee et al., 2021). The ecological consequence of these observations is, however, difficult to infer from genotypic and phenotypic testing, in part due to the lack of a quantifiable method to measure the cost of various degrees of phage resistance in different bacteria-virus interactions in natural ecosystems.

Population-based measurements have been a long-running standard in classical microbiological methods (Brehm-Stecher and Johnson, 2004), but from a theoretical perspective, microbial ecology ultimately depend on the traits and interactions of

single microbial cells. To build a theoretical framework encompassing community-level diversity and effects on higher-level functions such as biogeochemical cycling, the basic origin and maintenance of this diversity on the cellular level needs to be understood. While an individual-based model predicts trade-offs to be important in explaining virus-host coexistence and evolutionary outcomes (**Paper 1**), and phage-bacterium interactions and phage resistance has been studied using single-cell approaches (Chaudhry et al., 2020; Simmons et al., 2020; Attrill et al., 2021), methods to quantify the cost of resistance on a single-cell level remains underdeveloped.

When zooming in on microbial interactions at the cellular level, we need to face the crude complexity of myriads of interactions and the countless challenges in their interpretation. One strategy in dealing with complexity in ecological interactions is to focus on the fundamental processes in simple model communities (Bohannan and Lenski, 2000a). Protein synthesis is a fundamental and universal process in living organisms. The bulk biomass of bacterial cells consists of protein (Ingraham et al., 1983b), and the protein synthetic rate is tightly regulated to supply the growing cells with building blocks and functional components such as signaling and transport systems (Li et al., 2014; Scott et al., 2014; Hu et al., 2020). Moreover, as DNA codes for proteins, the protein synthetic machinery is likely the first to respond to phage resistance mutations, making it an attractive target for measuring the cost of resistance. The tracking of protein synthetic production of single microbial cells has recently been facilitated using a method called bioorthogonal non-canonical amino acid tagging (BONCAT). The method uses synthetic amino acid analogues that bacteria take up and incorporate into proteins that are then selectively fluorescently stainable and measurable using fluorometric techniques such as flow cytometry (**Paper 2**; **Paper 3**; Lindivat et al., 2020; Lindivat et al., 2021). The method further has the benefit of being culture-independent, and potentially applicable to diverse microbial communities (Hatzenpichler et al., 2014; Samo et al., 2014; Pasulka et al., 2018).

Although BONCAT has shown promise in tracking protein synthetic activity in various microbial systems and quantification efforts have been made (Samo et al., 2014), using the method for the quantification of cost of resistance have not been attempted. Before applying the method to complex communities, the method's performance in measuring trade-offs from phage resistance needs to be validated in a simple bacterial model system. Simple bacterial model systems, like *Escherichia coli* and lytic phage, although relying on cultivability, are useful for developing an understanding of methodological outcomes, because they are reproducible, easy to maintain, and can be complemented with experimental trade-off testing using previously established methods for confirmation. Furthermore, simple bacterium-phage systems allow for the isolation and subculturing of phage-resistant mutants that can be characterized on a phenotypic and genotypic level, enriching the single-cell BONCAT data.

2. Aims of the Ph.D. thesis

The main aim of the thesis is to quantify the cost of resistance through potential changes in protein synthetic activity in phage-resistant bacteria (*E. coli*), and simultaneously evaluate BONCAT's ability to be applied to reach this aim. This thesis focuses on experimental and methodological work motivated by an individual-based model developed in **Paper 1**, highlighting the importance of trade-offs in traits at a single cell level and strengthened by laboratory infection experiments with *E. coli* and T4-like phage G28.

The main objectives to reach the main aim are:

1. Explore the potential of simple life-strategy trade-offs such as cost of resistance that promote coexistence in artificial virus-host communities (**Paper 1**)
2. Assess the effect of the BONCAT amino acid analogues on the test system (**Paper 2**)
3. Validate the ability of BONCAT to measure changes in growth modes in *E. coli* (Chapter 5)
4. Characterize the link between genotype and phenotype in phage-resistant *E. coli* through whole-genome sequencing and testing of multiple traits: maximum growth rate, nutrient affinity, yield (**Paper 3**)
5. Evaluate the applicability of BONCAT to quantify the cost of phage resistance (**Paper 3**)

3. The model system: Why *E. coli*?

"Anything that is true for *E. coli* must be true for elephants, except more so."

- Jaques Monod (1954), as cited in Morange (2010)

Escherichia coli, originally *Bacterium coli* commune (Escherich, 1886), is a common intestinal Gram-negative gammaproteobacterium (Scheutz and Strockbine, 2005), and one of best-understood organisms in science (Cronan, 2014). The comprehensive knowledge of the bacterium and its phages makes *E. coli* a good candidate for ecological and evolutionary models (Bohannan and Lenski, 2000a). Moreover, *E. coli* is a versatile model organism that can grow in a wide variety of growth media (Lessard, 2013; Elbing and Brent, 2019), can be engineered to express wanted traits (Chen et al., 2017; Ibrahim et al., 2021), and due to the global distribution of the bacterium (Lagerstrom and Hadly, 2021), *E. coli*-infecting phages are widespread especially in aquatic environments (Nappier et al., 2019), should new ones need to be isolated.

But, how is the bacterium *E. coli* a good model trade-offs in microbial communities consisting of other species of bacteria, or even multicellular organisms? The biochemical organization of life is similar in all living organisms; the amino acids, nucleotides and phospholipids are shared between all kingdoms of life (Westerhoff et al., 2009). Jaques Monod famously compared *E. coli* to elephants (Morange, 2010), capturing the idea of shared biological processes between the two arguably very different life forms. As it happens, viruses also share biochemical composition with living organisms, although they are not organisms in their own right. Moreover, phages are the most abundant biological entities on the planet (Mann, 2005), providing researchers with a widespread pool of diverse model viruses to draw from (Campbell, 1960).

The *E. coli* test system for **Paper 1 – 3** was chosen based on similar motivations that traditionally involved the bacterium as a model organism in biology and phage

research; its simplicity, easy maintenance, and predictable growth in laboratory media (Ellis and Delbrück, 1939; Summers, 1993). What was perhaps not anticipated when choosing the model system, was that the eighty-or-so years at the forefront of phage research and intricate background knowledge of *E. coli* provides a framework for putting together molecular-level puzzle pieces and linking together observations of the population-level to single-cell measurements (**Paper 2**; **Paper 3**).

3.1 E. coli as a workhorse in phage research

The peculiar tendency of bacterial cultures to lyse spontaneously was observed by many scientists around the end of the 1800s. The first report on filtrates that could clear bacterial cultures was published in the 1890s (Hankin, 1896, translated 2011). About 20 years later, two scientists independently isolated and identified viruses – phages – as the causative agents for bacterial lysis (Twort, 1915; d'Herelle, 1917). Subsequently, phages became the focus of several scientists trying to understand their interactions and dynamics with their bacterial hosts (Summers, 1993; Ruiz and Silhavy, 2022).

E. coli was introduced in phage research in the 1930s followed by the isolation of phages active on the bacterium from sewage (Ellis and Delbrück, 1939; Summers, 1993). The early aims for the *E. coli*-phage research were to understand the role of bacteria and viruses in cancer (Summers, 1993), however, the results obtained from the subsequent series of experiments were also basis for modern molecular biology and genetics (Sharp, 2001; Ullmann, 2011; Ruiz and Silhavy, 2022). *E. coli* contributed to the development of several important phage methodologies, such as the one-step growth curve (Ellis and Delbrück, 1939), as well as the concept of phage burst size (Delbrück, 1940). To enable rapid progress in the field, it was proposed to standardize the research by focusing on a restricted group of bacteria and phages (Delbrück, 1945); And so, focus was put on *E. coli* and a number of so-called "T-phages" named T1 through T7 (Delbrück, 1946; Sharp, 2001).

Here, it is worth noting that "the" model organism *E. coli* is predominantly two strains of the bacterium: *E. coli* strain B, used by the Phage Group (e.g., Luria and Delbrück, 1943) and *E. coli* K-12 used for the discovery of genetic recombination (Lederberg and Tatum, 1947; Lederberg, 1947) and DNA restriction (Arber, 1974). Notably, strain B and strain K-12 are physiologically distinct from each other, which makes both better suited for specific research applications. For instance, *E. coli* strain B shows higher membrane permeability than K-12, probably due to different composition of outer membrane porins (Yoon et al., 2012), which can allow for e.g., more effective fluorescence staining (Herrera et al., 2002). While strain K-12 was initially thought to be a typical *E. coli* (Hobman et al., 2007), it was discovered that it lacks the ability to express genes for O-antigen synthesis (Liu and Reeves, 1994; Browning et al., 2013). Some evidence suggests that the ancestral *E. coli* K-12 had a functioning O-antigen synthesis (Hobman et al., 2007), indicating that the antigen loss was a result of a mutation early in the strain's laboratory adaptation. The phage susceptibility between the strains also differs, notably strain B being susceptible to phages T1 – T7 (Demerec and Fano, 1945), while K12-derivates are less permissive to non-glycosylated T-phages, such as T2 and T6 (Revel, 1967). Due to differences in cell surface composition, the same phage can infect both *E. coli* strain B and K-12 using different receptors (as in the case of phage T4; Yu and Mizushima, 1982; Washizaki et al., 2016; Subedi and Barr, 2021). However, differences in phage susceptibility were not found in the *E. coli* strain B and K-12 derivate strain tested for the current thesis (Table 1).

3.2 The workhorse of this thesis: E. coli DSM 103246

While much focus has been put on trusted laboratory strains like *E. coli* strain B and K12 strains, the model organism of this thesis is a "newcomer" to the laboratory environment; The *E. coli* I chose for my doctoral research was *E. coli* DSM 103246, also known as *E. coli* E28 (**Paper 1**; Schmidt et al., 2017; Kittler et al., 2020; Korf et al., 2020). The strain was originally isolated from a chicken carcass in Germany year

2012 and has been identified as serotype O186:H34 (Schmidt et al., 2017; Korf et al., 2020). As is common for *E. coli* isolated from animal production environments (EFSA and ECDC, 2023), the strain is toxin-producing and resistant to multiple antimicrobials (Schmidt et al., 2017; Korf et al., 2020). To date, the strain has been used as a model in research aimed at testing the applicability of phage therapy to control *E. coli* colonization in poultry (Kittler et al., 2020; Korf et al., 2020). Although the strain is a relatively recent addition to *E. coli*-research, it has been whole genome sequenced twice (**Paper 3**; Schmidt et al., 2017), providing detailed genetic information about the strain as well as providing an insight into the mutational activities that have occurred between sequencings.

The strain is highly susceptible to the lytic phage DSM 103876, also known as phage G28 (**Paper 1**; **Paper 3**; Kittler et al., 2020; Korf et al., 2020), which was isolated from manure in 2016 (Korf et al., 2020). The phage is tailed phage identified to the genus *Tequatrovirus* bearing similarities with phage T4, but with notable difference in e.g., a putative phage tail fiber adhesion protein (Korf et al., 2020). The phage has been used as a part of a phage cocktail to experimentally control *E. coli* gut colonization in chickens (Kittler et al., 2020), and was noted for its "outstanding performance" in lysing its host culture (Korf et al., 2020). For clarity, due to similarities in the collection designation of both the *E. coli* strain and phage, I will refer to *E. coli* as "DSM 103246" and to the phage as "G28". The one-step growth dynamics of *E. coli* DSM 103246 and phage G28 were tested and subsequently published in **Paper 1**, showing that at virus-to-host ratio as 1 virus to 100 hosts resulted in lysis of the *E. coli* culture (**Paper 1**). Importantly, both the *E. coli* strain and the phage are available at the German Collection for Microorganisms and Cell Cultures (DSMZ) and can be purchased by anybody qualified to work with biosafety level 2 microorganisms and interested in reproducing the results in this thesis.

3.3 Other E. coli-phage systems

Before deciding on the *E. coli* strain, I tested out a couple of other strains: the classical *E. coli* strain B (DSM 613) and a K-12-derived strain (DSM 4230), both purchased from DSMZ. However, neither of the *E. coli* strains were found suitable for the planned experiments; *E. coli* strain B showed poor growth in M9 media (Appendix 1.5), which is an amino acid-free medium important for the main method of this thesis. It also tended to sediment in liquid culture, which is typical for the strain as its flagellar biosynthesis is impaired (Yoon et al., 2012). The K-12 strain DSM 4230 was unable to grow in minimal media without amino acid supplementation, which interfered with the method relying on amino-acid-free media for the uptake of synthetic amino acid analogues (described in detail in Chapter 5). There could perhaps have been opportunity to optimize the protocol to include the strain B or the K12 strain, however, I opted for focusing on *E. coli* DSM 103246 due to its reliable growth and convincing performance in M9 media without amino acid supplementation. I also appreciated the traits of DSM 103246 coinciding with *E. coli* from animal production environments, making it a potentially useful model from an applied perspective, such as in phage therapy context (Kittler et al., 2020; Korf et al., 2020).

In connection with the testing of different *E. coli* strains, I also tried out a few other phages for my experiments. The T-series phages T5 (DSM 16353) and T7 (DSM 4623) were initially purchased from DSMZ to pair with the *E. coli* DSM 613 and DSM 4230, however, I also tested their activity on *E. coli* DSM 103246. Using spot assays (Appendix 2.c), both *E. coli* DSM 613 and DSM 4230 were found susceptible to all phages tested, while *E. coli* DSM 103246 was resistant to phage T5 and T7 (Table 1). Notably, I was only able to produce high titer lysate from phage T5 in nutrient broth (Appendix 1.12), making it a poor candidate for experiments using minimal media. On the other hand, phage T7 was found to lyse a liquid culture of a susceptible *E. coli* strain in M9 media in about an hour when incubated at 37 °C. While neither of these phages were used in further experiments, the work with the other *E. coli*-phage pairs was not completely wasted, as *E. coli* DSM 613 and phage

T7 were subsequently used for a phage exercise at the undergraduate course "BIO101 Organismal Biology" at the University of Bergen.

Table 1. *E. coli* strains and their susceptibility to different phages (G28 = DSM 103876; T5 = DSM 16353; TR7 = DSM 4623) where "+" indicates susceptibility and "-" indicates resistance. The phage resistance was tested using spot assays.

E. coli strain:	G28	T5	T7
DSM 613	+	+	+
DSM 4230	+	+	+
DSM 103246	+	-	-

3.4 Limitations of E. coli model systems

The famous comparison of *E. coli* and elephants made by Monod captures the idea of shared biochemical principles between life forms, but it overlooks the key differences that make each species unique in the biosphere. Not surprisingly, the use of *E. coli* to model processes in eukaryotic, multi-cellular organisms has been extensively criticized (Thieffry, 1996; Brachet et al., 1997; Loison, 2013). For instance, *E. coli* was used as an early model for embryonic development (Thieffry, 1996; Brachet et al., 1997; Morange, 2010; Loison, 2013), which is understandably paradoxical for a species reproducing through binary fission.

Even for modelling of microbial interactions, the dynamic between bacteria and bacterivorous predators (e.g., nematodes; Nair et al., 2019) differ from virus-host dynamics in the defensive strategies involved. *E. coli* fends off predators through toxin production (Lainhart et al., 2009; Koudelka et al., 2018), the genes for which can originate from phage interactions (O'Brien et al., 1984; Herold et al., 2004; Koudelka et al., 2018), indicating that phages, rather than being exclusively predatorial, can provide bacteria with predator-defense traits. Phage defense, on the other hand, predominantly involves preventing the phage from interacting with

surface receptors (Chapter 4) or through DNA exclusion systems such as CRISPR-Cas (Westra et al., 2015; Landsberger et al., 2018). As many bacterivorous predators can be maintained in laboratory cultures (Lainhart et al., 2009; Nair et al., 2019), it would perhaps be motivated to use relevant predators for predator-prey modelling, instead of phages.

Aside from being general model organisms, common laboratory strains of *E. coli* are potentially poor representatives of their own species (Hobman et al., 2007). Incidentally, the dependence on laboratory strains (strain B and K-12) of *E. coli* has resulted in erroneous conclusions about the species; It was believed, based on strain K-12, that *E. coli* lacked the reverse transcriptase enzyme (Lim and Maas, 1989; Hobman et al., 2007), even though the enzyme was later found to be present in other strains of the bacterium (Lampson et al., 1989), including strain B (Lim and Maas, 1989). While laboratory strains have been maintained under laboratory conditions since their isolation about a century ago, "wild" *E. coli* present in the environment today have evolved under natural selection and adapted to anthropogenic conditions, such as industrial animal production that only appeared during the latter half of the 20th century (Hart and Mayda, 1998).

The difference between laboratory strains and other *E. coli* is especially prominent from the genetic perspective; the genome of *E. coli* K-12 is about 859 000 base pairs smaller than the genome of the pathogenic strain *E. coli* O157:H7 (Hayashi et al., 2001). Part of this genetical difference stems from the fact that laboratory adaptation of *E. coli* K-12 has led to the loss of traits that allows it to survive its natural environment (Stevenson et al., 1994; Cronan, 2014). Likewise, *E. coli* strain B has been identified to have one of the smallest *E. coli* genomes of sequenced (Lukjacenko et al., 2010). Similarly, the traditional *E. coli*-infecting T-series phages, originally isolated around 80 years ago, have been propagated using various hosts and have undergone genetic changes over the years (Subedi and Barr, 2021).

3.5 The dark wild side of the "harmless" lab rat

While *E. coli* is an common member of the intestinal microbiome in humans and other mammals (Scheutz and Strockbine, 2005) and has been a biological model organism for over a century (Ullmann, 2011), its global recognition is not only due to digestive benefits or scientific breakthroughs; *E. coli* is a problematic pathogen, both in humans (Russo and Johnson, 2003; Murray et al., 2022) and livestock (Kolenda et al., 2015; Luppi et al., 2016; Apostolakos et al., 2021), and due to the increasing prevalence of antimicrobial resistance, the species is listed among the leading threats to global health and of critical priority for new treatment developments (Tacconelli et al., 2018). The cost – financial burden and loss of life – of resistance in *E. coli* is substantial, responsible for the highest number of deaths attributable to antimicrobial resistance globally (Murray et al., 2022) adding to the estimated one trillion $USD impact on the global gross domestic product due to drug-resistant infections by 2030 (Jonas et al., 2017). Many aspects that make *E. coli* a versatile and useful model organism – such as metabolic diversity and genetic plasticity – make it into a hardy and opportunistic disease agent readily adapting to infect new hosts and evolving new modes of infection (Vigil et al., 2010; Shaked et al., 2012; Braz et al., 2020; Ormsby et al., 2023). Its evolutionary potential has further made it evasive of sterilization techniques, evolving heat tolerance surviving up to 85 °C in meat processing facilities (Guragain et al., 2023), and has also been observed to evolve resistance to wastewater treatments, co-evolving with increased antimicrobial resistance (Yu et al., 2022). Owing to its adaptability, *E. coli* has been observed to become naturalized in aquatic environments (Koh et al., 2022) and soil (Ishii et al., 2006), leading to concerns of increased emergence of stable, pathogenic environmental populations in connection to climate change (Carlton et al., 2016; Hellberg and Chu, 2016; Robert et al., 2021).

I am aware that *E. coli* DSM 103246 has properties, like resistance genes (Schmidt et al., 2017; Korf et al., 2020) and a spontaneously inducible prophage (Schmidt et al., 2017), that might interfere with the study of cost of phage resistance. Arguably, the use of standard strains like *E. coli* strain B or K-12 would be motivated by their long history as model organisms and for better comparability of results in the literature.

However, these properties (antimicrobial resistance genes, virulence determinants and prophages) are commonly present in *E. coli* genomes (e.g., Stocki et al., 2002; Eppinger et al., 2011; Luppi et al., 2016; Subedi et al., 2018) but are less common or absent in *E. coli* laboratory strains (Brown and Curtiss III, 1996; Hayashi et al., 2001; Perna et al., 2001; Stocki et al., 2002; Kaper, 2004). Even if they contribute to noise and confounding outcomes, these genetic properties might play an important role in phage interactions. In my opinion, the chosen strain is a better representative of a "modern-day" *E. coli* and might provide better insight into the real-world ecology of the species.

Finally, I consider the use of phages to treat infections an important option to investigate as *E. coli* showing resistance to last-resort antimicrobials are encountered at an increasing frequency (Benzerara et al., 2017; Azam et al., 2018; Nkansa-Gyamfi et al., 2019; Wang et al., 2020b; Zurfluh et al., 2020). Therefore, while my work was aimed at a primarily ecological question of the fitness cost of phage resistance in the bacterial host, any insight into the phage resistance properties in *E. coli* can be valuable when evaluating the effects and risks of phage therapy applications (**Paper 1**; **Paper 3**). While the common laboratory strains of *E. coli* were originally focused on to speed up progress in the field, I argue that we have come far enough to include modern traits of the species in research, to broaden the horizons of the field and to answer important questions related to *E. coli*.

4. Resistant mutants and resistance mutations

"It is likely that resistance to phage varies quantitatively in *E. coli*, with some mutants completely resistant to phage attack and others partially resistant."

- Bohannan et al. (2002)

Before proceeding with the presentation of the phage-resistant isolates in my work, the interaction between *E. coli* and its phages (sometimes referred to as coliphages, e.g., Nappier et al., 2019) will be briefly described. Due to the global distribution of *E. coli* as an intestinal bacterium in animals (Lagerstrom and Hadly, 2021), coliphages are widespread especially in aquatic, agriculture-associated, and fecal contaminated environments (Cole et al., 2003; Gentry-Shields et al., 2015; Nappier et al., 2019). They are mainly categorized into two groups: lysogenic and lytic phages. Lysogenic phages imbed themselves into the genome of the host cell and replicate together with the host cell's division cycle (Chatterjee and Rothenberg, 2012). This thesis concerns a lytic phage (Korf et al., 2020), which hijack the cellular machinery of a susceptible cell to produce new phage particles and destroy the host cell through lysis, releasing phage progeny back into the environment.

The life cycle of a lytic phage begins with absorption to the host cell, which initiates as a reversible binding to a specific receptor molecule on the cell surface, and terminates as irreversible attachment (Molineux, 2001; Washizaki et al., 2016). The most common phage receptor site in *E. coli* is the outer membrane protein OmpC (Kortright et al., 2020). Some phages can have affinity for more than one receptor, and use e.g., both an outer membrane protein receptor and a cell surface glycoconjugate, such as the lipopolysaccharide (LPS, Yu and Mizushima, 1982; Washizaki et al., 2016), as receptors. The LPS is an outer membrane component in Gram-negative bacteria and is divided into three parts: an anchoring lipid, a core polysaccharide, and a repeating O polysaccharide unit (O-antigen; Lugtenberg and van Alpen, 1983; Wang and Quinn, 2010). The long O-antigens protrude outward from the outer membrane and cover the cell surface of *E. coli* like a "fur coat" (Hantke, 2020). The receptor molecule which phages interact with can be e.g., a

specific unbranched glucose residue in the LPS (Washizaki et al., 2016). Potentially in part due to phage predation, *E. coli* shows an enormous diversity in surface glycoconjugate and antigen structures across strains (Lugtenberg and van Alpen, 1983; Knirel et al., 2015; Liu et al., 2019; Leclercq et al., 2021), and specific phages can absorb through only a subset of e.g., LPS conformations (Washizaki et al., 2016; Zhong et al., 2020).

Following absorption, the injection of phage DNA, transcription of host genes is blocked (Onodera, 2009), while host RNA polymerase is used to catalyze the initial phage DNA transcription (Molineux, 2001; Onodera, 2009). The phage-associated enzymes interact with the bacterial chromosome (Gauss et al., 1994) and initiate the replication phage DNA and synthesis of phage components. Phage enzymes also destroy the host genome (Onodera, 2009). Consequently, the bacterial cell becomes an efficient factory – or a virocell (Forterre, 2012) – producing phage particles, which are assembled during a period of latency terminating in the lysis (bursting; through the enzymatic degradation of the cell wall; Onodera, 2009). Lysis can be observed in liquid bacterial cultures as an abrupt reduction in culture turbidity, which can be measured using spectrometric instruments (**Paper 1**).

Bacteria develop phage resistance by preventing phage absorption (Picken and Beacham, 1977; Braun-Breton and Hofnung, 1981; Riede and Eschbach, 1986; Scholl et al., 2005; Zhong et al., 2020; McGee et al., 2021; Zulk et al., 2022), blocking phage DNA injection by superinfection systems (Cumby et al., 2012), cleaving injected phage DNA once it has entered the cell (Arber, 1965; Korona and Levin, 1992; Wilkowska et al., 2020), or through abortive infection processes leading to the death of the bacterial cell (Parma et al., 1992; Refardt et al., 2013; Strotskaya et al., 2017). Advancements in sequence-based techniques have led to the ability to systematically map bacterial genomes for potential phage defense systems (Doron et al., 2019; Kortright et al., 2020; Mutalik et al., 2020; Vassallo et al., 2022). In this thesis, I am focusing on phage resistance through absorption prevention, as this appears to be the main resistance mechanism found in the phage G28-resistant *E. coli* mutants presented in **Paper 3**.

Phage absorption can be prevented through the modification of the phage receptor inhibiting phage attachment or absorption (Picken and Beacham, 1977; Morona et al., 1984; Zhong et al., 2020), blocking of phage receptors using competitive inhibitors (Braun-Breton and Hofnung, 1981; Riede and Eschbach, 1986), production of decoys (outer membrane vesicles; Manning and Kuehn, 2011), or through the production of an extracellular matrix (**Paper 3**; Chaudhry et al., 2020) or capsule (Scholl et al., 2005) preventing the phage from accessing the receptor on the cell surface. Sequence-based methods have shown that the underlying mutations preventing phage absorption often result from relatively minor, spontaneous mutations, resulting in amino acid substitutions (**Paper 3**; Morona et al., 1985; McGee et al., 2021), deletions (Zhong et al., 2020), and sometimes loss of entire genes (Korf et al., 2020; Sørensen et al., 2021). Mutations have been linked to the loss of outer membrane proteins (Henning and Haller, 1975; Chai and Foulds, 1977; Korf et al., 2020), and the loss of function of the receptor proteins (Braun-Breton and Hofnung, 1981). Likewise, mutations affecting LPS synthesis can result in the truncation of the LPS structure (Hantke, 2020; Zhong et al., 2020). Interestingly, phage-resistant *E. coli* often show mutations that are not directly linked to phage defense (Sørensen et al., 2021), which likely result from the background mutation rate in the bacteria.

4.1 Characterizations of phage-resistant E. coli isolates

Three phage-resistant mutants from the model strain *E. coli* DSM 103246 were produced specifically for the experiments conducted for **Paper 3**. They were all isolated from infection trials where *E. coli* DSM 103246 was exposed to phage G28 in soft M9 agar (Appendix 1.8). The chosen phage-resistant mutants were designated TR5, TR7, and ISO24A; TR5 and TR7 were isolated as a part of the first successful attempts at isolating phage-resistant strains using the soft agar method (Appendix 2.d), while ISO24A was isolated as a part of the undergraduate course “BIO299 Research Practice” (University of Bergen) by student Karen Erstad who I had the pleasure to supervise while she successfully isolated resistant strains following my

protocol. Notably, TR5 and ISO24A were designated *fully resistant* to phage G28 (efficiency of plating (EOP) of > 10^{-7}, whereas TR7 was designated *partially resistant* showing an EOP of 10^{-2} (**Paper 3**; designation based on Hancock and Reeves, 1975).

I found it fascinating to compare my observations with classical phage research articles from the 1940s; Among the earliest characteristics of phage-resistant *E. coli* in ever reported, apart from the lack of affinity for phage absorption (Luria and Delbrück, 1943), was a change in colony morphology (Luria and Delbrück, 1943; Demerec and Fano, 1945). Likewise, change colony morphology was observed in two of the phage G28-resistant isolates, ISO24A and TR7 (**Paper 3**; Figure 1). The change in colony size, shape, color, and texture provide insight into potential physiological effects, and heterogeneous outcomes of phage exposure, as several colony morphologies can occur in subcultured mutants resistant to the same lytic phage (Luria and Delbrück, 1943; Demerec and Fano, 1945); Based on colony morphology alone, resistance to phage G28 presents with two distinct outcomes: similar colony morphology as wildtype (smooth colonies with a white/grey color) or large, mucoid colonies (**Paper 3**; Figure 1).

Mucoidy in *E. coli* is linked to mutations in genes regulating the synthesis of colanic acid (**Paper 3**; Wielgoss et al., 2016; Mutalik et al., 2020), which is an exopolysaccharide produced during biofilm formation (Danese et al., 2000) and cellular stress responses (Wang et al., 2020a). Mucoidy is a readily observable property that is indicative of a phage resistance mechanism: the production of an extracellular matrix preventing the phage from reaching surface receptors (Chaudrhy et al., 2020). While it is frequently observed in association with phage resistance (Hancock and Reeves, 1975; Wielgoss et al., 2016; Chaudhry et al., 2020), mucoid phenotypes do not form in all strains of *E. coli* (Lenski, 1988).

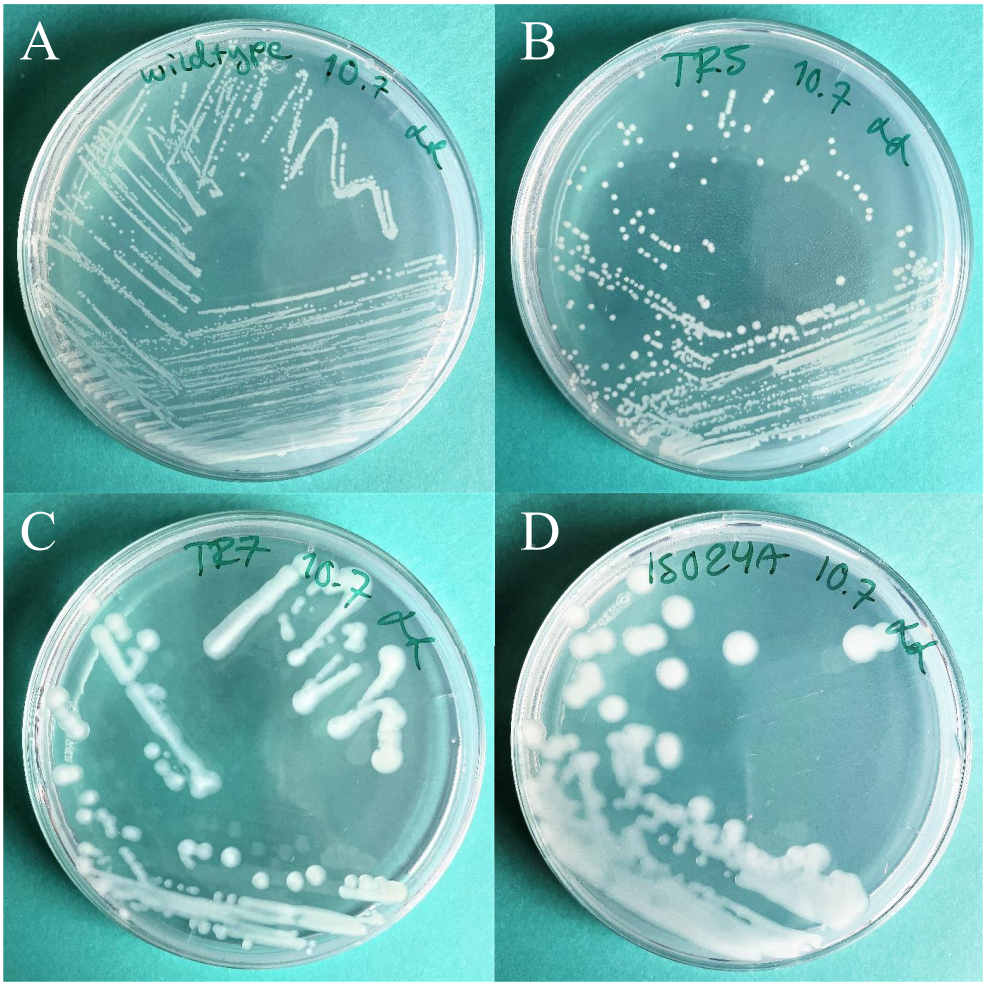

Figure 1. Colony morphology of wildtype *Escherichia coli* DSM 103246 (**A**), compared to phage G28-resistant isolates TR5 (**B**), TR7 (**C**), and ISO24A (**D**) on M9 agar (Appendix 1.7) after 32 h incubation at 37 °C. TR5 shows similar morphology to the wildtype, while TR7 and ISO24A shows a mucoid colony morphology. Photographs taken using iPhone 12 mini by Lotta Landor.

It is worth noting here, that although the field of microbiology is moving towards culture-independent and single-cell methods (e.g., Hatzenpichler et al., 2020; Grujcic et al., 2022), the culturing of the phage G28-resistant *E. coli* on agar was immensely helpful in interpreting the results described in **Paper 3**; The mucoid colony

morphologies of isolates ISO24A and TR7 contributed to establishing a link between the genetic data, phage susceptibility and growth phenotype. It could perhaps have been possible to infer the mucoidy from the sequence data and growth characteristics alone, however, the visual proof of mucoid colonies (Figure 1) coinciding with mutations in genes involved in colanic acid (mucus) synthesis regulation attributed to more confident conclusions.

4.2 Challenges in isolating phage-resistant E. coli

In the literature, it is often mentioned how, with relative ease, phage-resistant mutants can be isolated from phage-infected cultures (such as in the quote in the beginning of this chapter; Luria and Delbrück, 1943). Nonetheless, it is not always straightforward to isolate resistant mutants from all *E. coli*-phage systems (Lenski, 1984), and in some cases resistant mutants have not been successfully isolated using specific protocols (Korf et al., 2020). In my case, it took several attempts to isolate phage-resistant isolates from the *E. coli* DSM 103246 and phage G28 system, because the majority of isolates isolated using the soft agar method (Appendix 2.d) remained susceptible to phages. I tested alternative methods to isolate phage-resistant bacteria, including liquid lysis (adapted from Habusha et al., 2019; and Jørgensen et al., 2022), but the soft agar method was found to be the only one successful.

Specifically, four isolates (TR3, TR5, TR6, and TR7) were found to show changed susceptibility to phage G28 out of 64 isolates tested. The isolate TR6 later lost its resistance when passaged on M9 agar (Appendix 1.7) to remove contaminant phages (and new attempts at cleaning the isolate were not made) and TR3 proceeded to DNA extraction for whole genome sequencing (**Paper 3**) before its severe phage contamination was observed. As a part of the course BIO299, a further 5 resistant and partially resistant isolates were found out of an additional 25 isolates tested. Taken together, the success rate of the method to isolate phage-resistant bacteria was about 10 %, however, the success rate appears to be variable.

Notably, many of the isolates that showed no change in phage susceptibility, showed mucoid colony morphologies, indicating that the phage exposure had resulted in some form of change in the isolates. Interestingly, mucoidy has been suggested as a mechanism facilitating the co-existence between susceptible bacteria and virulent phages (Chaudhry et al., 2020), which could explain the lack of resistance in many of the mucoid isolates. A few studies have shown the tendency of mucoid resistant phenotypes to revert to a non-mucoid phage susceptible state (Wielgoss et al., 2016; Chaudhry et al., 2020), indicating perhaps that mucoidy is costly to the cell and that selection favors non-mucoid phenotypes. The tendency of G28-exposed isolates to revert back to a non-mucoid morphology was observed in several of the isolates, as well.

Another challenge in isolating the phage-resistant isolates was phage contamination; Several of the isolated phage-resistant isolates (TR5 – TR7, specifically) were found to contain phages after isolation, which was initially discovered through flow cytometric counts (Figure 2). The main issue concerning phage contamination was the disruption of flow cytometric analysis, as the phage particles, stained with a DNA-stain, overshadowed the bacterial population in the samples (Figure 2). Moreover, some "resistant" isolates were observed, as in the case of TR3, to spontaneously lyse in liquid culture, which I hypothesize resulted from a combination of phage contamination and the loss of resistance in the isolates affected.

The issue with phage contamination was addressed by adding an agar passage step to the isolation protocol (Appendix 2.e), where the isolates were passaged on phage-free M9 agar 3 times, followed by flow cytometric analysis to confirm the absence of phages in the cultures. However, repeated agar passage comes with the risk of potentially reversing the phage resistance in the bacteria (as observed in Wielgoss et al., 2016; Jørgensen et al., 2022); Indeed, of the resistant isolates in the study, two (TR5 and TR7) were observed to lose their resistance to phage G28 through passage on agar 5 – 6 times. Isolate TR6 lost its resistance after only 3 passages, while phages still being present in the isolate.

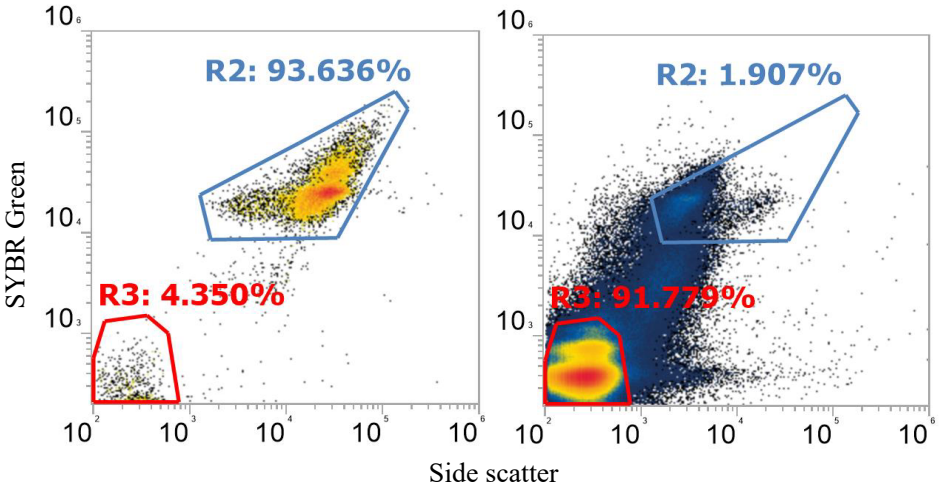

Figure 2. Flow cytometric density plots of single cells of wildtype *E. coli* DSM 103246 (**A**) and phage G28-resistant isolate TR5 (**B**) stained with nucleic acid stain SYBR Green I. Gate R2 (blue) marks where bacterial cells are expected to appear, whereas R3 (red) marks potential viral particles and small-particle debris, both gates show percentage of gated events. As apparent, the majority (R3 > 91 %) of the sample of TR5 consists of potential contaminant phages. Notably, the liquid culture, from which these flow cytometric counts were performed, of TR5 was not lysed and appeared similar to that of the wildtype in terms of turbidity. After this observation, the TR5 isolate was cleaned from the phage through serial passage. The logarithmic X-axis ranges from 10^2 – 10^6 arbitrary units (unit for light scatter; de Rond et al., 2020), and Y-axis 2.0 × 10^2 – 10^6 relative fluorescence units.

Due to this unstable nature of the phage-resistant phenotypes, passaging of cultures were kept to a minimum, and frozen glycerol stocks (stored at –80 °C; Appendix 2.a) were produced from the strains to preserve the resistance traits as unchanged as possible throughout the experiments. Furthermore, spot assays (Appendix 2.c) were used as controls before and after all experiments using phage-resistant isolates, to ensure that the phage resistance remained unchanged.

4.3 The potential receptor site(s) for phage G28

One tricky aspect of the relatively recently isolated system of *E. coli* DSM 103246 and phage G28, is the fact that the cell surface receptor for phage G28 is unknown. However, the whole-genome sequencing of the resistant isolates revealed new clues for a potential receptor(s) of phage G28 (**Paper 3**). Based on previous work performed by Korf et al. (2020), their whole-genome sequenced phage G28-absorpion deficient mutant *E. coli* E28.G28R3 showed a 55-kb deletion in its genome affecting genes involved in both the outer membrane protein families of OmpA and OmpC, which they hypothesized could be important for phage G28 absorption. However, none of these proteins were directly affected by mutations in any of the resistant strains in **Paper 3**. Instead, the resistant isolate ISO24A showed a mutation in a gene coding for transmembrane protein IgaA, which unlikely serves as a receptor (Mutalik et al., 2020), but is a part of the Rcs regulatory pathway (Cho et al., 2014; Wall et al., 2018). While no phage receptors in Rcs core components have been reported (to the best of my knowledge), the Rcs system is connected to membranal proteins such as the potential phage G28-receptor OmpA (Cho et al., 2014; Dekoninck et al., 2020; Korf et al., 2020). Similarly, TR5 showed a mutation in genes coding for DsbA, an enzyme that forms disulfide bonds in proteins (Maskos et al., 2003), such as OmpA (Santos-Martin et al., 2021), indicating that the structure of OmpA could be altered in the isolate. The mutation profile of TR5 also involved mutations in a gene important for O-antigen synthesis (**Paper 3**; Bertani and Ruiz, 2018), indicating that the LPS might be involved in G28-infection. It is possible that phage G28 uses a combination of an LPS-based and an outer membrane protein receptor, similar to what is observed in phage T4 (Yu and Mizushima, 1982; Washizaki et al., 2016). What complicates the determination of the potential receptor sites affected in TR5 is the low frequency of both unique mutations (Table 2), indicating that either mutation unlikely explains the resistance alone.

4.4 Resistance mutations, mechanisms, and possible implications

Phage receptors are primarily functional components of the bacterial cell surface and outer membrane that are important for the survival and growth of *E. coli* cells. While phage resistance is beneficial to survive phage exposure, surface modifications resistance can compromise the primary function of the receptor, which can have implication for bacterial fitness (Burmeister et al., 2020). One direct consequence of the modification of surface receptors is the impaired transport of sugars across the cell membrane (Wandersman and Schwartz, 1982). In some cases, phage resistance can completely block the function of the receptor, like in the case of the iron-transporter FhuA, where the competitively inhibiting lipoproteins (that provides phage resistance) restricts the transport of iron into the cell (Braun et al., 1994).

The sequenced genome of TR5 showed mutations involved in the O-antigen synthesis and periplasmic protein folding, suggesting changes in the LPS and function of DsbA substrates (**Paper 3**). This is further indicated by observations that TR5 produced sediment in liquid culture, as mutations in genes involved in LPS synthesis and disulfide bond formation can impair motility of cells (Parker et al., 1992; Dailey and Berg, 1993; Zuo et al., 2019). Further implications of the mutations could be increased membrane permeability (Zhong et al., 2020), and can reduce that cells' tolerance to antimicrobials (Parker et al., 1992; Zhong et al., 2020; Furniss et al., 2022; McGee et al., 2023), hydrophobic compounds (Parker et al., 1992), and surfactants (Zhong et al., 2020). The methodological implications for the potential change in membrane integrity of TR5 is discussed further in **Paper 3** and Chapter 6 of this thesis. Preliminary disc diffusion testing (adapted from Hudzicki, 2009) using 10 µg chloramphenicol discs, showed smaller growth-free zones in TR5 compared to the wildtype *E. coli* DSM 103246, indicating increased tolerance to phenicol antimicrobials in the phage-resistant isolate (unpublished).

Table 2 (adapted from **Paper 3**). Unique mutations in phage G28-resistant *E. coli* isolates.

Isolate	Mutation	Frequency	Protein affected	Role
TR5	Insertion	25 – 46 %	Wzy	O-antigen synthesis (1)
	Insertion	47 %	DsbA	Protein folding (2)
TR7	SNP (transversion)	99 %	RscC	Regulation of colanic acid/capsule synthesis, biofilm formation (3, 4)
ISO24A	SNP (transition)	100 %	IgaA	Negative regulator of Rcs phosphorelay (5)

Refs. 1: Woodward et al., (2010); 2: Hiniker and Bradwell (2004); 3: Lee et al. (1996); 4: Ferrières and Clarke (2003); 5: Wall et al. (2020)

The Rcs phosphorelay is associated with resistance to several phages in *E. coli* (Mutalik et al., 2020). It involves several membranal protein components that regulate gene expression in response to stress signals from the outer membrane and periplasm (Wall et al., 2018; Wall et al., 2020). As the Rcs (regulation of capsular polysaccharide synthesis) system regulates the production of capsular polysaccharides and colanic acid (Lee et al., 1996; Wall et al., 2018), mucoid phenotypic outcomes from mutations in Rcs-associated genes have been observed (**Paper 3**; Wall et al., 2018; Mutalik et al., 2020; Wall et al., 2020). Both mucoid phage G28-resistant mutants showed mutations in genes coding for core components of the Rcs: genes *yrfF* (ISO24A) and *rcsC* (TR7), coding for the transmembrane protein IgaA and hybrid sensory kinase RcsC, respectively (Table 2). While TR5 does not show mutations directly designated to the Rcs phosphorelay, perturbations, or mutations in LPS synthesis can trigger the Rcs cascade (Wall et al., 2018), indicating that the system's activity could be altered in TR5. Interestingly, DsbA also has substrates linked to the Rcs (Wall et al., 2018; Santos-Martin et al., 2021),

however, if and how the mutation in this protein affects the Rcs system in TR5 is unknown.

Due to the complex nature of the Rcs cascade (Wall et al., 2018), the full-scale fitness consequence of the mutations in genes coding for the system's components is probably impossible to infer based on the experiments performed in **Paper 3** alone. Nevertheless, I hypothesize that the mucoidy and potentially impaired stress-response pathways that the Rcs-related mutations cause could impact ISO24A and TR7 both through energetic cost (excessive mucus production) and through a potentially reduced ability to respond to disturbances. The tendency for phage G28-resistant mutants to show mutations in Rcs-associated genes could explain the difficulty of isolating phage-resistant mutants from the *E. coli* DSM 103246 and phage G28 system, as an upregulation of colanic acid biosynthesis could provide refuge from phages without the need of genetic mutation (Chaudhry et al., 2020).

An overall reduced growth rate is frequently reported for phage-resistant *E. coli* (**Paper 3**; Korf et al., 2020; Sørensen et al., 2021; Zulk et al., 2022), and the reduction in growth rate is sometimes linked to specific genetic changes (Sørensen et al., 2021). However, bacterial growth is influenced by several factors (Ingraham et al., 1983a), and a reduced growth rate could be an indirect consequence of different functional changes in the bacterial cell. Nonetheless, an overall reduction in growth rate was observed in ISO24A and TR7 compared to the wildtype *E. coli* DSM 103246 across the range of glucose concentrations tested (**Paper 3**), which fits with the hypothesis of costly mucus production. On the other hand, TR5 showed a similar growth phenotype to the wildtype *E. coli* DSM 103246 (**Paper 3**), which is consistent at least from the *wzy*-mutation perspective with previous findings (Zuo et al., 2019).

One challenge when trying to determine the fitness implication of specific phage resistance mechanisms is the lack of competition and environmental context. For instance, the growth phenotypes of phage-resistant *E. coli* can be similar to the wildtype in nutrient-rich laboratory media, while showing reduced growth in environmentally relevant media compositions (Zulk et al., 2022). Furthermore,

important fitness implications *in vivo* might not show up in laboratory cultures; The O-antigen plays an important role in colonization and invasion in animal host tissues (Sheng et al., 2008; Zuo et al., 2019), and while TR5 maintains similar growth to the wildtype in laboratory media, its mutation in a gene involved in O-antigen synthesis might indicate that it is unable to colonize, or persist in, its natural habitat (the chicken gut; Korf et al., 2020). In addition, phage resistance might not evolve as readily in environmentally relevant conditions. As observed in a plant pathogen (*Pseudomonas syringae*) and phage system, phage-resistant bacteria emerged readily *in vitro* but did not emerge when co-cultured in the tomato leaf apoplast (Hernandez and Koskella, 2019). Another important issue when it comes to studies of bacterial fitness is that fitness traits tend to be tested in isolation, and the outcome is dependent on the choice of traits in any given study. As such, **Paper 3** highlights the importance of choosing multiple fitness parameters to provide a comprehensive view of the different fitness outcomes.

4.5 The cost of acquired antimicrobial resistance in E. coli?

The cost of resistance is not limited to phage resistance only. Antimicrobial resistance can develop as a result of mutations (Mwangi et al., 2007); however, antimicrobial resistance is often achieved by the acquisition of antimicrobial resistance genes through horizontal gene transfer rather than spontaneous mutations (Miao et al., 2012). One proposed remedy for the looming global antimicrobial resistance crisis is the phasing out and reduction of antimicrobial use, anticipating that the fitness cost associated with redundant antimicrobial resistance genes would result in negative selection and eventually in a reduction in the prevalence of antimicrobial resistance in bacterial populations (Raymond, 2019). However, the cost of acquired antimicrobial resistance genes has been observed to be reduced by compensatory mutations (Björkman et al., 1998; Bird et al., 2023), which potentially could make the resistance genes difficult to eradicate.

I decided to investigate if the acquisition of a large (approximately 185-kb) plasmid would engender a measurable fitness cost on the growth of *E. coli* by performing a conjugation experiment using wildtype *E. coli* DSM 103246 as well as a plasmid donor *Aeromonas salmonicida* subsp. *salmonicida* P20-1A/17, a fish pathogenic bacterium. The conjugation experiment was performed using an adapted version of the protocol described by McIntosh et al. 2008 (Appendix 2.h). The plasmid donor carried a plasmid known to contain a florfenicol (*floR*) as well as a mercury resistance gene (unpublished). The gene *floR* also confers resistance to chloramphenicol (Doublet et al., 2005), which was used as a selective antimicrobial for the experiment. Wildtype *E. coli* DSM 103246 cannot grow in the presence of 10 µg/mL chloramphenicol (Figure 3), however, after the conjugation experiment, the isolated *E. coli* transconjugant CR showed the ability to do so but did not reach the same optical density as the antimicrobial-free culture (Figure 3).

Interestingly, however, the growth phenotype of the transconjugant was similar to the wildtype in antimicrobial-free media (Figure 3), which does not indicate an immediate fitness cost from the plasmid, at least not when it comes to growth in laboratory media. It would be tempting to assume that if *E. coli* encountered this plasmid under chloramphenicol or mercury selection in nature, it could become established in the population. The experiment was not replicated, and further investigation of the *E. coli* transconjugant was not done.

The ability of transconjugant to grow exposed to chloramphenicol indicates the successful conjugation between *A. salmonicida* subsp. *salmonicida* and *E. coli*, which is also the largest inter-specific “leap” the plasmid in question has been observed to successfully achieve. This also shows the compatibility of antimicrobial resistance conferring plasmids between aquatic and terrestrial animal production environments, as both bacterial isolates in this experiment were isolated from farmed animals.

While the sequence analysis is not performed as a part of this thesis, the plasmid as well as the plasmid donor *A. salmonicida* subsp. *salmonicida* P20-1A/17, together with a few other *Aeromonas* spp. strains that previously had been recipients of the

plasmid, were sequenced. I hope to be able to identify the plasmid and characterize its genetic contents and close the chapter on this transferable linked antimicrobial and mercury resistance story in the future.

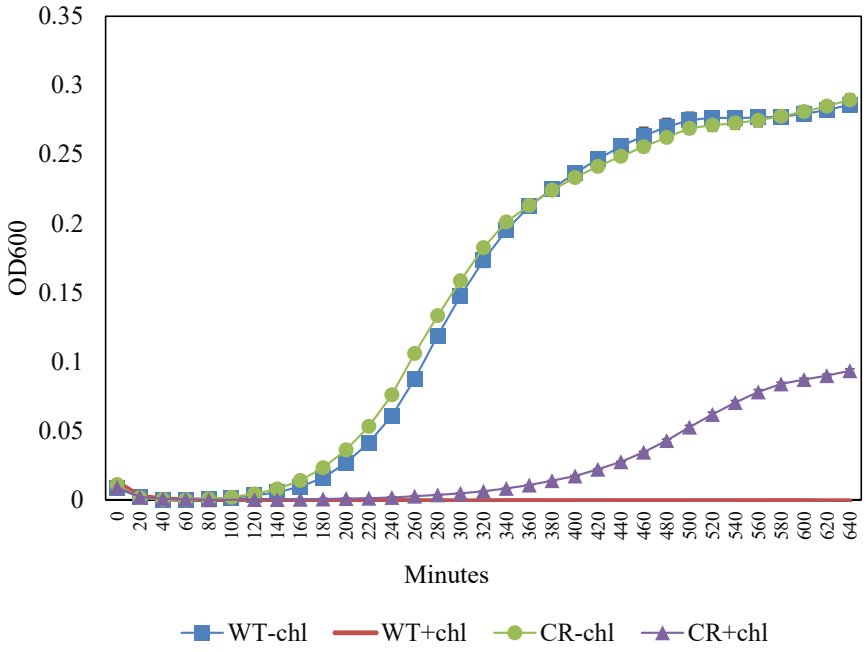

Figure 3. Optical density (600 nm, OD600) growth curves of wildtype *E. coli* DSM 103246 (WT) growing in the absence (-chl) and presence (+chl) of 10 µg/mL chloramphenicol, as well as chloramphenicol-resistant transconjugant *E. coli* (CR) grown in the absence (-chl) and presence (+chl) of the same concentration of chloramphenicol. Error bars are standard deviation of the mean of 21 wells (barely visible).

5. How BONCAT works

"The selective identification of a newly synthesized proteome has been hindered by the basic fact that all proteins, new and old, share the same pool of amino acids and thus are chemically indistinguishable."

- Dieterich et al. (2006)

Advancements in microbiological methodology have led to the development of methods with the ability to measure microbial activity to a single-cell level. Some of the methods, like Raman microspectrometry, are remarkably precise, with the potential ability to detect specific genetic expressions within single cells (Germond et al., 2018). While these methods are increasing in use in microbial applications, their use in the wider microbiological community is limited by i.e., low sample throughput (e.g., 200 – 500 cells/h for an automated Raman-based cell sorting platform: Lee et al., 2019), reliance on radioactivity (microautoradiography: Nielsen et al., 2003), or expensive instrumentation and sample preparation (NanoSIMS: Gao et al., 2016). An alternative approach to study microbial activity is the use of synthetical biomolecules that can be visualized within single cells. Recently, a method using synthetic amino acids has been found successful in measuring protein synthetic activity of single cells without prior modification of the studied system (Dietrich et al., 2006; Hatzenpichler et al., 2014). Following a general introduction to the method, I discuss experiments performed to validate and assess the method's applicability to quantify the cost of resistance in bacteria (**Paper 3**; Chapter 6).

5.1 Using synthetic amino acids to track microbial protein synthesis

Bioorthogonal non-canonical amino acid tagging (BONCAT, Dietrich et al., 2006) is a proteomic approach which allows for the detection of newly synthesized proteins in cells. The method uses non-canonical (unnatural, synthetic) amino acid analogues (NCAAs) which are distinct from their natural amino acid counterpart by having a terminal alkyne or azide group. These terminal groups make the analogues detectable

through selective staining with the help of an alkyne-azide “click” reaction, where analogues with an alkyne group can be labelled or stained (I will use the words “stained” and “labelled” interchangeably throughout this text) using an azide-bearing fluorophore. Likewise, analogues with a terminal azide group can be labelled using fluorescence dyes containing a complementary alkyne group (Kiick et al., 2002).

The two most used NCAAs for BONCAT applications are *L*-azidohomoalanine (AHA) and *L*-homopropargylglycine (HPG) which are azide-, and alkyne-bearing, respectively (Hatzenpichler et al., 2020). Both AHA and HPG are methionine analogues and replace the amino acid in synthesized proteins (Kiick et al., 2002; Hatzenpichler et al. 2020; Ječmen et al., 2023). Each of these analogues can be dissolved in an aqueous media in which suspended cells can incorporate them into proteins through cellular translational activity, without the requirement for genetic manipulation of the target cells (Beatty et al., 2005; Hatzepichler et al., 2020). Other non-canonical amino acids, like azidonorleucine (Aln), azide-bearing, can be used in BONCAT applications with the help of genetically modified target cells expressing a bioengineered methionyl tRNA synthetase, which incorporates Aln into cellular proteins (Franco et al., 2018). Aln is especially useful for targeting specific cells’ protein synthesis activity in systems with several different cell types, such as intracellular bacteria (Franco et al., 2018).

Within the cells, the terminal groups of incorporated NCAAs structurally survive the translational activity (Kiick et al., 2002) and are highly distinguishable from other cellular components because the alkyne or azide groups are rarely metabolically produced in natural systems. The only organism known to produce an azide-containing metabolite is the dinoflagellate *Karenia brevis* (Hossain et al., 1985; Griffin, 1994) whereas alkyne-containing natural metabolites are somewhat more common and in cyanobacteria (Chai et al., 2016) and in acidic metabolites in plants (Shi Shun and Tykwinski, 2006). Cells that intrinsically produce alkyne or azide compounds are unlikely to be good candidates for BONCAT studies, as the alkyne-azide reactivity would interfere with the method.

5.2 The alkyne-azide click reaction

The staining of NCAA-containing proteins within cells is done through either a copper(I)-catalyzed (Rostovtsev et al., 2002) or a strain-promoted reaction (Agard et al., 2004) using fluorescence dyes containing a complementary alkyne or azide moiety (Hatzenpichler et al., 2014). In my work, I used the copper(I)-catalyzed reaction to label cells suspended in aqueous buffer in BONCAT experiments (**Paper 2**; **Paper 3**; Appendix 2.f). The copper(I)-catalyzed reaction is dependent on the copper(I) oxidation state driving the alkyne-azide cycloaddition reaction (Rostovtsev et al., 2002; Hong et al., 2010) which connects – "clicks" – the functional terminal in NCAA-containing proteins within the cells to the complementary terminal in the fluorophore containing labelling dye (Beatty et al., 2005; Hatzenpichler and Orphan, 2015). Because the copper(I) catalyst is toxic for living cells (Hong et al., 2010), cells are normally fixed before staining to prevent cellular stress processes to interfere with the method, although BONCAT labelling of live cells has proven successful with some adjustments (Hatzenpichler et al., 2014).

To facilitate the reaction, the copper(I) oxidation state is first achieved by the reduction of copper(II) in $CuSO_4$ by the addition of sodium ascorbate. However, due to the instability of copper(I) (Hatzenpichler and Orphan, 2015) and the production of reactive oxygen species by the copper(I)-ascorbate system under aerobic conditions (Houghton and Nicholas, 2008; Hong et al., 2010), the chelating ligand tris[(1-hydroxypropyl-1H-1,2,3-triazol-4-yl)methyl]amine (THPTA) is added to stabilize the copper catalyst and curb the production of free radicals (Hong et al., 2010; Hatzenpichler and Orphan, 2015). To further stabilize the system and to prevent ascorbate byproducts from reacting with protein side chains (Hong et al., 2010) and to prevent precipitation (Hatzenpichler and Orphan, 2015), aminoguanidine is added. In the stabilized copper(I)-environment, the alkyne-azide click reaction is readily and effectively achieved by the addition of concentrated fluorescence dye with the complementary alkyne or azido terminal group. One advantage of the BONCAT-labelling protocols is that the reagent molecules are small enough to penetrate cell walls and membranes without the need for permeabilization steps (Samo et al., 2014).

5.3 Measuring BONCAT fluorescence signal

The fluorescence from labelled BONCAT samples can be detected using different fluorometric instruments, including fluorescence microscopy (Hatzenpichler et al., 2014; Samo et al., 2014; Pasulka et al., 2018) and fluorescence-activated cell sorting (Reichart et al., 2020; Valentini et al., 2020). Flow cytometry, recently introduced in BONCAT applications (**Paper 2**; **Paper 3**; Lindivat et al., 2020; Lindivat et al., 2021), adds a quantitative aspect to the method, as it allows for high-speed multivariate analysis of a large number of cells (e.g., 300 – 800 cells per second; **Paper 3**). Furthermore, flow cytometry offers a wide variety of methods to add dimensions of information to BONCAT samples through multi-label analysis (Davey and Kell, 1996; Beatty et al., 2010; Lindivat et al., 2021). I applied a nucleic acid stain, SYBR Green I (Thermo Fisher Scientific, United States), to detect all DNA-containing cells in addition to their BONCAT fluorescence (**Paper 2**; **Paper 3**).

5.4 Non-activity effects on BONCAT fluorescence

While the BONCAT method specifically should track the newly synthesize proteins in the test system, working with the method has led me to consider that factors independent of bacterial activity are affecting the fluorescence of the BONCAT-incubated cells. As mentioned above, the chemistry involved in the click reaction mainly concerns the stabilization of copper(I) and the neutralizing of destructive products from the resulting chemical reactions. However, I suspect that the system is difficult to stabilize completely, hypothetically resulting in a staining/experiment-dependent fluorescence, which I have frequently observed. Even mixing is probably very important for stabilization of the copper(I)-catalyzed click reaction, but mixing also bears the risk of oxygenation which can affect the reducing conditions required for copper(I) system (Hatzenpichler and Orphan, 2015). I learned early on that the correct storage (–20 °C) and quality (low number of freeze-thaw cycles) of THPTA, specifically, is crucial for fluorescence of stained samples (Figure 4). Given the number of reagents needed for the successful click reaction to occur, individual

reagent quality control is not necessarily feasible to do, especially when there are no BONCAT quality standards to compare to.

Sample processing can impact the fraction of BONCAT-fluorescent cells. Namely, the freezing of BONCAT-incubated samples in NCAA-free buffer without cryoprotectant leads to the disproportionate loss of BONCAT-negative cells. For instance, in the pilot study for the BONCAT time-course experiments in **Paper 3**, BONCAT-incubated samples were frozen after the removal of AHA in sterile phosphate-buffered saline (PBS) without cryoprotectant. The active fraction (%BONCAT+) of both wildtype *E. coli* DSM 103246 and phage G28-resistant isolate ISO24A increased to > 80 % after 15 minutes of incubation and remained at that level throughout the incubation period (170 min, Figure 5).

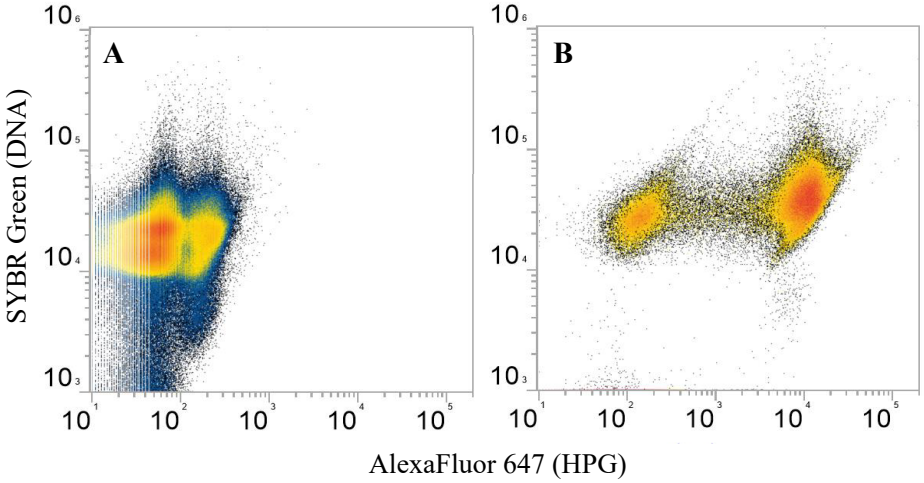

Figure 4. Difference in BONCAT-fluorescence in *E. coli* DSM 103246 incubated with 100 µM HPG, after staining with THPTA-reagent stored at the wrong temperature (**A**) and at the correct temperature (**B**). The logarithmic scale Y-axis (DNA stain SYBR Green I) ranges 10^3 – 10^6, and the X-axis (AlexaFluor 647 picolyl azide) 10^1 – 2.0×10^5 relative fluorescence units, respectively.

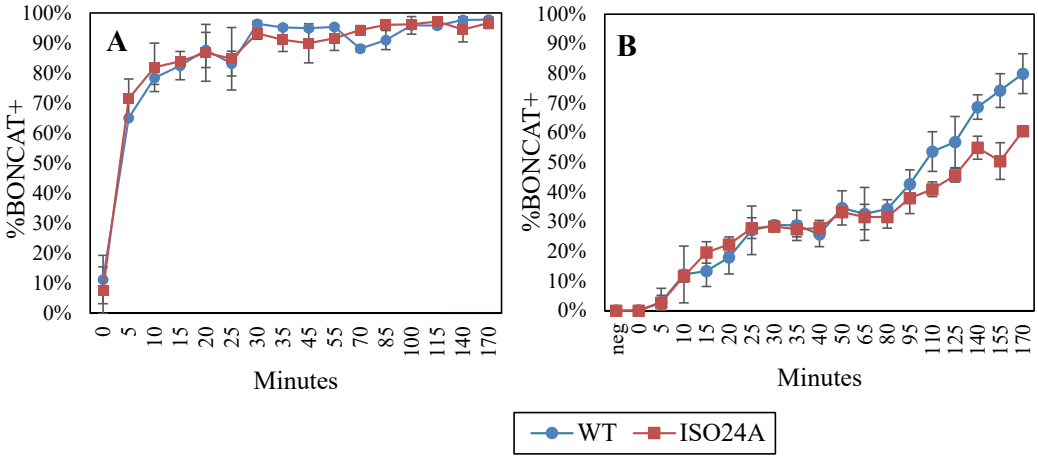

Figure 5. The mean fraction of active cells (%BONCAT+) over time (minutes) in samples of wildtype *E. coli* DSM 103246 (WT) and phage-resistant mutant ISO24A incubated with 50 µM AHA. Samples in chart **A** were frozen in AHA-free buffer without cryoprotectant, and samples in chart **B** were frozen in AHA-free buffer containing 20 % glycerol (data adapted from **Paper 3**), before staining and flow cytometric analysis. In **B**, "neg" is a negative control without AHA not included in **A**. Due to the loss of inactive cells (BONCAT-negative), the active fraction of cells in chart **A** is higher than in chart **B**. Error bars are standard deviation of the mean of 3 (**A**) and 3 (**B**) replicate samples.

In contrast, freezing the samples in PBS containing 20 % glycerol allowed for the preservation of BONCAT-negative cells proportionally similar to non-frozen samples (Paper 2). As %BONCAT+ cells (or virus particles; Pasulka et al., 2018) frequently are reported in the literature (Hatzenpichler et al., 2016; Leizeaga et al., 2017; Couradeau et al., 2020; Valentini et al., 2020; Chen et al., 2021), sample processing might be important to avoid misrepresenting the active fraction of microbial cells or viruses in any given system. Of course, my observations were done for *E. coli* in minimal media, and there could be species/media-specific differences in freezing effect of on BONCAT-negative cells. It is also not clear whether the loss of BONCAT-negative cells is due to increased cell permeability from freezing leading to higher labelling efficiency or due to the loss of truly BONCAT-negative cells. As a final note, I have not tested the effect of glycerol on the staining efficiency through

the click reaction, and therefore recommend removing the glycerol-containing buffer before staining (Appendix 2.f).

5.5 Method validation

BONCAT has been validated for several bacterial systems (Samo et al., 2014; Lindivat et al., 2020), and applied to virus-host systems (Pasulka et al., 2018). No previous attempts at quantifying the cost of resistance have been made using this method, however. Thus, I performed a couple of validating exercises to gain insight into how the method performs in the light of the new research question. To confirm that BONCAT and its components are not affecting the bacterial system, a straightforward growth test was initially performed using *E. coli* exposed to the alkyne-bearing analogue HPG at a previously used concentration (100 µM HPG: Samo et al., 2014; Hatzenpichler and Orphan, 2015; Leizeaga et al., 2017; Pasulka et al., 2018). The test was set up similarly to the microwell assays described in **Paper 2**.

The premise of BONCAT is non-toxicity – hence "bioorthogonal" meaning non-interfering with living functions (Hatzenpichler at al., 2016). Indeed, the metabolic effect of NCAAs on microbial systems had been studied previously, and it was initially concluded that NCAA-supplementation (50 µM HPG or AHA) only cause minor perturbations on *E. coli* metabolism (Steward et al., 2020). Despite this, no growth was observed in my validation test *E. coli* treated with 100 µM HPG, while the HPG-free culture showed a complete growth curve (Figure 6). This finding was found to be remarkable, and motivated the study in **Paper 2**, where the antibacterial effects of NCAAs were further scrutinized, showing HPG had negative, AHA less so, and methionine positive effect on *E. coli* growth. These results were later confirmed by Ječmen et al. (2023), who also found HPG to be growth-inhibiting in their *E. coli*. They further showed that both AHA and HPG exposure induced expression of phage shock protein A in *E. coli*, which is indicative of a stress response that they hypothesized could be related to the NCAA-exposure. Stress responses have been found to be triggered by HPG exposure in *Synechococcus* systems (Michels et al.,

2021), as well. Additionally, pulse-labelling using HPG has been found to reduce growth in *Salmonella enterica* and *Mycobacterium tuberculosis*, but the growth recovered some time after the HPG-pulse (van Elsland et al., 2018).

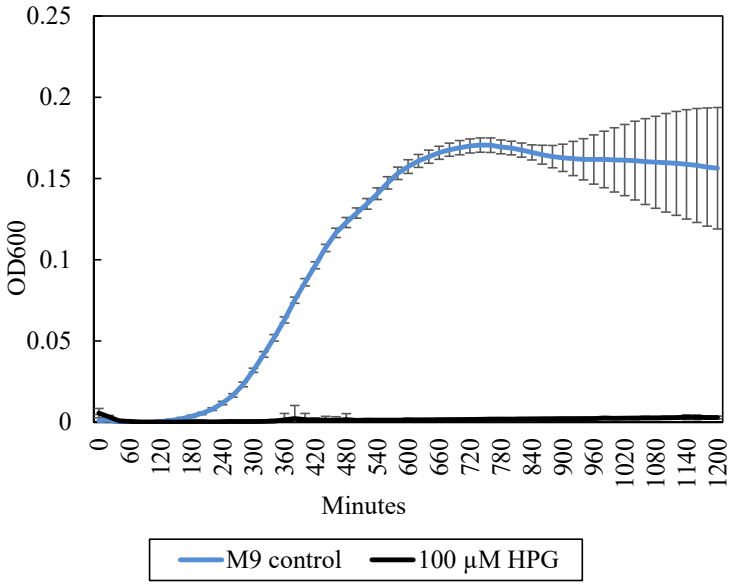

Figure 6. Optical density measured at 600 nm (OD600) of *Escherichia coli* DSM 103246 grown in M9 media containing 100 µM *L*-homopropargylglycine (100 µM HPG, black), or in HPG-free M9 media (M9 control, grey), at 37 °C over time (minutes). All measurements are baseline corrected. Error bars are standard deviation from the mean of 27 wells per treatment.

Naturally, all protocols were adjusted to allow for as unaffected growth as possible, using least-affecting concentrations of AHA. Due to its antibacterial effects, HPG was found to be an unsuitable NCAA for any future cost of resistance experiments. In the light of these findings, I hypothesize that the alkyne moiety in HPG is the most likely cause for its growth inhibiting effect in *E. coli*, as this is the main distinction between the analogue and the non-toxic methionine. Indeed, other alkyne-containing compounds have been found to have a range of biological effects, including potential antimicrobial and antitumor properties and have thus garnered interest for

pharmaceutical applications (Ott et al., 2005; Erol et al., 2015). As HPG was found to have significant effects on growth at nM-concentrations, HPG or other alkyne-bearing compounds might have potential as a target for antimicrobial drug development to target drug-resistant *E. coli* in the future.

5.5.1 BONCAT responds to bacterial growth rate

My second validation experiment was aimed at testing BONCAT's ability to detect changes in growth rate in *E. coli*. To address this, the temperature-dependent growth rate of bacterial cells was used to test the ability of BONCAT to respond to different growth rates in the same bacterial strain (Appedinx 2.g). At optimal temperature range (20 – 37 °C, Farewell and Neidhardt, 1998), *E. coli* will increase its growth rate in response to increasing temperature (Ingraham et al., 1983c; Farewell and Neidhardt, 1998; Yang et al., 2020). The full temperature-range of *E. coli* DSM 103246 was not specifically tested for the study, but a range of temperatures was chosen based on the literature, as well as the temperature-range of the instrument used.

The test confirmed that *E. coli* DSM 103246 showed the highest mean maximum growth rate at 37 ºC (1.05 ± 0.12 h^{-1}), declining to 0.63 ± 0.03 h^{-1} at 28 ºC, and further declining to 0.29 ± 0.11 h^{-1} at 15 ºC in M9 media (Appendix 1.5). Likewise, for AHA-incubated samples, the BONCAT-signal showed a similar trend, showing the strongest fluorescence signal at 37 ºC for all concentrations tested, and showing a declining trend with declining temperature (Figure 7). Additionally, a positive fluorescence-concentration relationship is observed (Figure7). The results here are presented in peak relative fluorescence units (peak RFU), whereas the mean RFU per cell was used in later experiments as this was found to be more informative (**Paper 2**; **Paper 3**).

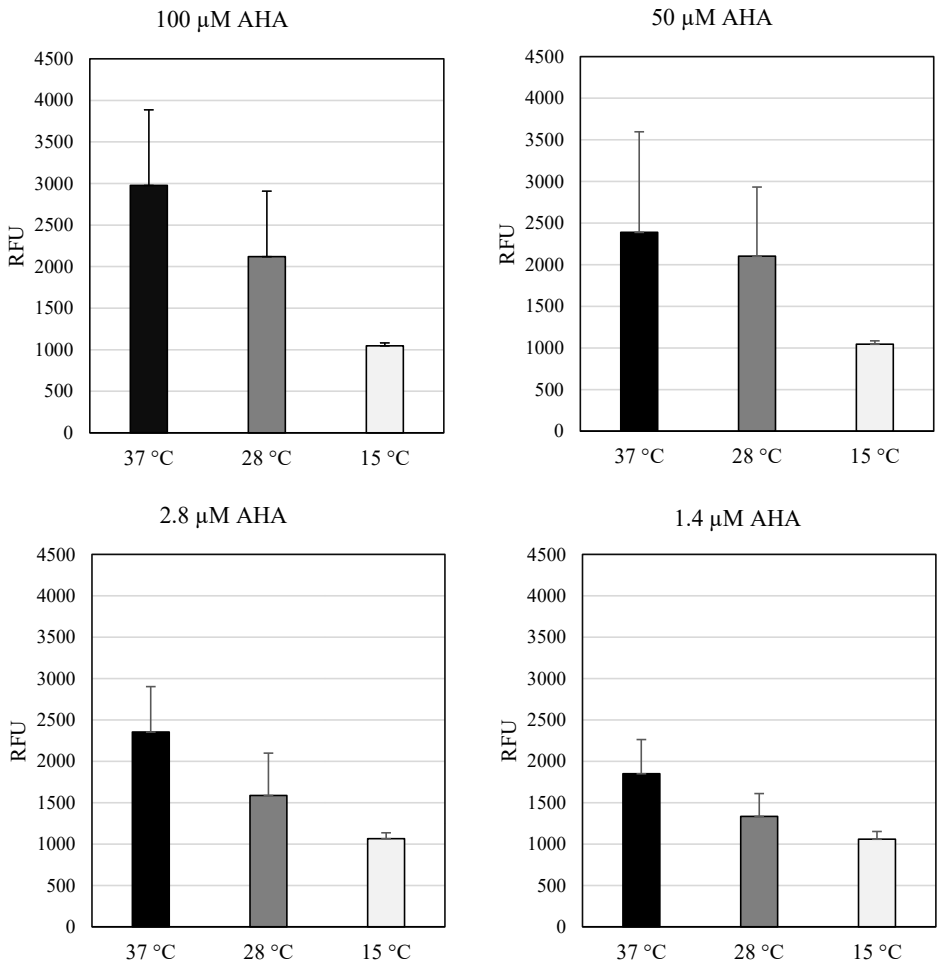

Figure 7. BONCAT signal in mean peak relative fluorescence units (RFU) in *E. coli* DSM 103246 incubated with different concentrations of *L*-azidohomoalanine (AHA; 100 µM; 50 µM; 2.8 µM; 1.4 µM) for 30 minutes at different temperatures (37 °C = black; 28 °C = dark grey; 15 °C = light grey). Error bars are standard deviation of the mean of 12 replicate measurements.

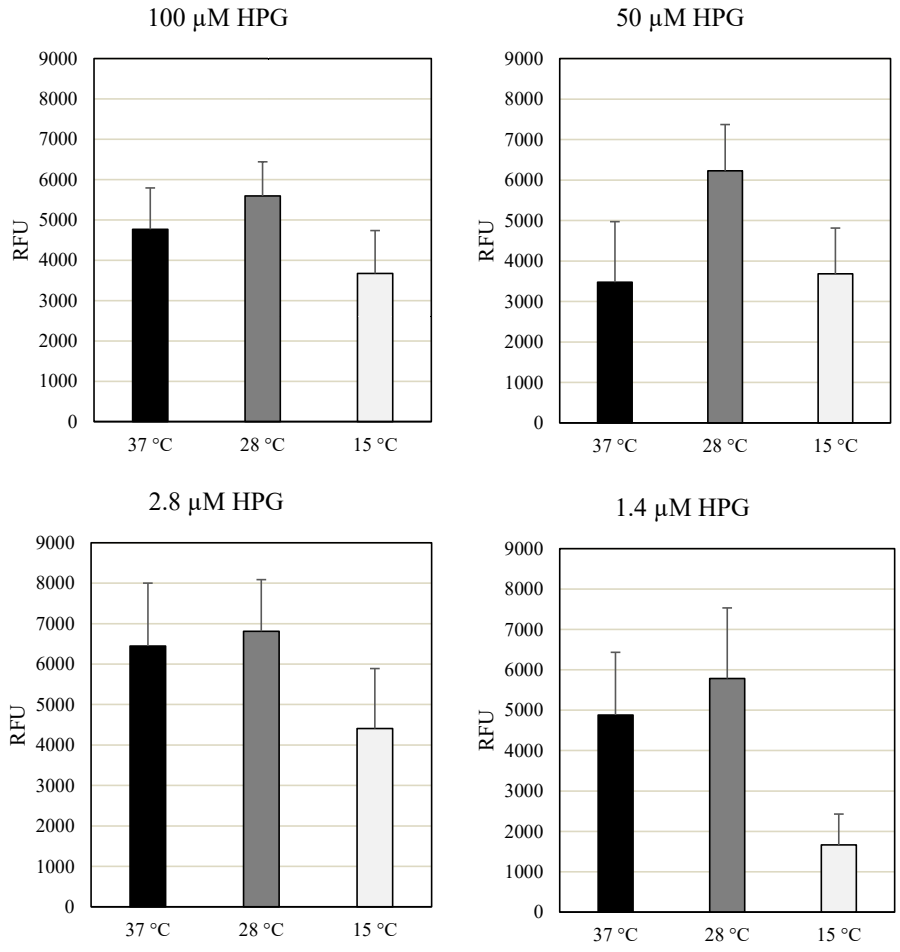

Figure 8. Mean peak relative fluorescence units (RFU) of *E. coli* DSM 103246 incubated with different *L*- homopropargylglycine (HPG; 100 µM; 50 µM; 2.8 µM; 1.4 µM) for 30 minutes at different temperatures (37 °C = black; 28 °C = dark grey; 15 °C = light grey). Error bars are standard deviation of the mean of 12 replicate measurements.

The same temperature-fluorescence-relationship was not found when the above-mentioned experiment was conducted using HPG, and no direct fluorescence-concentration relationship was observed (Figure 8). The peak fluorescence was notably higher in HPG treatments compared to AHA treated cells. I hypothesize that the growth-inhibiting or growth-affecting HPG concentrations used (**Paper 2**) likely

affected the bacterial system, which could explain the lack of expected pattern for the NCAA. In conclusion, the methionine analogue AHA showed ability to respond to bacterial growth rate, whereas due to its antibacterial properties, HPG was found to be a poor candidate for further studies where unaltered bacterial growth is an important factor, as concluded in **Paper 2**.

5.5.2 BONCAT responds to the bacterial growth phase

To further investigate the relationship between the fluorescence signal and the growth activity of the bacterial system, a BONCAT experiment was set up in parallel with the infection experiment presented in **Paper 1**. At five chosen time-points, based on the growth of a phage-free culture of *E. coli* DSM 103246, samples were taken and incubated in separately with 100 µM AHA for 30 minutes at 37 °C. The growth phases were estimated by the tracking of the optical density (OD, measurements every 20 minutes) of the growing culture under 150 rpm agitation at 37 °C and were designated: early exponential phase (OD = 0.07); exponential phase (OD = 0.23): late exponential phase (OD = 0.56); stationary phase (OD = 0.7); and late stationary phase (OD = 0.68; 480 minutes after the stationary phase sample). The growth rate of the culture at each growth phase was estimated based on the OD measurements according to Kurokawa and Ying, (2017).

After BONCAT-labelling and flow cytometric analysis (Appendix 2.f.), the BONCAT signal was observed to be the strongest at the early exponential phase and decreasing with each subsequent growth phase (Figure 9). Likewise, the active fraction of the of the samples was the highest at the early exponential phase, where 93 ± 2.9 % of the cells were found to be BONCAT-positive. The active fraction declined in subsequent growth phases, from 69 ± 7.9 % during the exponential phase, to 35 ± 10 % during the late exponential phase. Once the stationary phase was reached, only 17 ± 4.6 % were active, and 480 minutes later, less than 1 % of cells (0.2 ± 0.0 %) were active. While the active fraction of any bacterial population might be an interesting measurement to report, its value in batch culture experiments, where

cultures are expected to growth in an exponential fashion, is debatable. Regardless, these findings suggest that BONCAT is sensitive to the growth phase of bacterial batch cultures, and that culturing conditions and culture growth need to be carefully controlled for reproducibility of results.

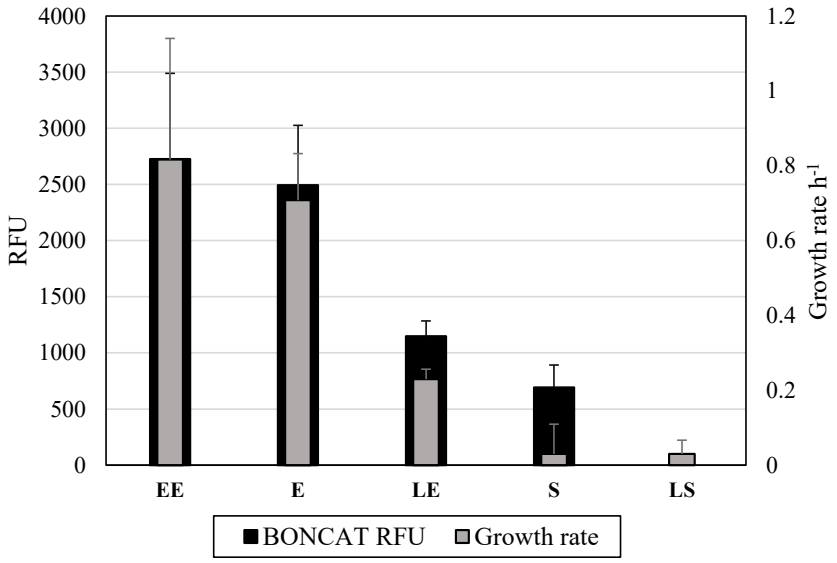

Figure 9. BONCAT signal as mean relative fluorescence units (RFU) per cell (black) at different growth rates (grey) of *E. coli* DSM 103246 incubated with 100 µM *L*-azidohomoalanine (AHA) for 30 min at each growth phase: EE = early exponential phase; E = exponential phase; LE = late exponential phase; S = stationary phase; LS = late exponential phase. Error bars are standard deviation of the mean of 4 (BONCAT) and 3 (growth rate) replicate measurements.

6. Attempting to quantify the cost of resistance

"Models indicate the presence of [cost of resistance (COR)] and observational evidence for it exists, but COR remains difficult to measure and is not always confirmed experimentally."

- Våge et al. (2012)

The ability of BONCAT to measure and quantify the cost of resistance is foremostly facilitated by the high sensitivity of the method. My validation experiments showed the methods response to different growth rates in *E. coli*. This was further confirmed in **Paper 3**, as > 1 % of cells responded to the substrate immediately after AHA addition, followed by a rapid increase in fluorescence during the first minutes of incubation. Similar observations have been made previously, showing detectable BONCAT fluorescence after only 2 % of the generation time in *E. coli* (Hatzenpichler et al., 2014).

The sensitivity of the method to the growth phase of batch cultured bacteria implied that a single snapshot of bacterial protein synthetic activity likely would not be very informative. Therefore, time course incubation – a series of snapshots – was opted for to sufficiently capture not just the difference in BONCAT fluorescence, but also its development over time, between the test bacteria. The multiple measurements over time were further motivated by the potential to estimate and quantify the protein synthetic rate of single cells based on their BONCAT signal (**Paper 2**). In addition, complementary methods were used to test the implication of the resistance mutations in the phage G28-resistant isolates, which proved to be helpful in portraying an overview of the phenotypic consequences of the resistance mutations (**Paper 3**; Table 3).

Here, it is important to note, that although BONCAT is applicable for single-cell resolution (e.g., Hatzenpichler et al., 2014; Samo et al., 2014), the flow cytometric analyses I performed are essentially population-based measurements. The BONCAT fluorescence per cell is reported as mean label intensity per cell using gating to separate the populations of interest; That is, depending on the population gating, the

single-cell fluorescence signal changes. Nonetheless, the flow cytometric data shows characteristic two populations in NCAA-incubated samples; One population with low fluorescence (BONCAT-negative population) and one population showing increasing fluorescence over the incubation time (BONCAT-positive population). These populations are connected by intermediately fluorescent cells in between (Figure 10, left), indicating heterogenous activities of cells within the same sample. However, it is impossible to retrieve the single cell measurements using the Attune NxT platform, and extraction of the single-cell data would require additional software.

Table 3 (adapted from data in **Paper 3**). A schematic overview of mutations and the metabolic role of affected proteins of phage G28-resistant isolates, and changes in different traits (+ increase; - decrease; = no change; parentheses () indicate a statistically non-significant change) compared to the wildtype *E. coli* DSM 103246.

		Effect on trait compared to wildtype				
Isolate	**Colony morphology**	**α%**	**μ**	**Y**	**B**	**%+**
TR5	smooth	62%	=	-	+	+
TR7	mucoid	45%	-	=	(-)	=
ISO24A	mucoid	12%	-	=	-	-

Abbreviations: **α%** - nutrient affinity compared to wildtype (100%) in percent (%); **μ** = growth rate; **Y** = yield; **B** = BONCAT-fluorescence per cell; **%+** = active fraction of cells.

Trade-offs between phage resistance and different traits were found in all isolates tested (**Paper 3**). In both the mucoid isolates ISO24A and TR7, a similar pattern of reduced growth rate was observed (Table 3), ISO24A also showing a more pronounced reduction BONCAT fluorescence, nutrient affinity and fraction of active cells at the end of the incubation period compared to the wildtype *E. coli* DSM 103246. Perhaps due to its partial resistance, TR7 showed the highest similarity with

the wildtype, although this similarity was only expressed in two fitness traits (yield and active fraction of cells; Table 3). The trade-off pattern of TR5 stood out from the other isolates, only showing a reduction in nutrient affinity and yield, but increased BONCAT-fluorescence and fraction of active cells compared to the wildtype (Table 3). These findings, from three different resistant *E. coli* isolates, prompt the question: How is cost of resistance expected to be expressed in protein synthesis?

Protein synthetic rate of bacterial cells is constrained by ribosomal availability and is expected to respond proportionally to the cellular growth rate at optimal temperature range (Cox, 2003; Scott and Hwa, 2011; Scott et al., 2014; Li et al., 2018). As protein synthesis is the most energetically costly process in bacterial cells (Stouthamer, 1975; Russell and Cook, 1995), the protein synthetic activity needs to be tightly regulated to optimize the energy economy of the cell. The reduced BONCAT fluorescence, indicative of reduced protein synthetic activity, in ISO24A can thus be explained by the lower growth rate in the isolate (Table 3) but is also a sign of a well-balanced protein economy. The same cannot necessarily be said for TR7, that although showed a significantly reduced growth rate, only showed slightly lower (not statistically significant) BONCAT fluorescence compared to the wildtype (**Paper 3**). Remarkably, TR5 maintained the same growth rate as the wildtype, yet increased protein synthetic activity (increased BONCAT fluorescence), indicating perhaps a trade-off from increased energetic expenditure to protein production per generation.

If the cost of resistance can be expressed as either an increased or a decreased BONCAT-signal, applying the method as a means of quantifying resistance trade-offs in natural systems would require background knowledge of wildtype fluorescence to accurately interpret the results. It may on the other hand be hypothesized that phage resistance could result in the disruption of protein synthetic regulation in bacterial cells, and to that end increased protein synthetic activity should be considered a possible cost of resistance.

Although this thesis shows different BONCAT signals in phage-resistant *E. coli* using flow cytometric measurements, the cost of resistance remains short from being

quantified in my test system. As discussed below, due to unanswered physiological questions regarding the resistant isolates and methodological limitations of BONCAT, the quest to quantify the cost of resistance is not quite over yet.

6.1 Methodological limitations complicating quantification

The idea of quantifying the cost of resistance by measuring the protein synthetic activity is appealing. However, despite attempts at quantifying the rate of protein synthesis previously (Samo et al., 2014), BONCAT has limitations which deem the method "semi-quantitative" (Hatzenpichler and Orphan, 2015). The different levels of methionine residues per protein make the absolute quantification of the protein synthetic rate difficult, especially when comparing different species of bacteria with potentially differing protein profiles (Hatzenpichler and Orphan, 2015). The method cannot provide information on the specific polypeptide produced without the use of complementary methods (Hatzenpichler et al., 2016) and it is currently not known how much individual proteins with varying methionine content contribute to the total fluorescence of any given cell (Samo et al., 2014; Hatzenpichler and Orphan, 2015). It is also unclear to what extent protein folding affects the fluorescent signal of recombinant proteins, as the tertiary structure of a protein hypothetically could shield the azide/alkyne moieties from labelling reagents or from laser beams during fluorometric analysis. As the phage-resistant isolate TR5 has a mutation in genes affecting an enzyme involved in the protein folding machinery in the periplasm (**Paper 3**; Hiniker and Bardwell, 2004), it is possible that the protein folding differs from the wildtype, which in turn could affect the fluorescence of the proteins in TR5. In spite of these limitations BONCAT corresponds well with other proteomic approaches, such as ^{3}H-leucine incorporation (Leizeaga et al., 2017), indicating that it at least performs at par with similar methods.

While methionine is the most frequent protein synthetic initiation sequence in *E. coli*, the methionine incorporation frequency in the bacterium is one of the lowest per protein residue (Saier, 2008). Moreover, the incorporation frequency of BONCAT

methionine analogues differ from each other, as AHA has an incorporation frequency significantly lower than HPG (Ječmen et al., 2023). There might also be differences in uptake affinity or rate of NCAA incorporation between microbial species (Samo et al., 2014), as there has been shown to be strain-specific incorporation differences in *E. coli* (Ječmen et al., 2023). While the activation rate of the methionyl-tRNA synthase, which incorporate AHA/HPG into polypeptides, is known in one transformed strain of *E. coli* (Kiick et al., 2002), this rate might differ in other strains and bacterial species. In my test system, it might be argued that the differences in NCAA-affinity and incorporation could be consequences of phage resistance on "protein synthetic activity" in the phage-resistant *E. coli*. Further investigation would nonetheless be needed to decipher whether protein synthetic rate or the affinity/incorporation frequency of AHA is affected in the phage G28-resistant isolates.

The competitive exclusion of NCAA by free methionine in the environment or experimental system, in the intracellular amino acid pool, as well as the *de novo* methionine synthesis in test microorganisms, are concerns affecting the performance of the method (Hatzenpichler and Orphan, 2015; Valentini et al., 2020). When testing out different *E. coli* model systems, I observed the effect of casamino acid supplementation on the BONCAT signal (Figure 10). The method's sensitivity to amino acid composition of the media limits the applicability of culturable bacteria with specific and growth requirements, such as *E. coli* DSM 4230 (Chapter 3). Methionine starvation of cellular systems before BONCAT incubation can improve the BONCAT signal, but the effect of methionine-depletion might also impact the system in an unforeseen manner (Bagert et al., 2014). The balancing of methionine and NCAA concentrations in test media has been suggested to reduce deteriorative effects (30:1 AHA:methionine; Bagert et al., 2014), however, due to the potentially differential methionine/NCAA incorporation rates of different bacterial strains/species this would require careful testing for each test system.

The route of uptake of NCAA by microbial cells has yet to be shown (Hatzenpichler and Orphan, 2015; Hatzenpichler et al., 2020. In my test system, the mucoidy of

ISO24A and TR7 could play a part in preventing the cells from readily taking up AHA from the media, potentially explaining the isolates' lower BONCAT fluorescence. Further, the metabolic fate of the recombinant proteins during the cell cycle is not completely understood, and observations in **Paper 2** suggest that NCAA-containing proteins do not appear to be passed on to next generations; Conversely, in **Paper 3**, the increase in BONCAT fluorescence per cell appears to level off periodically, corresponding approximately to the generation time of *E. coli* DSM 103246. This stagnation could hypothetically be due to the division of NCAA-containing proteins between daughter cells, resulting in a lower fluorescence per cell, indicating that the NCAAs might be passed to next generations after all. Nevertheless, either to avoid loss of active cells due to cellular division or depletion of free NCAA in the media over time, for several-generation incubation times the replenishing of the system with NCAAs is recommended (Hatzenpichler and Orphan, 2015), although the long-term physiological effect of NCAA-containing proteins on microbial cells remains unknown.

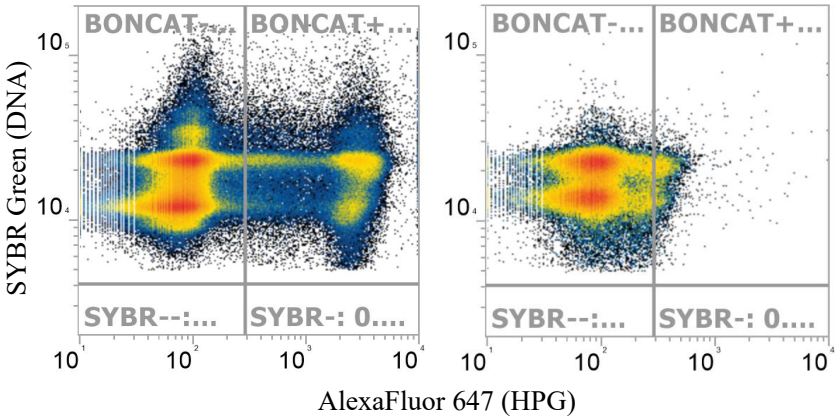

Figure 10. *E. coli* DSM 103246 incubated with 100 µM *L*-homopropargylglycine (HPG) in M9 media (left) and in M9 media supplemented with casamino acids (right). The top-left quadrant gates the HPG-negative events, whereas the top-right quadrant gates HPG-positive events. The HPG-signal was affected by casamino acid supplementation. The bottom quadrants show SYBR Green-negative events but are gated clear of cells for clarity. The logarithmic X-axis ranges from 10^1 – 10^4, and the Y-axis 10^3 – 1.1×10^5 relative fluorescence units, respectively.

The extent to which the method perturbs the test system also needs to be considered. Apart from their impact on bacterial growth (**Paper 2**), both AHA and HPG incubation has been shown to change intracellular amino acid profiles in *E. coli*, specifically increasing the levels of acetylated amino acids (Steward et al., 2020). Induction of stress responses during NCAA incubation have been reported for *E. coli* and *Synechococcus* (Michels et al., 2021; Ječmen et al., 2023). As bacterial stress responses involve expression of various proteins (e.g., vanBogelen et al., 1987; Brissette et al., 1990), the undisturbed protein synthetic activity in any sample might not be accurately reflected in the BONCAT fluorescence. Due to its possible effect on the test system, the method should ideally be tested for toxicity and cellular stress responses in each bacterial species tested, which in practice is difficult to do, especially for unculturable systems. As discussed in **Paper 3**, due to the mutations related to the Rcs system, which is involved stress signaling (Wall et al., 2018), the stress responses in ISO24A and TR7 to AHA incubation could differ from that of wildtype, potentially affecting the BONCAT signal.

Finally, while the components of the click reaction are small and readily penetrate cell walls and membranes (Samo et al., 2014), bias in labelling efficiency between different cell types may exist and permeabilization treatments of samples have been shown to improve the labelling efficiency (Leizeaga et al., 2017). One implication of phage resistance can be increased membrane permeability (Zhong et al., 2020; Kortright et al., 2022), and this could potentially affect the labelling efficiency of phage-resistant *E. coli*. The phage-resistant isolate TR5 shows a mutation in a gene related to O-antigen synthesis (**Paper 3**), which potentially could affect the structural integrity of the LPS and subsequently the permeability of the cell (Zhong et al., 2020). Similarly, TR5 also shows a mutation in a protein folding enzyme responsible for folding of e.g., OmpA (Santos-Martin et al., 2021), the misfolding of which could affect the membranal integrity of the isolate (Wang, 2002; Kortright et al., 2022), although, *dsbA* deletion mutants have not been associated with increased membrane permeability previously (Furniss et al., 2022). Without additional investigation into the membrane permeability of TR5, a potential labelling bias of isolate needs to be considered as a factor when interpreting its BONCAT-signal. Similarly, the mucoidy

or potential capsular polysaccharides in isolates ISO24A and TR7 could affect the labelling efficiency of the cells (**Paper 3**), if the labelling agents do not penetrate through the extracellular matrix as readily as in the wildtype. Given the propensity of phage-resistant bacteria to show different surface modifications (Mangalea and Duerkop, 2020), permeabilization steps should be considered to ensure unbiased labeling efficiency in future cost of resistance studies using BONCAT.

In summary, the BONCAT fluorescence is affected by several factors that might be independent of the protein synthetic activity of the test system (Table 4). While these limitations inhibit quantification of the cost of resistance in my test system, they are not necessarily impossible to overcome through further investigation into the relationship between fluorescence, protein synthesis, and methodological effects of BONCAT in different test systems.

6.2 Future prospects

The three resistant mutants characterized showed several interesting characteristics and trade-offs that would require further investigation to fully explain. In part due to the wealth of knowledge associated with *E. coli*, several possible causes for the trade-offs observed in **Paper 3** were proposed, but not proven. For instance, the effect of the mutation in the O-antigen polymerase gene *wzy* and the disulfide oxidoreductase gene *dsbA* on the O-antigen structure or DsbA substrates in isolate TR5 was not possible to infer from the sequence or experimental data alone. Given that the wildtype *E. coli* is an extended spectrum β-lactamase producing strain (Korf et al., 2020), and disulfide bonds are important for β-lactamase function (Furniss et al., 2022), the antimicrobial susceptibility profile of TR5 would be interesting to investigate. Another potentially important target for future studies would be to identify the receptor molecule(s) of phage G28, which could shed light on the exact resistance mechanism in the resistant isolates.

Table 4. Factors affecting BONCAT-fluorescence in bacteria. Abbreviations: AHA = L-azidohomoalanine; NCAA = non-canonical amino acid analogue

Factor	Effect on fluorescence	Reference
Methionine in the test system	Decreased	Bagert et al. (2014)
Permeabilization	Increased	Leizeaga et al. (2017)
Concentration of AHA	Concentration-dependent	This thesis, Samo et al. (2014)
Reagent quality	Decreased	This thesis
Nutrient rich media (e.g., LB broth)	Decreased	Hatzenpichler and Orphan (2015)
Alkaline (> pH 7) and sulfide (> 1mM) using AHA	Potentially decreased due to reduction of azide group	Hatzenpichler at al. (2014)
Azide/alkyne metabolites in the test system	Hypothetically decreased	Hatzenpichler and Orphan (2015)
Treatment with ribosome-targeting antimicrobials	Fluorescence-reduction to background levels	Reichart et al. (2020)
Incubation time	Variable	**Paper 2**; **Paper 3**; Samo et al. (2014); Leizeaga et al. (2017), Lindivat et al. (2020)

Methodological limitations aside, based on findings in the current work, BONCAT was able to measure a fluorescence difference in phage susceptible and phage-resistant bacteria. An interesting next step in the quest of quantifying the cost of resistance would be to apply the method to mixed communities with direct competition between susceptible and resistant mutants, as this would be one step closer to applying the method to natural systems. Long-term co-culturing of *E. coli* DSM 103246 and phage G28 potentially would allow for the natural emergence of phage-resistant mutants that would be exposed to competition against wildtype bacteria and other emerged phage-resistant mutants. The hypothetical ability of phage G28 to use several receptors could allow for viral host-range mutants to occur. A

continuous flow platform, such as a chemostat, would be ideal for this purpose, allowing for a steady-state environment (Gresham and Hong, 2014), and solving potential problems accumulation of toxic waste products that inherently affect batch cultures (Osborne et al., 2021). I will suggest the use of BONCAT to be applied to quantify the cost of resistance in this co-evolutionary set-up, with the expectation that the method is able distinguish different populations of bacteria based on their cost of resistance (Figure 11). However, a few issues of the BONCAT method need to be settled before such implementation, such as how to incubate a continuous flow co-culture with NCAAs.

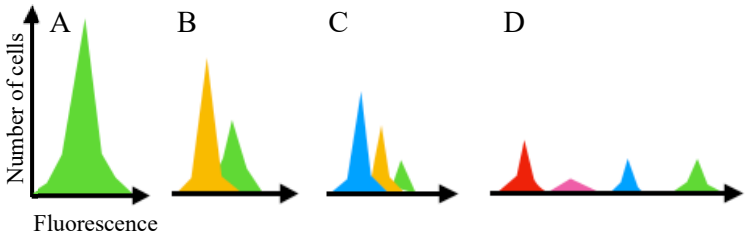

Figure 11. Idealized scenario of bacterium-phage co-evolution visualized by bioorthogonal non-canonical amino acid tagging (BONCAT): (**A**) Wildtype fluorescence (green) peak based on protein synthetic activity before phage addition; (**B**) After phage addition, resistant cells (yellow) appear, but show lower fluorescence than the susceptible wildtype (green); (**C**) as co-evolutionary dynamics commence, the phage has evolved the ability to infect the resistant (yellow) population, and a new resistant phenotype (blue) appears, hypothetically with a lower protein synthetic rate that both the wildtype (green) and the first resistant phenotype (yellow); (**D**) At the end of the experiment, several populations of co-evolved populations might co-exist, separated by their BONCAT-fluorescence.

The successful application of BONCAT to measure cost of resistance would ultimately depend on its ability to visualize separate populations through BONCAT fluorescence (Figure 11). Although not included in **Paper 3**, the time-course incubations involved a batch co-culture of wildtype *E. coli* DSM 103246 and one phage G28-resistant mutant each. However, the BONCAT fluorescence of the wildtype-resistant mutant mix did not show separate populations, perhaps indicating

that BONCAT is unable to distinguish between phage susceptible and phage-resistant bacteria. However, the co-culture was an artificial mix of equal ratio of wildtype and phage-resistant isolate, and it is possible that any competition between the two strains was not detectable during the first few generations of co-culturing (the experiment ran for approximately five generations based on the wildtype's generation time).

Given the differential mutational outcomes of the phage G28-resistant isolates (**Paper 3**), cell sorting, and single-cell sequencing would be an informative addition to any co-evolutionary study of the *E. coli*-phage G28 system. However, as the phages might periodically outnumber the bacterial cells during virus-host dynamics (**Paper 1**; Bohannan and Lenski, 1997; Bohannan and Lenski, 2000b), the relative phage concentration could become a problem for both for BONCAT flow cytometric analysis and cell sorting. This could potentially be solved by adjusting the flow cytometric and cell sorting instruments to only detect bacteria-size cells. If successful, this coevolutionary set-up would allow for phenotype-genotype measurements on a single-cell resolution.

7. Conclusions

Here I present my conclusion with regards to the *main objectives* of this thesis:

1. *Explore the potential of simple life-strategy trade-offs such as cost of resistance that promote coexistence in artificial virus-host communities:* As shown in **Paper 1**, individual-level trade-offs were found to be important to explain coexistence in a simulated bacterium-phage system, the dynamics of which were strengthened using laboratory experiments.

2. *Assess the effect of the BONCAT amino acid analogues on the test system:* The BONCAT method was found to affect bacterial growth, but the effect differed depending on which methionine analogue was used (**Paper 2**). Furthermore, non-growth affecting concentrations of AHA were identified.

3. *Validate the ability of BONCAT to measure changes in growth modes in E. coli:* BONCAT was found to respond to bacterial growth rates at different temperatures and at different growth phases during an exponential growth curve (Chapter 5).

4. *Characterize the link between genotype and phenotype in phage-resistant E. coli through whole-genome sequencing and testing of multiple traits: maximum growth rate, nutrient affinity, yield:* Whole genome sequencing revealed unique mutations in each phage-resistant *E. coli* and trade-offs were found in each isolate. The partial resistant isolate TR7 showed a slight indication of lower fitness impact compared to the fully resistant isolates. However, while suggestions for potential phage resistance mechanisms were made based on the phenotypic tests (**Paper 3**), the exact mechanism(s) for phage G28 resistance and receptor used by the phage requires further investigation.

5. *Evaluate the applicability of BONCAT to quantify the cost of phage resistance:* BONCAT coupled with flow cytometry was able to measure different fluorescence in

the phage-resistant isolates compared to the wildtype *E. coli* (**Paper 3**). This indicates that phage resistance affects protein synthetic activity, and that the cost of resistance can manifest as changes in protein synthetic rate and efficiency. Further assessment of proteomic differences and labelling efficiency is needed for confirmation of the protein synthetic activity of the resistant isolates, though. Furthermore, the lack of competition and environmental context in the test system might make the relevance of the trade-offs hard to interpret. The cost of resistance cannot be definitively quantified using BONCAT at this time but following the line of suggestions to address methodological limitations I give in the current thesis, the method has the potential to do so.

References

Abedon, S.T. (2022) ‘Pleiotropic costs of phage resistance’ In: *Bacteriophages as Drivers of Evolution*, pp. 253 – 262, Springer, Cham, Switzerland

Agard, N.J., Prescher, J.A., and Bertozzi, C.R. (2004) ‘Strain-promoted [2 + 3] azide-alkyne cycloaddition for covalent modification of biomolecules in living systems’ *Journal of American Chemical Society* 126(46), 15046 – 15047

Apostolakos, I., Laconi, A., Mughini-Gras, L., Yapicier, Ö.S. and Piccirillo, A. (2021) ‘Occurrence of colibacillosis in broilers and its relationship with avian pathogenic *Escherichia coli* (APEC) population structure and molecular characteristics’ *Frontiers in Veterinary Sciences* 8, 737720

Arber, W. (1965) ‘Host controlled modification of bacteriophage’ *Annual Reviews in Microbiology* 19, 365 – 368

Arber, W. (1974) ‘DNA modification and restriction’ In: Cohn, W.E. (ed.) *Progress in nucleic acid research and molecular biology*, volume 14, pp. 1 – 36, Academic Press, New York

Attrill, E.L., Claydon, R., Lapinska, U., Recker, M., Meaden, S, Brown, A.T., Westra, E.R., Harding, S.V. and Pagliara, S. (2021) ‘Individual bacteria in structured environments rely on phenotypic resistance to phage’ *PLoS Biology* 19(10), e3001406

Avrani, S. and Lindell, D. (2015) ’Convergent evolution toward an improved growth rate and a reduced resistance range in *Prochlorococcus* strains resistant to phage’ *PNAS* 112(17)), E2191 – E2200

Azam, M., Jan, A.T., Kumar, A., Siddiqui, K., Mondal, A.H., Haq, Q.M.R. (2018) 'Study of pandrug and heavy metal resistance among *E. coli* from anthropogenically influenced Delhi stretch of river Yamuna' *Brazilian Journal of Microbiology* 49(1), 471 – 480

Bargert, J.D., Xie, Y.J., Sweredoski, M.J., Qi, M., Hess, S., Schuman, E.M. and Tirrell, D.A. (2014) 'Quantitative, time-resolved proteomic analysis by combining bioorthogonal noncanonical amino acid tagging and pulsed stable isotope labeling by amino acids in cell culture' *Molecular & Cellular Proteomics* 13, 1352 – 1358

Beatty, K.E., Xie, F., Wang, Q. and Tirrell, D.A. (2005) 'Selective dye-labelling of newly synthesized proteins in bacterial cells' *Journal of the American Chemical Society* 127(41), 14150 – 14151

Beatty, K.E., Fisk, J.D., Smart, B.P., Lu, Y.Y., Szychowski J., Hangauer, M.J., Baskin, J.M., Bertozzi, C.R. and Tirrell, D.A. (2010) 'Live-cell imaging of cellular proteins by a strain-promoted azide-alkyne cycloaddition' *ChemBioChem* 11(15), 2092 – 2095

Benzerara, Y., Gallah, S., Hommerli, B., Genel, N., Decré, D., Rottamn, M. and Arlet, G. (2017) 'Emergence of plasmid-mediated fosfomycin-resistance genes among *Escherichia coli* isolates, France' *Emerging Infectious Diseases* 23(9), 1564 – 1567

Bertani, B. and Ruiz, N. (2018) 'Function and biogenesis of lipopolysaccharides' *EcoSal Plus* 8(1), 10.1128/ecosalplus.ESP-0001-2018.

Bird, S.M., Ford, S., Thompson, C.M.A., Little, R., Hall, J.P.J., Jackson, R.W., Malone, J., Harrison, E. and Brockhurst, M.A. (2023) 'Compensatory mutations reducing the fitness cost of plasmid carriage occur in plant rhizosphere communities' *FEMS Microbiology Ecology* 99(4), fiad027

Björkman, J., Hughes, D. and Andersson, D.I. (1998) 'Virulence of antibiotic-resistant *Salmonella typhimurium*' *PNAS* 95(7), 3949 – 3953

vanBogelen, R.A., Kelley, P.M. and Neidhard, F.C. (1987) ‘Differential induction of heat shock, SOS, and oxidation stress regulons and accumulation of nucleotides in *Escherichia coli*’ *Journal of Bacteriology* 169(1), 26 – 32

Bohannan, B.J.M. and Lenski, R.E. (1997) ’Effect of prey heterogeneity on the response of a model food chain to resource enrichment’ *Ecology* 78(8), 2303 – 2315

Bohannan, B.J.M. and Lenski, R.E. (2000a) ’Linking genetic change to community evolution: insights from studies of bacteria and bacteriophage’ *Ecology Letters* 3(4), 362 – 377

Bohannan, B.J.M. and Lenski, R.E. (2000b) ’The relative importance of competition and predation varies with productivity in a model community’ *The American Naturalist* 156(4), 329 – 340

Bohannan, B.J.M., Kerr, B., Jessup, C.M., Hughes, J.B. and Sandvik, G. (2002) ‘Trade-offs and coexistence in microbial microcosms’ *Antonie van Leeuwenhoek* 81, 107 – 115

Brachet, J., Sapp, J., Thieffry, D. and Burian, R. (1997) ‘Interview of Jean Brachet by Jan Sapp Arco Felice, Italy, December 10, 1980’ *History and Philosophy of the Life Sciences* 19(1), 113 – 140

Braun, V., Killmann, H. and Herrmann, C. (1994) ‘Inactivation of FhuA at the cell surface of *Escherichia coli* K-12 by a phage T5 lipoprotein at the periplasmic face of the outer membrane’ *Journal of Bacteriology* 176(15), 4710 – 4717

Braun-Breton, C. and Hofnung, M. (1981) ‘In vivo and in vitro functional alterations of the bacteriophage Lambda receptor in *lamB* missense mutants of *Escherichia coli* K-12’ *Journal of Bacteriology* 148(3), 845 – 852

Braz, V.S., Melchior, K. and Moreira, C.G. (2020) ‘*Escherichia coli* as a multifaceted pathogenic and versatile bacterium’ *Frontiers in Cellular and Infection Microbiology* 10, 548492

Brehm-Stecher, B.F. and Johnson, E.A. (2004) ‘Single-cell microbiology: tools, technologies, and applications’ *Microbiological and Molecular Biology Reviews* 68(3), 538 – 559

O’Brien, A.D., Newland, J.W., Miller, S.F., Holmes, R.K., Smith, H.W. and Formal, S.B. (1984) ‘Shiga-like toxin-converting phages from *Escherichia coli* strains that cause hemorrhagic colitis or infantile diarrhea’ *Science* 226(4675), 694 – 696

Brissette, J.L., Russel, M., Weiner, L. and Model, P. (1990) ‘Phage shock protein, a stress protein in *Escherichia coli*’ *PNAS* 87(3), 862 – 866

Brockhurst, M.A., Buckling, A and Rainey, P.B. (2005) ‘The effect of a bacteriophage on diversification of the opportunistic bacterial pathogen, *Pseudomonas aeruginosa*’ *Proceedings. Biological Sciences* 272(1570), 1385 – 1391

Brockhurst, M.A., Fenton, A., Roulston, B. and Rainey, P.B (2006) ‘The impact of phages on interspecific competition in experimental populations of bacteria’ *BMC Ecology* 6, 19

Brown, P.L. and Curtiss III, R. (1996) ‘Unique chromosomal regions associated with virulence of an avian pathogenic *Escherichia coli* strain’ *PNAS* 93(20), 11149 – 11154

Browning, D.F., Wells, T.J., França, L.S., Morris, F.C., Sevastsyanovich, Y.R., Bryant, J.A., Johnson, M.D., Lund, P.A., Cunningham, A.F., Hobman, J.L., May, M.A., Webber, M.A. and Henderson, I.R. (2013) ‘Laboratory adapted *Escherichia coli* K-12 becomes a pathogen of *Caenorhabditis elegans* upon restoration of O antigen biosynthesis’ *Molecular Microbiology* 87(5), 939 – 950

Burmeister, A.R., Fortier, A., Roush, C., Lessing, A.J., Bender, R.G., Barahman, R., Grant, R., Chan, B.R. & Turner, P.E. (2020) ‘Pleiotropy complicates a trade-off between phage resistance and antibiotic resistance’ *PNAS* 117(21), 11207 – 11216

Cairns, J., Frickel, J., Jalasvuori, M., Hiltunen, T. and Becks, L. (2017) 'Genomic evolution of bacterial populations under coselection by antibiotics and phage' *Molecular Ecology* 26(7), 1848 – 1859

Campbell, A. (1960) 'Conditions for the existence of bacteriophage' *Evolution* 15(2), 153 – 165

Carlton, E.J., Woster, A.P., DeWitt, P., Goldstein, R.S. and Levy, K. (2016) 'A systematic review and meta-analysis of ambient temperature and diarrhoeal diseases' *International Journal of Epidemiology* 45(1), 117 – 130

Chai, T-J. and Foulds, J. (1977) '*Escherichia coli* K-12 *tolF* mutants: Alterations in protein composition of the outer membrane' *Journal of Bacteriology* 130(2), 781 – 786

Chatterjee, S. and Rothenberg, E. (2012) 'Interaction of bacteriophage λ with its *E. coli* receptor, LamB' *Viruses* 4(11), 3162 – 3178

Chaudhry, W., Lee, E., Worthy, A., Weiss, Z., Grabowicz, M., Vega, N. and Levin, B. (2020) 'Mucoidy, a general mechanism for maintaining lytic phage in populations of bacteria' *FEMS Microbial Ecology* 96(10), fiaa162

Chen, Z., Sun, X., Li, Y., Yan, Y. and Yuan, Q. (2017) 'Metabolic engineering of *Escherichia coli* for microbial synthesis of monolignols' *Metabolic Engineering* 39, 102 – 109

Chen, L., Zhao, B., Li, X., Cheng, Z., Wu, R. and Xia, J. (2021) 'Isolating and characterizing translationally active fraction of anammox microbiota using biorthogonal non-canonical amino acid tagging' *Chemical Engineering Journal* 418, 129411

Cho, S-H., Szewczyk, J., Pesavento, C., Zietek, M., Banzhaf, M., Roszczenko, P., Asmar, A., Laloux, G., Hov, A-K., Leverrier, P., Van der Henst, C., Vertommen, D., Typas, A. and Collet, J-F. (2014) 'Detecting envelope stress by monitoring β-barrel assembly' *Cell* 159(7), 1652 – 1664

Cole, D., Long, S.C. and Sobsey, M.D. (2003) 'Evaluation of F+ RNA and DNA coliphages as source-specific indicators of fecal contamination in surface waters' *Applied and Environmental Microbiology* 69(11), 6507 – 6514

Couradeau, E., Sasse, J., Goudeau, D., Nath, N., Hazen, T.C., Bowen, B.P., Chakraborty, R., Malmstrom, R.R. and Northen, T.R: (2019) 'Probing the active fraction of soil microbiomes using BONCAT-FACS' *Nature Communications* 10, 2770

Cox, R.A. 'Correlation of the rate of protein synthesis and the third power of the RNA:protein ratio in *Escherichia coli* and *Mycobacterium tuberculosis' Microbiology* 149(3), 729 – 737

Cronan, J.E. (2014) '*Escherichia coli* as an experimental organism' In: *Encyclopedia of Life Sciences*, John Wiley & Sons, Ltd, Chichester

Cumby, N., Edwards, A.M., Davidson, A.R. and Maxwell, K.L. (2012) 'The bacteriophage HK97 gp15 moron element encodes a novel superinfection exclusion protein' *Journal of Bacteriology* 194(18), 5012 – 5019

Dailey, F.E. and Berg, H.C. (1993) 'Mutants in disulfide bond formation that disrupt flagellar assembly in *Escherichia coli*' PNAS 90(3), 1043 – 1047

Davey, M.H. and Kell, D.B. (1996) 'Flow cytometric analysis of heterogeneous microbial populations: the importance of single-cell analysis' *Microbiological Reviews* 60(4), 641 – 696

Dekoninck, K., Létoquart, J., Laguri, C., Demange, P., Bevernaegie, R., Simorre, J-P., Dehu, O., Iorga, B.I., Elias, B., Cho, S-H. and Collet, J-F. (2020) 'Defining the function of OmpA in the Rcs stress response' *eLife* 9, e60861

Delbrück, M. (1940) 'The growth of bacteriophage and lysis of the host' *Journal of General Physiology* 23(5), 643 – 660

Delbrück, M. (1945) ‘Interference between bacterial viruses: The mutual exclusion effect and the depressor effect’ *Journal of Bacteriology* 50(2), 151 – 170

Delbrück, M. (1946) ‘Bacterial viruses or bacteriophages’ *Biological Reviews of the Cambridge Philosophical Society* 21, 30 – 40

Demerec, M. and Fano, U. (1945) ‘Bacteriophage-resistant mutants in *Escherichia coli*’ *Genetics* 30(2), 119 – 136

Dietrich, D.C., Link, A.J., Graumann, J., Tirrell, D.A. and Schuman, E.M. (2006) ‘Selective identification of newly synthesized proteins in mammalian cells using bioorthogonal noncanonical amino acid tagging (BONCAT)’ PNAS 103(25), 9482 – 9487

Doron, S., Melamed, S., Ofir, G., Leavitt, A., Lopatins, A., Keren, M., Amitai, G. and Sorek, R. (2018) ‘Systematic discovery of anti-phage defense systems in the microbial pan-genome’ *Science* 359(6379), eaar4120

Doublet, B., Schwars, S., Kehrenberg, C. and Cloeckaert, A. (2005) ‘Florfenicol resistance gene *floR* is part of a novel transposon’ *Antimicrobial Agents and Chemotherapy* 49(5), 2106 – 2108

Du, Z. and Behrens, S.F. (2021) ’Tracking *de novo* protein synthesis in the activated sludge microbiome using BONCAT-FACS’ *Water Research* 205, 117696

EFSA (European Food Safety Authority) and ECDC (European Centre for Disease Prevention and Control, 2023) ‘The European Union summary report on antimicrobial resistance in zoonotic and indicator bacteria from humans, animals and food in 2020/2021’ *EFSA Journal* 21(3), 7867

Elbing, K. and Brent, R. (2019) ‘Recipes and tools for culture of *Escherichia coli*’ *Current Protocols in Molecular Biology* 125(1), e83

Ellis, E.L. and Delbrück, M. (1939) ‘The growth of bacteriophage’ *Journal of General Physiology* 22(3), 365 – 384

van Elsland, D.M., Pujals, S., Bakkum, R., Bos, E., Oikonomeas-Koppasis, N., Berlin, I., Neefjes, J., Meije, A.H., Koster, A.J., Albertzzi, L. and van Kasteren, S.I. (2018) 'Ultrastructural imaging of *Salmonella*–host interactions using super-resolution correlative light-electron microscopy of bioorthogonal pathogens' *ChemBioChem* 19(16), 1766 – 1770

Eppinger, M., Mammel, M.K., Leclerc, J.E., Ravel, J. and Cebula, T.A. (2011) 'Genomic anatomy of *Escherichia coli* O157:H7 outbreaks' *PNAS* 108(50), 20142 – 20147

Erol, I., Özcarik, R. and Gürler, Z. (2015) 'Novel functional methacrylate copolymers with side chain tertiary amine and alkynes and their some properties' *Journal of Polymer Research* 22, 635

Escherich, T. (1886) 'Die Darmbakterien des Säuglings und ihre Beziehungen zur Physiologie der Verdauung' *Verlag von Ferdinand Enke*, Stuttgart, Germany

Farewell, A. and Neidhardt, F.C. (1998) 'Effect of temperature on in vivo protein synthetic capacity in *Escherichia coli*' *Journal of Bacteriology* 180(17), 4707 – 4710

Ferenci, T. (2016) 'Trade-off mechanisms shaping the diversity of bacteria' *Trends in Microbiology* 24(3), 209 – 223

Ferrières, L. and Clarke, D.J. (2003) 'The RcsC sensor kinase is required for normal biofilm formation in *Escherichia coli* K-12 and controls the expression of a regulon in response to growth on a solid surface' *Molecular Microbiology* 50(5), 1665 – 1682

Forterre, P. (2012) 'The virocell concept and environmental microbiology' *The ISME Journal* 7, 233 – 236

Franco, M., D'haeseleer, P.M., Branda, S.S., Liou, M.J., Haider, Y., Segelke, B.W. and El-Etr, S.H. (2018) 'Proteomic profiling of *Burkholderia thailandensis* during host infection using bio-orthogonal noncanonical amino acid tagging' *Frontiers in Cellular and Infection Microbiology* 8, 370

Fuhrman, J.A. (1999) ‘Marine viruses and their biogeochemical and ecological effects’ *Nature* 399, 541 – 548

Furniss, R.C.D., Kaberabkova, N., Barker, D., Bernal, P., Maslova, E., Antwi, A.A.A., McNeil, H.E., Pugh, H.L., Dortet, L., Blair, J.M.A., Larrouy-Maumus, G., McCarthy, R.R., Gonzalez, D. and Mavridou, D.A.I. (2022) ‘Breaking antimicrobial resistance by disrupting extracytoplasmic protein folding’ *eLife* 11, e57974

Gao, D., Huang, X. and Tao, Y. (2016) ‘A critical review of NanoSIMS in analysis of microbial metabolic activities at single-cell level’ *Critical Reviews in Biotechnology* 36(5), 884 – 890

Gauss, P., Park, K., Spencer, T.E. and Hacker, K.J. (1994) ‘DNA helicase requirements for DNA replication during bacteriophage T4 infection’ *Journal of Bacteriology* 176(6), 1667 – 1672

Gentry-Shields, J., Myers, K., Pisanic, N., Heaney, C. and Stewart, J. (2015) ‘Hepatitis E virus and coliphages in waters proximal to swine concentrated animal feeding operations’ *Science of the Total Environment* 505, 487 – 493

Germond, A., Ichimura, T., Horinouchi, T., Fujita, H., Furusawa, C. and Watanabe, T.W. (2018) ‘Raman spectral signature reflects transcriptomic features of antibiotic resistance in *Escherichia coli*’ *Communications Biology* 1, 85

Gregory, A.C., Zayed, A.A., Conceicao-Neto, N., Temperton, B., Bolduc, B., Alberti, A., Ardyna, M., Arkhipova, K., Carmichael, M., Cruaud, C., Dimier, C., Domínguez-Huerta, G., Ferland, J., Kandels, S., Liu, Y., Marec, C., Pesant, S., Picheral, M., Pisarev, S., Poulain, J., Tremblay, J-E., Vik, Dean, Babin, M., Bowler, C., Culleu, A.I., de Vargas, C., Dutilh, B.E., Iudicone, D., Karp-Boss, L., Roux, S., Sunagawa, S., Wincker, P. and Sullivan, M.B. (2019) ‘Marine DNA viral macro- and microdiversity from pole to pole’ *Cell* 177, 1109 – 1123

Gresham, D. and Hong, J. (2014) ‘The functional basis of adaptive evolution in chemostats’ *FEMS Microbiology Reviews* 39(1), 2 – 16

Griffin, R.J. (1994) ‘The medicinal chemistry of the azido group’ In: Ellis, G.P. and Luscombe, D.K. (eds.) *Progress in Medicinal Chemistry*, vol. 31, Elsevier Science B.V.

Grujcic, V., Taylor, G.T. and Foster, R.A. (2022) ‘One cell at a time: Advances in single-cell methods and instrumentation for discovery in aquatic microbiology’ *Frontiers in Microbiology* 13, 881018

Guragain, M., Schmidt, J.W., Dickey, A.M. and Bosilevac, J.M. (2023) ‘Distribution of extremely heat-resistant *Escherichia coli* in the beef production and processing continuum’ *Journal of Food Protection* 86(1), 100031

Habusha, M., Tzipilevich, E. and Ben-Yehuda, S. (2019) ‘A mutant bacteriophage evolved to infect bacteria gained a broader host range’ *Molecular Microbiology* 111(6), 1463 – 1475

Hancock, R.E.W. and Reeves, P. (1975) ‘Bacteriophage resistance in *Escherichia coli* K-12: General pattern of resistance’ *Journal of Bacteriology* 121(3), 983 – 993

Hankin, M.E. (2011) ‘Hankin ME. The bactericidal action of the waters of the Jamuna and Ganges rivers on Cholera microbes. Ann. Inst. Pasteur 10:511–523 (1896)’ *Bacteriophage* 1(3), 117 – 126

Hantke, K. (2020) ‘Compilation of *Escherichia coli* K-12 outer membrane phage receptors – their function and some historical remarks’ *FEMS Microbiology* 367(2), fnee013

Hart, J.F. and Mayda, C. (1998) ‘The industrialization of livestock production in the United States’ *Southwestern Geographer* 38(1), 58 – 78

Hatzenpichler, R., Scheller, S., Tavormina, P.L., Babin, B.M., Tirrell, D.A. and Orphan, V.J. (2014) ‘In situ visualization of newly synthesized proteins in environmental microbes using amino acid tagging and click chemistry’ *Environmental Microbiology* 16(8), 2568 – 2590

Hatzepichler, R. and Orphan, V. (2015) 'Detection of protein-synthesizing microorganisms in the environment via bioorthogonal noncanonical amino acid tagging (BONCAT)' In: McGenity, T.J., et al. (eds.) *Hydrocarbon and Lipid Microbiology Protocols*, Springer Protocol Handbooks, Springer-Verlag, Berlin

Hatzenpichler, R., Connon, S.A., Goudeau, D., Malmstrom, R.R., Woyke, T. and Orphan, V.J. (2016) 'Visualizing in situ translational activity for identifying and sorting slow-growing archaeal-bacterial consortia' *PNAS* 113, E4069 – 78

Hatzenpichler, R., Krukenberg, V., Spietz, R.L. and Jay, Z.J. (2020) 'Next-generation physiology approaches to study microbiome function at single cell level' *Nature Reviews Microbiology* 18, 241 – 256

Hayashi, T., Makino, K., Ohnishi, M., Kurokawa, K., Ishii, K., Yokoyama, K., Han, C-C., Ohtsubo, E., Nakayama, K., Murata, T., Tanaka, M., Tobe, T., Iida, T., Takami, H., Honda, T., Sasakawa, C., Ogasawara, N., Yasunaga, T., Kuhara, S., Shiba, T., Hattori, M. and Shinagawa, H. (2001) 'Complete genome sequence of enterohemorrhagic *Eschelichia coli* O157:H7 and genomic comparison with a laboratory strain K-12' *DNA Research* 8, 11 – 22

Hellberg, R.S. and Chu, E. (2016) 'Effects of climate change on the persistence and dispersal of foodborne bacterial pathogens in the outdoor environment: A review' *Critical Reviews in Microbiology* 42(4), 548 – 572

Henning, U. and Haller, I. (1975) 'Mutants of *Escherichia coli* lacking all 'major' proteins of the outer cell envelope membrane' *FEBS Letters* 55(1), 161 – 164

d'Herelle, F. (1917) 'Sur un microbe invisible antagoniste des bacilles dysentériques' *Comptes Rendus de l'Académie des Sciences* 165, 373 – 375 Translated by Ackermann, H-W. (2011) In: *Bacteriophage* 1(1), 3 – 5

Hernandez, C.A. and Koskella, B. (2019) 'Phage resistance evolution *in vitro* is not reflective of *in vivo* outcome in a plant-bacteria-phage system' *Evolution* 73(12), 2461 – 2475

Herold, S., Kerch, H. and Schmidt, H. (2004) 'Shiga toxin-encoding bacteriophages – genomes in motion' *International Journal of Medical Microbiology* 294(2 – 3), 115 – 121

Herrera, G., Martinez, A., Blanco, M. and O'Connor, J-E. (2002) 'Assessment of *Escherichia coli* B with enhanced permeability to fluorochromes for flow cytometric assays of bacterial cell function' *Cytometry* 49, 62 – 69

Hiniker, A. and Bardwell, J.C.A. (2004) '*In vivo* substrate specificity of periplasmic disulfide oxidoreductases' *Journal of Biological Chemistry* 279(13), 12967 – 12973

Hobman, J.L., Penn, C.W. and Pallen, M.J. (2007) 'Laboratory strains of *Escherichia coli*: model citizens or deceitful delinquents growing old disgracefully?' *Molecular Microbiology* 64(4), 881 – 885

Hong, V., Steinmetz, N.F., Manchester, M. and Finn, M.G. (2010) 'Labeling live cells by copper-catalyzed alkyne-azide click chemistry' *Bioconjugate Chemistry* 21(10), 1912 – 1916

Hossain, M.B., van der Helm, D., Sanduja, R. and Alam, M. (1985) 'Structure of 6-azidotetrazolo[5,l-α]phthalazine, $C_8H_4N_8$, isolated from the toxic dinoflaggelate *Gymnodinium breve*' *Acta Crystallographica Section C* 41, 1199 – 1202

Houghton, E.A. and Nicholas, K.M. (2008) 'In vitro reactive oxygen species production by histatins and copper(I,II)' *JBIC Journal of Biological Organic Chemistry* 14, 243 – 251

Hu, X-P., Dourado, H., Schubert, P. and Lercher, M.J. (2020) 'The protein translation machinery is expressed for maximal efficiency in *Escherichia coli*' *Nature Communications* 11, 5260

Hudzicki, J. (2009) 'Kirby-Bauer disk diffusion susceptibility test protocol' *American Society for Microbiology*, https://asm.org/Protocols/Kirby-Bauer-Disk-Diffusion-Susceptibility-Test-Pro (Accessed 10.10.2023)

Hug, LA., Baker, B.J., Anantharaman, K., Brown, C.T., Probst, A.J., Castelle, C.J., Butterfield, C.N., Hernsdorf, A.W., Amano, Y., Ise, K., Suzuki, Y., Dudek, N., Relman, D.A., Finstad, K.M., Amundson, R., Thomas, B.C. and Banfield, J.F. (2016) 'A new view of the tree of life' *Nature Microbiology* 1, 16048

Ibrahim, M., Raajaraam, L. and Raman, K. (2021) 'Modelling microbial communities: Harnessing consortia for biotechnological applications' *Computational and Structural Biotechnology Journal* 19, 3892 – 3907

Ingraham, J.L., Maaløe, O. and Neidhardt, F.C. (1983a) *Growth of the Bacterial Cell*, Sinauer Associates, Inc., Sunderland, Massachusetts

Ingraham, J.L., Maaløe, O. and Neidhardt, F.C. (1983b) 'Composition, organization, and structure of the bacterial cell' In: *Growth of the Bacterial Cell*, pp. 1 – 46, Sinauer Associates, Inc., Sunderland, Massachusetts

Ingraham, J.L., Maaløe, O. and Neidhardt, F.C. (1983c) 'Growth of cells and cultures' In: *Growth of the Bacterial Cell*, pp. 227 – 264, Sinauer Associates, Inc., Sunderland, Massachusetts

Ishii, A., Ksoll, W.B., Hicks, R.E. and Sadowsky, M.J. (2006) 'Presence and growth of naturalized *Escherichia coli* in temperate soils from Lake Superior watersheds' *Applied and Environmental Microbiology* 72(1), 612 – 621

Ječmen, T., Tuzhilkin, R. and Sulc, M. (2023) 'Photo-methionine, azidohomoalanine and homopropargylglycine are incorporated into newly synthesized proteins at different rates and differentially affect the growth and protein expression levels of auxotrophic and prototrophic *E. coli* in minimal medium' *International Journal of Molecular Sciences* 24(14), 11779

Jonas, O.B., Irwing, A., Berthe, F.C.J., Le Gall, F.G. and Marquez, P.V. (2017) 'Drug-resistant infections: a threat to our economic future (vol. 2): final report' *HNP/Agriculture Global Antimicrobial Resistance Initiative*, Washington, D.C., World Bank Group.

https://documents1.worldbank.org/curated/en/323311493396993758/pdf/final-report.pdf (Accessed 08.10.2023)

Jørgensen, J., Sundell, K., Castillo, D., Dramshøj, L.S., Jørgensen, N.B., Madsen, S.B., Landor, L., Wiklund, T., Donati, V.L., Madsen, L., Dalsgaard, I. and Middelboe, M. (2022) 'Reversible mutations in gliding motility and virulence genes: A flexible and efficient phage defence mechanism in *Flavobacterium psychrophilum*' *Environmental Microbiology* 24(10), 4915 – 4930

Kaper, J.B. (2004) 'Pathogenic *Escherichia coli*' *Nature Reviews Microbiology* 2, 123 – 140

Kiick, K.L., Saxon, E., Tirrell, D.A. and Bertozzi, C.R. (2002) 'Incorporation of azides into recombinant proteins for chemoselective modification by the Staudinger ligation' *PNAS* 99(1), 19 – 24

Kittler, S., Mengden R., Korf, I.H.E., Birebrodt, A., Wittmann, J., Plötz, M., Jung, A., Lehnherr, T., Rohde, C., Lehnherr, H., Klein, G. and Kehrenberg, C. (2020) 'Impact of bacteriophage-supplemented drinking water on the *E. coli* population in the chicken gut' *Pathogens* 9, 293

Knirel, Y.A., Prokhorov, N.S., Shashkov, A.S., Ovchinnikova, O.G., Zdorovenko, E.L., Lie, B., Kostryukova, E.S., Larin, A.K., Golomidova, A.K. and Letarov, A.V. (2015) 'Variations in O-antigen biosynthesis and O-acetylation associated with altered phage sensitivity in *Escherichia coli* 4s' *Journal of Bacteriology* 197(5), 905 – 912

Koh, X.P., Shen, Z., Woo, C.F., Yu, Y., Lun, H.I., Cheung, S.W., Kwan, J.K.C. and Lau, S.C.K. (2022) 'Genetic and ecological diversity of *Escherichia coli* and cryptic *Escherichia* clades in subtropical aquatic environments' *Frontiers in Microbiology* 13, 811755

Kolenda, R., Burdukiewicz, M. and Schierack, P. (2015) 'A systematic review and meta-analysis of the epidemiology of pathogenic *Escherichia coli* of calves and the

role of calves as reservoirs for human pathogenic *E. coli*' *Frontiers in Cellular and Infection Microbiology* 5, 23

Korf, I.H.E., Kittler, S., Bierbrodt, A., Mengden, R, Rohde, C., Rohde, M., Kroj, A., Lehnherr, T., Fruth, A., Flieger, A., Lehnherr, H. and Wittmann, J. (2020) '*In vitro* evaluation of phage cocktail controlling infections with *Escherichia coli*' *Viruses* 12, 1470

Kortright, K.E., Chan, B.K. and Turner, P.E. (2020) 'High-throughput discovery of phage receptors using transposon insertion sequencing of bacteria' *PNAS* 117(31), 18670 – 18679

Kortright, K.E., Done, R.E., Chan, B.E., Souza, V. and Turner, P.E. (2022) 'Selection for phage resistance reduces virulence of *Shigella flexneri*' *Applied and Environmental Microbiology* 88(2), e01514-21

Koudelka, G.B., Arnold, J.W. and Chakraborty, D. (2018) 'Evolution of STEC virulence: Insights from the antipredator activities of Shiga toxin producing *E. coli*' *International Journal of Medical Microbiology* 308(7), 956 – 961

Kurokawa, M. and Ying, B-W. (2017) 'Precise, high-throughput analysis of bacterial growth' *Journal of Visual Experiments* 127, e56197

Lagerstrom, K.M. and Hadly, E.A. (2021) 'The under-investigated wild side of *Escherichia coli*: genetic diversity, pathogenicity and antimicrobial resistance in wild animals' *Proceedings. Biological Sciences* 288(1948), 20210399

Lainhart, W., Stolfa, G. and Koudelka, G.B. (2009) 'Shiga toxin as a bacterial defense against a eukaryotic predator, *Tetrahymena thermophila*' *Journal of Bacteriology* 191(6), 5116 – 5122

Lampson, B.C., Sun, J., Hsu, M-Y., Vallejo-Ramirez, J., Inouye, S. and Inouye, M. (1989) 'Reverse transcriptase in a clinical strain of *Escherichia coli*: production of branched RNA-linked msDNA' *Science* 243(4894), 1033 – 1038

Landsberger, M., Gandon, S., Meaden, S,m Rollie, C., Chevallereau, A., Chabas, H., Buckling, A., Westra, E.R. and van Houte, S. (2018) 'Anti-CRISPR phages cooperate to overcome CRISPR-Cas immunity' *Cell* 174(4), 908 – 916

Leclercq, S.O., Branger, M., Smith, D.G.E. and Germon, P. (2021) 'Lipopolysaccharide core type diversity in the *Escherichia coli* species in association with phylogeny, virulence gene repertoire and distribution of type VI secretion systems' *Microbial Genomics* 7(9), 000652

Lederberg, J. and Tatum, E.L. (1946) 'Gene recombination in *Escherichia coli*' *Nature* 158, 558

Lederberg, J. (1947) 'Gene recombination and linked segregations in *Escherichia coli*' *Genetics* 32, 505 – 525

Lee, K.S., Palatinszky, M., Pereira, F., Nguyen, J., Fernandez, V.I., Mueller, A.J., Menolascina, F., Daims, H., Berry, D., Wagner, M. and Stocker, R. (2019) 'An automated Raman-based platform for the sorting of live cells by functional properties' *Nature Microbiology* 4, 1035 – 1048

Lee, S.H., Kim, I.C., Lee, W.S. and Byun, S.M. (1996) 'RcsC-mediated induction of colanic acid by secretion of streptokinase in *Escherichia coli* K-12' *FEMS Microbiology Letters* 139(2 – 3), 189 – 193

Leizeaga, A., Estrany, M., Forn, I. and Sebastián, M. (2017) 'Using click-chemistry for visualizing *in situ* changes of translational activity in planktonic marine bacteria' *Frontiers in Microbiology* 8, 2360

Lennon, J.T., Khatana, S.A.M., Martson, M.F. and Martiny, J.B.H. (2007) 'Is there a cost of virus resistance in marine cyanobacteria?' *The ISME Journal* 1, 300 – 312

Lenski, R.E. (1984) 'Two-step resistance by *Escherichia coli* B to bacteriophage T2' *Genetics* 107(1), 1 – 7

Lenski, R.E. (1988) ‘Experimental studies of pleiotropy and epistasis in *Escherichia coli*. II. Compensation for maladaptive effects associated with resistance to virus T4’ *Evolution* 42(3), 433 – 440

Lessard, J.C. (2013) ‘Growth media of *E. coli*’ *Methods of Enzymology* 533, 181 – 189

Li, G-W., Burkhardt, D., Gross, C. and Weissman, J.S. (2014) ‘Quantifying absolute protein synthesis rates reveals principles underlying allocation of cellular resources’ *Cell* 157(3), 624 – 635

Li, S.H-J., Li, Z., Park, J.O., King, C.G., Rabinowitz, J.D., Wingreen, N.S. and Gitai, Z. (2018) ‘*Escherichia coli* translation strategies differ across carbon, nitrogen and phosphorus limitation conditions’ *Nature Microbiology* 3, 939 – 947

Lim, D. and Maas, W.R. (1989) ‘Reverse transcriptase-dependent synthesis of a covalently linked, branched DNA-RNA compound in *E. coli* B’ *Cell* 56, 891 – 904

Lindivat, M., Larsen, A., Hess-Erga, O.K., Bratbak, G. and Hoell, I.A. (2020) ‘Bioorthogonal non-canonical amino acid tagging combined with flow cytometry for determination of activity in aquatic microorganisms’ *Frontiers in Microbiology* 11, 1929

Lindivat, M., Bratbak, G., Larsen, A., Hess-Erga, O-K. and Hoell, I.A. (2021) ‘Flow cytometric analysis of bacterial protein synthesis: monitoring vitality after water treatment’ *Frontiers in Microbiology* 12, 772651

Litchman, E., Edwards, K.F. and Klausmeier, C.A. (2015) ‘Microbial resource utilization traits and trade-offs: implications for community structure, functioning, and biogeochemical impacts at present and in the future’ *Frontiers in Microbiology* 6, 254

Liu, B., Furevi, A., Perepelov, A.V. Guo, X., Cao, h., Wang, Q., Reeves, P.R., Knirel, Y.A., Wang, L. and Widmalm, G. (2019) 'Structure and genetics of Escherichia coli O antigens' *FEMS Microbiology Reviews* 44(6), 655 – 683

Liu, C.G., Green, S.I., Min, L., Clark, J.R., Salazar, K.C., Terwilliger, A.L., Kaplan, H.B., Trautner, B.W., Ramig, R.F. and Maresso, A.W. (2020) 'Phage-antibiotic synergy is driven by a unique combination of antibacterial mechanism of action and stoichiometry' *mBio* 11(4)

Liu, D. and Reeves, P.R. (1994) '*Escherichia col*i K12 regains its O antigen' *Microbiology* 140(1), 49 – 57

Loison, L. (2013) 'Monod before Monod: enzymatic adaptation, Lwoff, and the legacy of general biology' *History and Philosophy of the Life Sciences* 35(2), 167 – 192

Lughtenberg, B., and van Alpen, L. (1983) 'Molecular architecture and functioning of the outer membrane of *Escherichia coli* and other gram-negative bacteria' *Biochimica et Biophysica Acta* 737(1), 51 – 115

Lukjancenko, O., Wassenaar, T.M and Ussery, D.W. (2010) 'Comparison of 61 sequenced *Escherichia coli* genomes' *Microbial Ecology* 60(4), 708 – 720

Luppi, A., Gibelli, M., Gin., Vangroenweghe, F., Vandenbroucke, V., Bauerfeind, R., Bonilauri, P., Labarque, G. and Hidalgo, Á. (2016)'Prevalence of virulence factors in enterotoxigenic *Escherichia coli* isolated from pigs with post-weaning diarrhoea in Europe' *Porcine Health Management* 2, 20

Luria, S.E. and Delbrück, M. (1943) 'Mutation of bacteria from virus sensitivity to virus resistance' *Genetics* 28(6), 491 – 511

Mann, N.H. (2005) 'The third age of phage" *PLoS Biology* 3(5), e182

Manning, A.J. and Kuehn, M.J. (2011) 'Contribution of bacterial outer membrane vesicles to innate bacterial defense' *BMC Microbiology* 11, 258

Mangalea, M.R. and Duerkop, B. A. (2020) ‘Fitness trade-offs resulting from bacteriophage resistance potentiate synergistic antibacterial strategies’ *Infection and Immunity* 88(7), e00926-19

Maskos, K., Huber-Wunderlich, M. And Glocksbuber, R. (2003) ’DsbA and DsbC-catalyzed oxidative folding of proteins with complex disulfide bridge patterns *in vitro* and *in vivo*’ *Journal of Molecular Biology* 325(3), 495 – 513

McGee, L.W., Barboush, Y., Shima, R. and Hennessy, M. (2023) ‘Phage-resistant mutations impact bacteria susceptibility to future phage infections and antibiotic response’ *Ecology and Evolution* 13(1), e9712

McIntosh, D., Cunningham, M., Ji, B., Fekete, F.A., Parry, E.M., Clark, S.E., Zalinger, Z.B., Glig, I.C., Danner, G.R., Johnson, K.A., Beattie, M. and Ritchie, R. (2008) ‘Transferable, multiple antibiotic and mercury resistance in Atlantic Canadian isolates of *Aeromonas salmonicida* subsp. *salmonicida* is associated with carriage of an IncA/C plasmid similar to the *Salmonella enterica* plasmid pSN254’ *The Journal of Antimicrobial Chemotherapy* 61(6), 1221 – 1228

Miao, V., Davies, D. and Davies, J. (2012) ‘Path to resistance’ In: Keen, P.L. and Montforts, M.H.M.M (eds.) *Antimicrobial Resistance in the Environment*, pp. 7 – 14, John Wiley & Sons, Incorporated, Hoboken, New Jersey

Michels, D.E., Lomenick, B., Chou, T-F., Sweredoski, M.J. and Pasulka, A. (2021) ‘Amino acid analogue induces stress response in marine *Synechococcus*’ *Applied Environmental Microbiology* 87(15), e0020021

Middelboe, M., Holmfeldt, K., Riemann, L., Nybroe, O. and Haaber, J. (2009) ‘Bacteriophages drive strain diversification in a marine *Flavobacterium*: implications for phage resistance and physiological properties’ *Environmental Microbiology* 11(8), 1971 – 1982

Molineux, I. J. (2001) 'No syringes please, ejection of phage T7 DNA from the virion is enzyme driven' *Molecular Microbiology* 40(1), 1 – 8

Morange, M. (2010) 'The scientific legacy of Jaques Monod' *Research in Microbiology* 161, 77 – 81

Morona, R., Klose, M. and Henning, U. (1984) '*Escherichia coli* K-12 outer membrane protein (OmpA) as a bacteriophage receptor: analysis of mutant genes expressing altered proteins' *Journal of Bacteriology* 159(2), 570 – 578

Morona, R., Krämer, C. and Henning, U. (1985) 'Bacteriophage receptor area of outer membrane protein OmpA of *Escherichia coli* K-12' *Journal of Bacteriology* 164(2), 539 – 543

Murray, C.J.L., Ikuta, K.S., Sharara, F., Swetschinski, L., Aguliar, G.R., Gray, A., Han, C., Bisignano, C., Rao, P., Wool, E., Johnson, S.C., Browne, A.J., Chipeta, M.G., Fell, F., Hackett, S., Haines-Woodhouse, G., Hamadani, B.H.K., Kumaran, E.A.P., McManigal, B., Achalapong, S., Agarwal, R., Akech, S., Albertson, S., Amuasi, J., Andrews, J., Aravkin, A., Ashley, E., Bani, F-X., Bailey, F., Baker, S., Basnyat, B., Bekker, A., Bander, R., Berkley, J.A., Bathou, A., Bielicki, J., Boonkasidecha, S., Bukoisa, J., Carvaheiro, C., Castaneda-Orjuela, C., Chansamouth, V., Chaurasia, S., Chiurchù, S., Crowdhury, F., Donatien, R.C., Cook, A.J., Cooper, B., Cressey, T.R., Criollo-Mora, E., Cunningham, M., Darbie, S., Day, N.P.J., Del Luca, M., Dokova, K., Dramowski, S., Dunachie, S.J., Bich, T.D., Eckmann, T., Eibach, D., Emami, A., Feasey, N., Fisher-Pearson, N., Forrest, K., Garcia, C., Garrett, D., Gastmeier, P., Giref, A.Z., Greer, A.C., Gupta, V., Haller, S., Haselback, A., Hay, S.I., Holm, M., Hopkins, S., Hsia, Y., Iregbu, K.C., Jacobs, J., Jarovsky, D., Javanmardi, F., Jenney, A.W.J., Khorana, M., Khusuwan, S., Kissoon, N., Kobeissi, E., Kostyanev, T., Krapp, F., Krumkamp, R., Kumar, A., Kyu, H.H., Lim, C., Lim, K., Manoharan, A., Marks, F., May, J., Mayxay, M., Mturi, N., Munera-Huertas, T., Musicha, P., Musila, L.A., Mussi-Pihata, M.M., Naidu, P.N., Nakamura, T., Nanavati, R., Nangia, S., Newton, P., Ngoun, C., Novotney, A., Nwakanma, D., Obiero, C.W., Ochoa, T.J., Olivas-Martinez, A., Olliaro, P., Ooko, E., Ortiz-Brizuela,

E., Ounchanum, P., Pak, G.D., Paredes, J.L., Peleg, A.Y., Perrone, C., Phe, T., Phommasone, K., Plakkal, N., Rattanevong, S., Roddell, A., Robets, T., Robotham, J.V., Roca, A., Rosenthal, V.D., Rudd, K.E., Russell, N., Sader, H.S., Saengchan, W., Schnall, J., Scott, J.A.G., Seekaew, S., Sharland, M., Shivamallappa, M., Stewardson, A.J., Stoeva, T., Tasak, N., Thaiprakong, A., Thwaites, G., Tigoi, C., Turner, C., Turner, P., van Doorn, H.R., Velaphi, S., Walson, J.L., Waner, S., Wangrangsimakul, T., Wannapinij, P., Wozniak, T., Lopez, A.D., Stergachis, A., Moore, C., Dolerek, C. and Naghavi, M. (2022) 'Global burden of bacterial antimicrobial resistance in 2019: a systematic analysis' *The Lancet* 399(10325), 629 – 655

Mutalik, V.K., Adler, B.A., Rishi, H.S., Piya, D., Zhong, C., Koskella, B., Kutter, E.M., Calendar, R., Novichkov, P.S., Price, M.N., Deutschbauer, A.M. and Arkin, A.P. (2020) 'High-throughput mapping of the phage resistance landscape in *E.coli' PLoS Biology* 18(10), e3000877

Mwangi, M.M., Wu, S.W., Zhou, Y. and Tomasz, A. (2007) 'Tracking the *in vivo* evolution of multidrug resistance in *Staphylococcus aureus* by whole-genome sequencing' *PNAS* 104(22), 9451 – 9456

Nappier, S.P., Hong, T., Ichida, A., Goldstone, A. and Eftim, S.E. (2019) 'Occurrence of coliphage in raw wastewater and in ambient water: a meta-analysis' *Water Research* 153, 263 – 273

Nair, R.R., Vasse, M., Wiegloss, S., Sun, L., Yu, Y-T.N. and Velicer, G.J. (2019) 'Bacterial predator-prey coevolution accelerates genome evolution and selects on virulence-associated prey defences' *Nature Communications* 10, 4310

Nielsen, J.L., Christensen, D., Kloppenberg, M. and Nielsen, P.H. (2003) 'Quantification of cell-specific substrate uptake by probe-defined bacteria under *in situ* conditions by microautoradiography and fluorescence *in situ* hybridization' *Environmental Microbiology* 5(3), 202 – 211

Nkansa-Gyamfi, N.A., Kazibwe, J., Traore, D.A.K. and Nji, E. (2019) 'Prevalence of multidrug-, extensive drug-, and pandrug-resistant commensal *Escherichia coli*

isolated from healthy humans in community settings in low- and middle-income countries: a systematic review and meta-analysis' *Global Health Action* 12(Suppl), 1815272

Onodera, K. (2009) 'Molecular biology and biotechnology of bacteriophage' In: Endo, I. and Nagamune, T. (eds.) *Nano/Micro Biotechnology. Advances in Biochemical Engineering / Biotechnology*, vol 119, pp. 17 – 43, Springer, Berlin, Heidelberg

Ormsby, M.J., White, H.L., Metcalf, R., Oliver, D.M. and Quilliam, R.S. (2023) 'Clinically important *E. coli* strains can persist, and retain their pathogenicity, on environmental plastic and fabric waste' *Environmental Pollution* 326, 121466

Osborne, M.G., Geiger, C.J., Corzett, C.H., Kram, K.E. and Finkel, S.E. (2021) 'Removal of toxic volatile compounds in batch culture prolongs stationary phase and delays death of *Escherichia coli' Applied and Environmental Microbiology* 87(24), e01860-21

Ott, I., Schmidt, K., Kirscher, B., Schumacher, P., Wiglenda, T. and Gust, R. (2005) 'Antitumor-active cobalt-alkyne complexes derived from acetylsalicylic acid: Studies on the mode of drug action' *Journal of Medicinal Chemistry* 48(2), 622 – 629

Parker, C.T., Kloser, A.W., Schaitman, CA., Stein, M.A., Gottesman, S. and Gibson, B.W. (1992) 'Role of the *rfaG* and *rfaP* genes in determining the lipopolysaccharide core structure and cell surface properties of *Escherichia coli* K-12' *Journal of Bacteriology* 174(8), 2525 – 2538

Parma, D.H., Snyder, M., Sobolevski, S., Nawroz, M., Brody, E. and Gold, L. (1992) 'The Rex system of bacteriophage λ: tolerance and altruistic cell death' *Genes & Development* 6, 497 – 510

Pasulka, A.L., Thamatrakoln, K., Kopf, S.H., Guan, Y., Poulos, B., Moradian, A., Sweredoski, M.J., Hess, S., Sullivan, M.B., Bidle, K.D. and Orphan, V.J. (2018)

‘Interrogating marine virus-host interactions and elemental transfer with BONCAT and nanoSIMS-based methods’ *Environmental Microbiology* 20(2), 671 – 692

Perna, N.T., Plunkett III, G., Burland, V., Mau, B., Glasner, J.D., Rose, D.J., Mayhew, G.F., Hackett, J., Klink, S., Boutin, A., Shao, Y., Miller, L., Grotbeck, E.J., Davis, N.W., Lim, A., Dimalanta, E.T., Potamousis, K.D., Apodaca, J., Anantharaman, T.S., Lin, J., Yen, G., Schwartz, D., Welch, R.A. and Blattner, F.R. (2001) ‘Genome sequence of enterohaemorrhagic *Escherichia coli* O157:H7’ *Nature* 409, 529 – 533

Picken, R.N. and Beacham, I.R. (1977) ‘Bacteriophage-resistant mutants of *Echerichia coli* K12. Location of receptors within the lipopolysaccharide’ *Journal of General Microbiology* 102, 305 – 318

Raymond, B. (2019) ‘Five rules for resistance management in the antibiotic apocalypse, a road map for integrated microbial management’ *Evolutionary Applications* 12(6), 1079 – 1091

Refardt, D., Bergmiller, T. and Kümmerli, R. (2013) ‘Altruism can evolve when relatedness is low: evidence from bacteria committing suicide upon phage infection’ *Proceedings of the Royal Society B* 280, 20123035

Reichart, N.J., Jay, Z.J., Kruckenberg, V., Parker, A.E., Spietz, R.L. and Hatzenpichler, R. (2020) ‘Activity-based cell sorting reveals responses of uncultured archaea and bacteria to substrate enrichment’ *The ISME Journal* 14, 2851 – 2861

Revel, H.R. (1967) ‘Restriction of nonglucosylated T-even bacteriophage: properties of permissive mutants of *Escherichia coli B* and K12’ *Virology* 31, 688 – 701

Riede, I. and Eschbach, M-L. (1986) ‘Evidence that TraT interacts with OmpA of *Escherichia coli*’ *FEBS Letters* 205(2), 241 – 245

Robert, E., Grippa, M., Nikiema, D.E., Kergoat, L., Koudouguo, H., Auda, Y. and Rochelle-Newall, E. (2021) ‘Environmental determinants of *E. coli*, link with the

diarrheal diseases, and indication of vulnerability criteria in tropical West Africa (Kapore, Burkina Faso)' *PLoS Neglected Tropical Diseases* 15(8), e0009634

de Rond, L., Coumans, F.A.W., Welsh, J.A., Nieuwland, R., van Leeuwen, T.G. and van der Pol, E. (2020) 'Quantification of light scattering detection efficiency and background in flow cytometry' *Cytometry Part A* 99(7), 671 – 679

Roossinck, M.J., Martin, D.P. and Roumagnac, P. (2015) 'Plant virus metagenomics: advances in virus discovery' *Phytopathology Review* 105(6), 716 – 727

Rostovtsev, V.V., Green, L.G., Fokin, V.V. and Sharpless, K.B. (2002) 'A stepwise Huisgen cycloaddition process: copper(I)-catalyzed regioselective "ligation" of azides and terminal alkynes' *Angewandte Chemie International Edition* 41(14), 2596 – 2599

Ruiz, N. and Silhavy, T.J. (2022) 'How *Escherichia coli* became the flagship bacterium of molecular biology' *Journal of Bacteriology* 204(9), e00230-22

Russell, J.B. and Cook, G.M. (1995) 'Energetics of bacterial growth: Balance of anabolic and catabolic reactions' *Microbiological Reviews* 59(1), 48 – 62

Russo, T.A. and Johnson, J.R. (2003) 'Medical and economic impact of extraintestinal infections due to *Escherichia coli*: focus on an increasingly important endemic problem' *Microbes and Infection* 5(5), 449 – 456

Samo, T.J., Smirga, S., Malfatti, F., Sherwood, B.P. and Azam, F. (2014) 'Broad distribution and high proportion of protein synthesis active marine bacteria revealed by click chemistry at the single cell level' *Frontiers in Marine Science* 1, 48

Santos-Martin, C., Wang, G., Subedi, P., Hor, L., Totsika, M., Paxman, J.J. and Heras, B. (2021) 'Structural bioinformatic analysis of DsbA proteins and their pathogenicity associated substrates' *Computational and Structural Biotechnology Journal* 19, 4725 – 4737

Scheutz, F. and Strockbine, N.A. (2005) 'Genus I. Escherichia Castellani and Chalmers 1919, 941T^{AL}' In: Brenner et al. (eds.) *Bergey's Manual® of Systematic Bacteriology Volume 2: The Proteobacteria, Part B: The Gammaproteobacteria*, pp. 607 – 623, Springer, New York, NJ

Schmidt, I., Riedel, T., Schober, I., Bunk, B., Spröer, C., Bierbrodt, A., Lehnherr, H. and Wittmann, J. (2017) 'Genome sequence of *Escherichia coli* E28, a multidrug-resistant strain isolated from a chicken carcass, and its spontaneously inducible prophage' *Genome Announcements* 5(22), e00348-17

Scholl, D., Adhya, S. and Merril, C. (2005) '*Escherichia coli* K1's capsule is a barrier to bacteriophage T7' *Applied and Environmental Microbiology* 71(8), 4872 – 4874

Scott, M. and Hwa, T. (2011) 'Bacterial growth laws and their applications' *Current Opinion un Biotechnology* 22(4), 559 – 565

Scott, M., Klumpp, S., Mateescu, E.M. and Hwa, T. (2014) 'Emergence of robust growth laws from optimal regulation of ribosome synthesis' *Molecular Systems Biology* 10, 747

Shaked, H., Samra, Z., Paul, M., Madar-Shapiro, L., Cohen, J., Pitlik, S. and Bishara, J. (2012) 'Unusual "flesh-eating" strains of *Escherichia coli*' *Journal of Clinical Microbiology* 50(12), 4008 – 4011

Sharp, R. (2001) 'Bacteriophages: biology and history' *Journal of Chemical Technology and Biotechnology* 76(7), 667 – 672

Sheng, H., Lim, J.Y., Watkins, M.K., Minnich, S.A. and Hovde, C.J. (2008) 'Characterization of an *Escherichia coli* O157:H7 O-antigen deletion mutant and effect of the deletion on bacterial persistence in the mouse intestine and colonization at the bovine terminal rectal mucosa' *Applied and Environmental Microbiology* 74(16), 5015 – 5022

Shi Shun, A.L.K. and Tykwinski, R.R. (2006) 'Synthesis of naturally occurring polyynes' *Angewandte Chemie International Edition*, 45, 1034 – 1057

Simmons, E.L., Bond, M.C., Koskella, B., Drescher, K., Bucci, V. and Nadell, C.D. (2020) 'Biofilm structure promotes coexistence of phage-resistant and phage-susceptible bacteria' *mSystems* 5(3), e00877-19

Stevenson, G., Neal, B., Liu, D., Hobbs, M., Packer, N.H., Batley, M., Redmond, J.W., Lindquist, L. and Reeves, P. (1994) 'Structure of the O antigen of *Escherichia coli* K-12 and the sequence of its *rfb* gene cluster' *Journal of Bacteriology* 176(13), 4144 – 4156

Steward, K.F., Eilers, B., Tripet, B., Fuchs, A., Dorle, M., Rawle, R., Soriano, B., Balasubramanian, N., Copie, V., Bothner, B and Hatzenpichler, R. (2020) 'Metabolic implications of using bioorthogonal non-canonical amino acid tagging (BONCAT) for tracking protein synthesis' *Frontiers in Microbiology* 11, 197

Stocki, S.L., Babiuk, L.A., Rawlyk, N.A., Potter, A.A. and Allan, B.J. (2002) 'Identification of genomic differences between *Escherichia coli* strains pathogenic for poultry and *E. coli* K-12 MG1655 using suppression subtractive hybridization analysis' *Microbial Pathogenesis* 33, 289 – 298

Storesund, J.E., Erga, S.R., Ray, J.L. and Thingstad, T.F. (2015) 'Top-down and bottom-up control on bacterial diversity in a western Norwegian deep-silled fjord' *FEMS Microbiology Ecology* 91(7), fic076

Stouthamer, A.H. (1975) 'A theoretical study on the amount of ATP required for synthesis of microbial cell material' *Antonie van Leeuwenhoek* 39, 545 – 565

Strotskaya, A., Savitskaya, E., Metlitskaya, A., Morozova, N., Datsenko, K.A., Semenova, E. and Severinov, K. (2017) 'The action of *Escherichia coli* CRISPR–Cas system on lytic bacteriophages with different lifestyles and development strategies' *Nucleic Acid Research* 45(4), 1946 – 1957

Subedi, M., Luitel, H., Debkota, B., Bhattarai, R.K., Phuyal, S., Panthi, P., Shrestha, A. and Chaudhary, D.K. (2018) 'Antibiotic resistance pattern and virulence genes

content in avian pathogenic *Escherichia coli* (APEC) from broiler chickens in Chitwan, Nepal' *BMC Veterinary Research* 14, 113

Subedi, D. and Barr, J.J. (2021) 'Temporal stability and genetic diversity of 48-year-old T-series phages' *mSystems* 6(1), 00990-20

Summers, W.C. (1993) 'How bacteriophage came to be used by the Phage Group' *Journal of the History of Biology* 26(2): 255 – 8267

Suttle, C.A. (2007) 'Marine viruses — major players in the global ecosystem' *Nature Reviews Microbiology* 5, 801 – 812

Sørensen, P.E., Baig, S., Stegger, M., Ingmer, H., Garmyn, A. and Butaye, P. (2021) 'Spontaneous phage resistance in avian pathogenic *Escherichia coli*' *Frontiers in Microbiology* 12, 782757

Tacconelli, E., Carrara, E., Savoldi, A., Harbarth, S., Mendelson, M., Monnet, D.L., Pulcini, C., Kahlmeter, G., Kluytmans, J., Carmeli, Y., Oullette, M., Outterson, K., Patel., J., Cavaleria, M., Cox, E.M., Houghens, C.R., Grayson, M.L., Hansen, P., Singh, N., Theuretxbacher, U., Margini, N. and WHO Pathogens Priority List Working Group (2018) 'Discovery, research, and development of new antibiotics: the WHO priority list of antibiotic-resistant bacteria and tuberculosis' *The Lancet Infectious Diseases* 18(3), P318 – 327

Thieffry, D. (1996) '*Escherichia coli* as a model system with which to study cell differentiation' *History and Philosophy of the Life Sciences* 18(2), 163 – 193

Thingstad, T.F. (2000) 'Elements of a theory for the mechanisms controlling abundance, diversity, and biogeochemical role of lytic bacterial viruses in aquatic systems' *Limnology and Oceanography* 45(6), 1320 – 1328

Thingstad, T.F., Våge, S., Storesund, J.E., Sandaa, R-A. and Giske, J. (2014) 'A theoretical analysis of how strain-specific viruses can control microbial species diversity' *PNAS* 111(21), 7813 – 7818

Thingstad, T.F. (2022) ‘Competition–defense trade-offs in the microbial world’ *PNAS* 119(37), e2213092119

Thompson, L.R., Sander, J.G., McDonald, D., Amir, A., Ladau, J., Locey, K.J., Prill, R.J., Tripathi, A., Gibbons, S.M., Ackermann, G., Navas-Molina, J.A., Janssen, S., Kopylova, E., Vázquez-Baeza, Y., González, A., Morton, J.T., Mirarab, S., Xu, Z.Z., Jiang, L., Haroon, M.F., Kanbar, J., Zhu, Q., Song, S.J., Kosciolek, T., Bokulich, N.A., Lefler, J., Brislawn, C.J., Humphrey, G., Owens, S.M., Hampton-Marcell, J., Berg-Lyons, D., McKenzie, V., Fierer, N., Fuhrman, J.A., Clauset, A., Stevens, R.L., Shade, A., Pollard, K., Goodvin, K.D., Jansson, J.K., Gilbert, J.A., Knight, R. and The Earth Microbiome Project (2017) ‘A communal catalogue reveals Earth’s multiscale microbial diversity’ *Nature* 551, 457 – 463

Tilman, D. (2000) ‘Causes, consequences and ethics of biodiversity’ *Nature* 405, 208 – 211

Twort, F.W. (1915) ‘An investigation on the nature of ultra-microscopic viruses’ *The Lancet* 2, 1241 – 1243

Ullmann, A. (2011) ‘*Escherichia coli* and the emergence of molecular biology’ *EcoSalPlus* 4(2)

Valentini, T.D., Lucas, S.K., Binder, K.A., Cameron, L.C., Motl, J.A., Dunitz, J.M. and Hunter, R.C. (2020) ‘Bioorthogonal non-canonical amino acid tagging reveals translationally active subpopulations of the cystic fibrosis lung microbiota’ *Nature Communications* 11, 2287

Vassallo, C.N., Doering, C.R., Littlehale, M.L., Teodoro, G.I.C. and Laub, M. (2022) ‘A functional selection reveals previously undetected anti-phage defence systems in the *E. coli* pangenome’ *Nature Microbiology* 7, 1568 – 1579

Vigil, K.J., Johnson, J.R., Johnston, B.D., Kontoyiannis, D.P., Mulanovich, V.E., Raad, I.I., DuPont, H.L. and Adachi, J.A. (2010) '*Escherichia coli* pyomyositis: An emerging infectious disease among patients with hematologic malignancies' *Clinical Infectious Diseases* 50(3), 374 – 380

Våge, S., Storesund, J. and Thingstad, F. (2012) 'Adding a cost of resistance description extends the ability of virus–host model to explain observed patterns in structure and function of pelagic microbial communities' *Environmental Microbiology* 15(6), 1842 – 1852

Våge, s., Storesund, J.E. and Thingstad, T.F. (2013) 'Adding a cost of resistance description extends the ability of virus-host model to explain observed patterns in structure and function of pelagic microbial communities' *Environmental Microbiology* 15(6), 1842 – 1852

Våge, S., Pree, B and Thingstad, T.F. (2016) 'Linking internal and external bacterial community control gives mechanistic framework for pelagic virus-to-bacteria ratios' *Environmental Microbiology* 18(11), 3932 – 3948

Våge, S., Bratbak, G., Egge, J., Heldal, M., Larsen, A., Norland, S., Lund, Paulsen, M., Pree, B., Sandaa, R-A., Foss Skjoldal, E., Tsagaraki, T., Øverås, L. and Thingstad, F. (2018) 'Simple models combining competition, defence and resource availability have broad implications in pelagic microbial food webs' *Ecology Letters* 21(9), 1440 – 1452

Wall, E., Majdalani, N. and Gottesman, S. (2018) 'The complex Rcs regulatory cascade' *Annual Reviews in Microbiology* 72, 111 – 139

Wall, E.A., Majdalani, N. and Gottesman, S. (2020) 'IgaA negatively regulates the Rcs phosphorelay via contact with the RcsD phosphotransfer protein' *PLoS Genetics* 16(7), e1008610

Wandersman, C. and Schwartz, M. (1982) 'Mutations that alter the transport function of the LamB protein in *Escherichia coli*" *Journal of Bacteriology* 151(1), 15 – 21

Wang, Y. (2002) ‘The function of OmpA in Escherichia coli’ *Biochemical and Biophysical Research Communications* 292(2), 396 – 401

Wang, X. and Quinn, P.J. (2010) ‘Lipopolysaccharide: Biosynthetic pathway and structure modification’ *Progress in Lipid Research* 49(2), 97 – 107

Wang, G., Zhang, H., Wang, J., Chen, S., Wang, Z., Zhao, L. and Wang, X. (2020a) ‘Colanic acid biosynthesis in *Escherichia coli* is dependent on lipopolysaccharide structure and glucose availability’ *Microbiological Research* 239, 126527

Wang, Y., Xu, C., Zhang, R., Chen, Y., Shen, Y., Hu, F., Liu, D., Lu., J., Guo, Y., Xia. X., Jiang, J., Wang, X., Fu, Y., Yang, L., Wang, J., Li, J., Cai, C., Yin, D., Che, J., Fan, R., Wang, Y., Qing, Y., Li, Y., Liao, K., Chen, H., Zou, M., Liange, L., Tang, J., Shen, Z., Walsh, T.R. and Shen, J. (2020b) ‘Changes in colistin resistance and *mcr-1* abundance in *Escherichia coli* of animal and human origins following the ban of colistin-positive additives in China: an epidemiological comparative study’ *The Lancet Infectious Diseases* 20(10), 1161 – 1171

Wannasrichan, W., Htoo, H.H., Suwansaeng, R., Pogliano, J., Nonejuie, P. and Chaikeeratisak, V. (2022) ‘Phage-resistant *Pseudomonas aeruginosa* against a novel lytic phage JJ01 exhibits hypersensitivity to colistin and reduces biofilm production’ *Frontiers in Microbiology* 13, 1004733

Washizaki, A., Yonesaki, T. and Otsuka, Y. (2016) ‘Characterization of the interactions between *Escherichia coli* receptors, LPS and OmpC, and bacteriophage T4 long tail fibers’ *MicrobiologyOpen* 5(6), 1003 – 1015

Weinbauer, M.G. and Rassoulzadegan, F. (2003) ‘Are viruses driving microbial diversification and diversity?’ *Environmental Microbiology* 6(1), 1 – 11

Westerhoff, H.V., Winder, C., Messiha, H., Simeonidis, E., Adamczyk, M., Verma, M., Bruggerman, F.J. and Dunn, W. (2009) ‘Systems biology: the elements and principles of life’ *FEBS Letters* 583, 3882 – 3890

Westra, E.R., van Houte, S., Oyesiku-Blakemore, S., Makin, B., Broniewski, J.M., Best, A., Bondy-Denomy, J., Davidson, A., Boots, M. and Buckling, A. (2015) 'Parasite exposure drives selective evolution of constitutive versus inducible defense' *Current Biology* 25, 1043 – 1049

Wielgoss, S., Bergmiller, T., Bischofberger, A.M. and Hall, A.R. (2016) 'Adaptation to parasites and cost of parasite resistance in mutator and nonmutator bacteria' *Molecular Biology and Evolution* 33(3), 770 – 782

Wilkowska, K., Mruk, I., Furmanek-Blaszk, B. and Sektas, M. (2020) 'Low-level expression of the Type II restriction–modification system confers potent bacteriophage resistance in *Escherichia coli*' *DNA Research* 27(1), dsaa003

Woodward, R., Yi, W., Li, L., Zhao, G., Eguchi, H., Perali, R.S., Guo, H., Song, J.K., Motari, E., Kelleher, P., Liu, X., Han, W., Zhang, E., Ding, Y., Li, M. and Wang, P.G. (2010) '*In vitro* bacterial polysaccharide biosynthesis: defining the functions of Wzy and Wzz' *Nature Chemical Biology* 6, 418 – 423

Yang, C-Y., Erickstad, M., Tadrist, L., Ronan, E., Gutierrez, E., Wong-Ng, J. And Groisman, A. (2020) 'Aggregation temperature of *Escherichia coli* depends on steepness of the thermal gradient' *Biophysical Journal* 118(11), 2816 – 2828

Yoon, S.H., Han, M-J., Jeong, H., Lee, C.H., Xia, X-X., Lee, D-H., Shim, J.H., Lee, S.Y., Oh, T.K. and Kim, J.F. (2012) 'Comparative multi-omics systems analysis of *Escherichia coli* strains B and K-12' *Genome Biology* 13, R37

Yu, F. and Mizushima, S. (1982) 'Roles of lipopolysaccharide and outer membrane protein OmpC of *Escherichia coli* K-12 in the receptor function for bacteriophage T4' *Journal of Bacteriology* 151(2), 718 – 722

Yu, D., Ryu, K., Zhi, S., Otto, S.J. and Neumann, N.F. (2022) 'Naturalized *Escherichia coli* in wastewater and the co-evolution of bacterial resistance to water treatment and antibiotics' *Frontiers of Microbiology* 13, 810312

Zhong, Z., Emond-Rheault, J-G., Bhandare, S., Lévesque, R. and Goodridge, L. (2020) 'Bacteriophage-induced lipopolysaccharide mutations in *Escherichia coli* lead to hypersensitivity to food grade surfactant sodium dodecyl sulfate' *Antibiotics* 9(9), 552

Zulk J.J., Clark, J.R., Ottinger, S., Ballard, M.B., Meija, M.E., Mercado-Evans, V., Heckmann, E.R., Sanchez, B.C., Trautner, B.W., Maresso, A.W. and Patras, K.A. (2022) 'Phage resistance accompanies reduced fitness of uropathogenic *Escherichia coli* in the urinary environment' *mSphere* 7(4), e00345-22

Zuo, J., Tu, C., Wang, Y., Qi, K., Hu, J., Wang, Z., Mi, R., Huang, Y., Chane, Z. and Han, X. (2019) 'The role of the *wzy* gene in lipopolysaccharide biosynthesis and pathogenesis of avian pathogenic *Escherichia coli*' *Microbial Pathogenesis* 127, 296 – 303

Zurfluh, K., Treier, A., Schmitt, K. and Stephan, R. (2020) 'Mobile fosfomycin resistance genes in Enterobacteriaceae—An increasing threat' *MicrobiologyOpen* 9(12), e1135

Paper 1

PLOS COMPUTATIONAL BIOLOGY

RESEARCH ARTICLE

Individual-based model highlights the importance of trade-offs for virus-host population dynamics and long-term co-existence

Fateme Pourhasanzade[1], Swami Iyer[2], Jesslyn Tjendra[1], Lotta Landor[1], Selina Våge[1]*

1 Department of Biological Sciences, University of Bergen, Bergen, Norway, **2** Computer Science Department, University of Massachusetts, Boston, Massachusetts, United States of America

* selina.vage@uib.no

OPEN ACCESS

Citation: Pourhasanzade F, Iyer S, Tjendra J, Landor L, Våge S (2022) Individual-based model highlights the importance of trade-offs for virus-host population dynamics and long-term co-existence. PLoS Comput Biol 18(6): e1010228. https://doi.org/10.1371/journal.pcbi.1010228

Editor: Amber M Smith, University of Tennessee Health Science Center College of Medicine Memphis, UNITED STATES

Received: November 30, 2021

Accepted: May 17, 2022

Published: June 8, 2022

Peer Review History: PLOS recognizes the benefits of transparency in the peer review process; therefore, we enable the publication of all of the content of peer review and author responses alongside final, published articles. The editorial history of this article is available here: https://doi.org/10.1371/journal.pcbi.1010228

Data Availability Statement: All relevant data are within the manuscript and its Supporting information files. An implementation of the IBM in

Abstract

Viruses play diverse and important roles in ecosystems. In recent years, trade-offs between host and virus traits have gained increasing attention in viral ecology and evolution. However, microbial organism traits, and viral population parameters in particular, are challenging to monitor. Mathematical and individual-based models are useful tools for predicting virus-host dynamics. We have developed an individual-based evolutionary model to study ecological interactions and evolution between bacteria and viruses, with emphasis on the impacts of trade-offs between competitive and defensive host traits on bacteria-phage population dynamics and trait diversification. Host dynamics are validated with lab results for different initial virus to host ratios (VHR). We show that trade-off based, as opposed to random bacteria-virus interactions, result in biologically plausible evolutionary outcomes, thus highlighting the importance of trade-offs in shaping biodiversity. The effects of nutrient concentration and other environmental and organismal parameters on the virus-host dynamics are also investigated. Despite its simplicity, our model serves as a powerful tool to study bacteria-phage interactions and mechanisms for evolutionary diversification under various environmental conditions.

Author summary

Genetic diversification in microbial communities is an important process with far-reaching consequences both for ecosystem functioning and public health. Yet, the mechanisms governing the selection of new microbial strains in ecosystems as well as developing infectious diseases are still relatively poorly understood. The sheer diversity in both bacterial and viral communities begs for a conceptual understanding of these regulatory mechanisms. Here we study one such presumably important mechanism, namely the trade-off between the host's growth and thus competitive abilities and its abilities to defend against the virus. To that end, we introduce an idealized individual-based model of bacterial and

the Python programming language is available at a public Github repository [24].

Funding: The work was funded by Trond Mohn Research Foundation (https://mohnfoundation.no/?lang=en) stipend TMS2018REK02 awared to SV. The funders had no role in study design, data collection and analysis, decision to publish, or preparation of the manuscript.

Competing interests: The authors have declared that no competing interests exist.

viral community to study the effects of trade-off based versus random interactions on short- and long-term population dynamics. Short-term infection dynamics emerging from our model are validated with experimental data. Our simulations show that long-term co-existence of the virus and host critically depends on the nature of trade-off regulating the virus-host interactions. Specifically, highest diversity in both host and viral communities and co-existence over long time scales are favored in regimes of trade-off based compatibility between viruses and their hosts.

Introduction

Viruses execute a wide range of functions in the biosphere, influencing biogeochemical cycles, affecting efficiencies of transport of energy and matter through food-webs and driving processes of evolutionary diversification [1–4]. These ecosystem-related functions may seem disentangled from the effects that pathogenic viruses can have on human health and society as demonstrated by the ongoing COVID-19 pandemic [5]. Yet, the underlying mechanisms driving the dynamics between viruses and their hosts are in principle the same.

Viral ecology has been growing as a field of research in the last decades, with sequencing techniques revealing enormous biodiversity in viral genomes [6]. The field, however, remains challenging, since advanced and at times intricate laboratory experiments are required to characterize viral traits as well as interactions with their hosts. Besides, much of the environmental viral metagenome remains unmapped or still undiscovered [7]. We conjecture that virology will grow as a field if we manage to focus on principles that unify different disciplines, from viral ecology to infectious disease research. To better understand the fundamental mechanisms that drive viral dynamics, conceptual models should be used as tools to identify principles that explain biodiversity and functioning in viral systems, be they ecological feedback mechanisms or emerging evolutionary dynamics.

Trait-based approaches have proved useful in identifying unifying and universally applicable mechanisms in ecology and were first established in terrestrial ecology [8, 9]. They have also been successfully applied to marine ecology [10], and in particular to microbial ecology [11–13]. A strength of trait-based approaches is that processes and interactions between organisms and their environment are described on a functional level, independent of particular taxa at hand. Besides, it brings trade-offs between organismal traits to the center of attention, which arise from chemical and physical constraints that are universal (ie, system-independent). Such trade-offs are crucial to understanding life [14–18]. In the marine microbial ecosystem, various processes and structures have been linked through fundamental trade-offs [19]. Trait- and trade-off based perspectives thus also promise to unify viral ecology [20].

In the present context, we use a simple evolutionary individual-based model to test the hypotheses that trade-offs between competitive and defensive traits are key to understanding virus-host population dynamics and evolutionary change. We define competitive traits as organism-specific traits to acquire limiting resources (in our case, nutrient affinities of hosts) and defensive traits as traits modifying the efficiency of a viral infection (here, the viral adsorption coefficient and the inverse of the host range of viruses). Following [21], we model each of these traits as genes being embedded in a phenotypic trait function, and we incorporate trade-offs between them by means of interaction functions that determine the likelihood of infection based on gene similarity of the host and virus ("compatibility function") and virus-intrinsic infection efficiency ("virulence function"). The model is highly idealized, with emphasis on

infection mechanisms that are important and applicable to both environmental as well as pandemic settings.

In the next section, we describe our individual-based model along with experimental methods used to characterize virus-host infection dynamics. This is followed by findings from our model, including a validation of the model dynamics with experimental results. We conclude the article by discussing the relevance and generality of our results for increased insights into virus-host interactions and evolutionary dynamics.

Materials and methods

Individual-based model

Individual-based models (IBMs) are in-silico models that describe the behavior of autonomous individuals (organisms). These models are widely used, not only in ecology [22] but also in other disciplines dealing with complex systems made up of autonomous entities [23]. In this section, we give an informal description of an evolutionary IBM to study the interaction patterns between bacteria and virus. For a formal description of the algorithm used in the IBM, we refer the reader to the pseudocode for the IBM in the Supporting Information section. An implementation of the IBM in the Python programming language is available at a public Github repository [24].

The state variables and parameters (environmental and organismal) of the IBM are listed in Table 1, each with a symbol, description, typical value [21], and units.

For simplicity, a single elemental resource is used in the model budget. Specifically, phosphorous is used as the model currency [25]. For ease of interpretation of the results, the total phosphorus concentration P is expressed in terms of the number of host individuals in the simulated volume, ie, $P \sim P/(P_h \cdot V)$. Similarly, the nutrient affinity α of a host and the adsorption coefficient β of a virus are normalized in terms of the simulated volume, ie, $\alpha \sim \alpha/V$ and $\beta \sim \beta/V$.

At the start of the simulation, we consider a nutrient medium of volume V. The medium is inoculated with a host population $\mathbf{H} = \{h_1, h_2, \ldots, h_{N_h^0}\}$, in which each host h_i has genotype $\{g_\alpha^0\}$ and mass m_i picked uniformly at random from the interval $\left[\frac{1}{2}, 1\right]$. The medium is also inoculated with a virus population $\mathbf{V} = \{v_1, v_2, \ldots, v_{N_v^0}\}$, in which each virus v_i has genotype $\{g_v^0, g_\beta^0\}$. Note that $\mathbf{H}$ and $\mathbf{V}$ are sets of individuals, which grow (or shrink) as dynamics unfold. The initial amount of dissolved phosphorus P_d^0 is calculated in units of host individuals as $P_d^0 = P - \Sigma_{i=1}^{N_h^0} m_i$.

At each time step $t \in [1, T]$ of the simulation, we update the current concentration P_d of dissolved phosphorus as $P_d = P_d + \omega(P_d^0 - P_d)$, which takes into account the inflow and outflow of phosphorus due to washout. We then carry out a round of host dynamics followed by a round of virus-host interaction dynamics as described below. Each time step t is fixed to 1 hour. With time-steps lasting 1 hour, rates in units h^{-1} can be translated into probabilties per time step.

During the host dynamics round, we consider each host $h_i \in \mathbf{H}$ in sequence. The host can be washed out of the medium with probability ω. If it remains in the medium, it can die with probability δ_h, in which case its biomass m_i is returned to the medium, ie, P_d is incremented to $P_d + m_i$. If the host does not die, it experiences a mass loss due to metabolism given by $\epsilon_h m_i$, which is subtracted from m_i and added to P_d. The host h_i grows during the time step t, and the resulting gain in mass is calculated as $\frac{\gamma g_\alpha P_d}{1+\frac{g_\alpha P_d}{\mu_h}}$ [26], which is subtracted from P_d and added to m_i. If m_i exceeds unity, then the host divides into two daughter cells, each with half the mass (ie,

Table 1. State variables and parameters of the IBM.

Symbol	Description	Value	Units
	State variables		
N_h	host abundance	variable	individuals
N_v	virus abundance	variable	individuals
	Environmental parameters		
T	simulation duration	3.6×10^1	h
t	time step duration	1	h
V	chemostat volume	10^{-6}	L
P	total phosphorus concentration	7.1×10^1	μmol-P L^{-1}
P_d	dissolved phosphorus concentration	variable	μmol-P L^{-1}
ω	chemostat dilution rate	2×10^{-1}	h^{-1}
N_h^0	initial value for N_h	4.6×10^1	individuals
N_v^0	initial value for N_v	8.1×10^2	individuals
VHR	virus to host ratio (the ratio N_v^0/N_h^0)	1.76×10^1	-
	Organismal parameters		
P_h	maximum phosphorus concentration in a host	8.3×10^{-8}	μmol-P
α	nutrient affinity of a host	1.6×10^{-7}	L h^{-1}
μ_h	maximum growth rate of a host	7.38×10^{-1}	h^{-1}
g_α	nutrient affinity gene of a host	variable $\in [0, 1]$	-
g_α^0	initial value for g_α	10^{-1}	-
m	mass of a host	variable $\in \left[\frac{1}{2}, 1\right]$	-
π_h	probability of mutation of host genotype	6×10^{-2}	-
σ_h	standard deviation of host genotype mutations	5×10^{-2}	-
δ_h	mortality rate of a host	1.4×10^{-2}	h^{-1}
ϵ_h	metabolic loss rate of a host	1.4×10^{-2}	h^{-1}
β	adsorption coefficient of a virus	6.2×10^{-11}	L h^{-1}
g_v	memory gene of a virus	variable $\in [0, 1]$	-
g_v^0	initial value of g_v	10^{-1}	-
g_β	adsorption coefficient gene of a virus	variable $\in [0, 1]$	-
g_β^0	initial value of g_β	10^{-1}	-
π_v	probability of mutation of virus genotype	6×10^{-3}	-
σ_v	standard deviation of virus genotype mutations	5×10^{-3}	-
κ	number of viruses produced per infection of a host	10^1	-
δ_v	decay rate of a virus	1.4×10^{-2}	h^{-1}

Symbol, description, typical value [21], and units.

https://doi.org/10.1371/journal.pcbi.1010228.t001

$m_i/2$) and the same genotype (ie, $\{g_\alpha\}$) as the host. With probability π_h, the genotype of the daughter cells mutates to $\{g'_\alpha\}$, where g'_α is sampled from a Gaussian distribution with mean g_α and standard deviation σ_h; and with probability $1 - \pi_h$, the genotype of the daughter cells remains the same as that of the parent cell. The daughter cells are added to the host population **H** and the parent cell is removed from it.

During the virus-host interaction round, we consider each virus-host pair (v_i, h_j), where $v_i \in \mathbf{V}$ and $h_j \in \mathbf{H}$. The virus v_i can be washed out of the medium with probability ω. If it remains in the medium, it can decay with probability δ_v. If the virus does not decay, then whether or not it infects the host h_j depends on its compatibility with the host and its virulence. The former is given by the compatibility function $\mathcal{C}$ and the latter by the virulence function $\mathcal{V}$. The

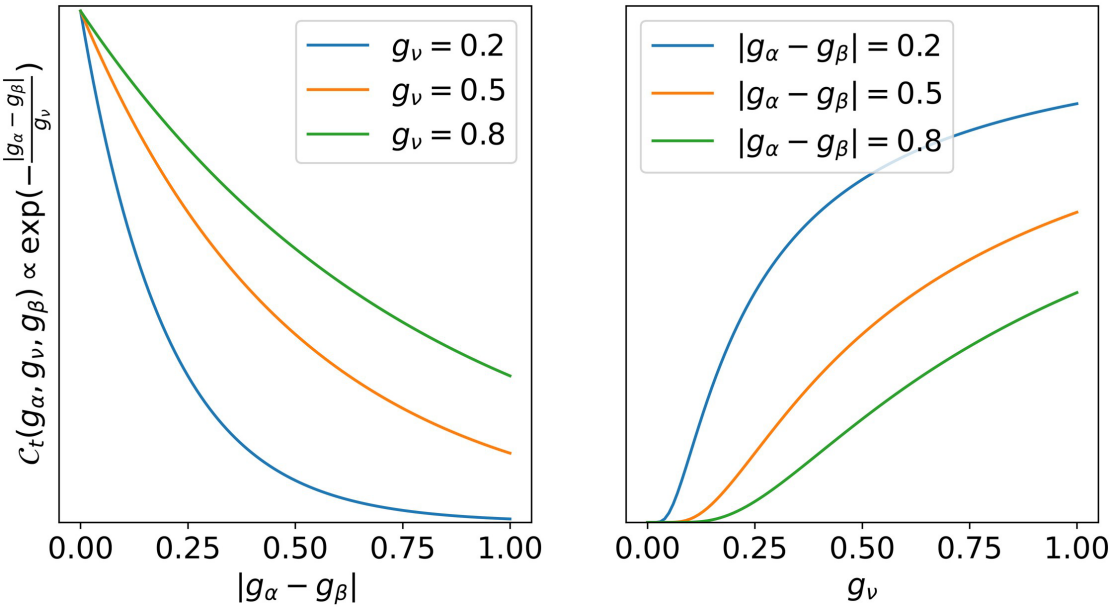

Fig 1. Trade-off based compatibility function $\mathcal{C}_t$. The left panel shows how $\mathcal{C}_t$ varies with $|g_\alpha - g_\beta|$ for fixed values of g_ν; $\mathcal{C}_t$ is high when g_α and g_β have similar values and low otherwise. The right panel shows how $\mathcal{C}_t$ varies with g_ν for fixed values of $|g_\alpha - g_\beta|$; $\mathcal{C}_t$ is high for high values of g_ν and low otherwise.

https://doi.org/10.1371/journal.pcbi.1010228.g001

values of both functions (also called interaction functions) are from the unit interval [0, 1], and are interpreted as probabilities. To test the effects of trade-off based vs random compatibility between hosts and viruses, we consider two compatibility functions: trade-off based compatibility $\mathcal{C}_t(g_\alpha, g_\nu, g_\beta) = \exp\left(-\frac{|g_\alpha - g_\beta|}{g_\nu}\right)$ and random compatibility $\mathcal{C}_r$, which samples a number uniformly at random from the unit interval. The function $\mathcal{C}_t$ (Fig 1) captures the trade-off between the host's nutrient affinity and the virus' adsorption coefficient, such that the compatibility is highest when the corresponding gene values g_α and g_β are similar. The virus-host compatibility is also enhanced when the virus' host range (expressed by its memory gene g_ν) is high.

We also consider two virulence functions: trade-off based virulence $\mathcal{V}_t(g_\nu, g_\beta) = \frac{\beta g_\beta}{g_\nu}$ and random virulence $\mathcal{V}_r$, which samples a number uniformly at random from the unit interval. The function $\mathcal{V}_t$ (Fig 2) captures the trade-off between the virus' adsorption coefficient g_β and its host range g_ν, whereby virulence of the infection is high for viruses with high adsorption (ie, high g_β) and narrow host range (ie, small g_ν). The virus v_i is compatible with host h_j with probability $\mathcal{C}$. If they are compatible, the virus can infect the host with probability $\mathcal{V}$. All viruses are assumed to by lytic, meaning that hosts die upon infection. If the host is infected, then it is removed from the host population **H**, its biomass is immediately recirculated into the dissolved nutrient pool P_d, and the virus produces κ copies of itself, each of which has the same genotype (ie, $\{g_\nu, g_\beta\}$) as the parent. With probability π_ν, the genotype of the copies mutates to $\{g'_\nu, g'_\beta\}$, where g'_ν and g'_β are sampled from a Gaussian distribution with mean g_ν and g_β respectively and standard deviation σ_ν; and with probability $1 - \pi_\nu$, the genotype of the copies

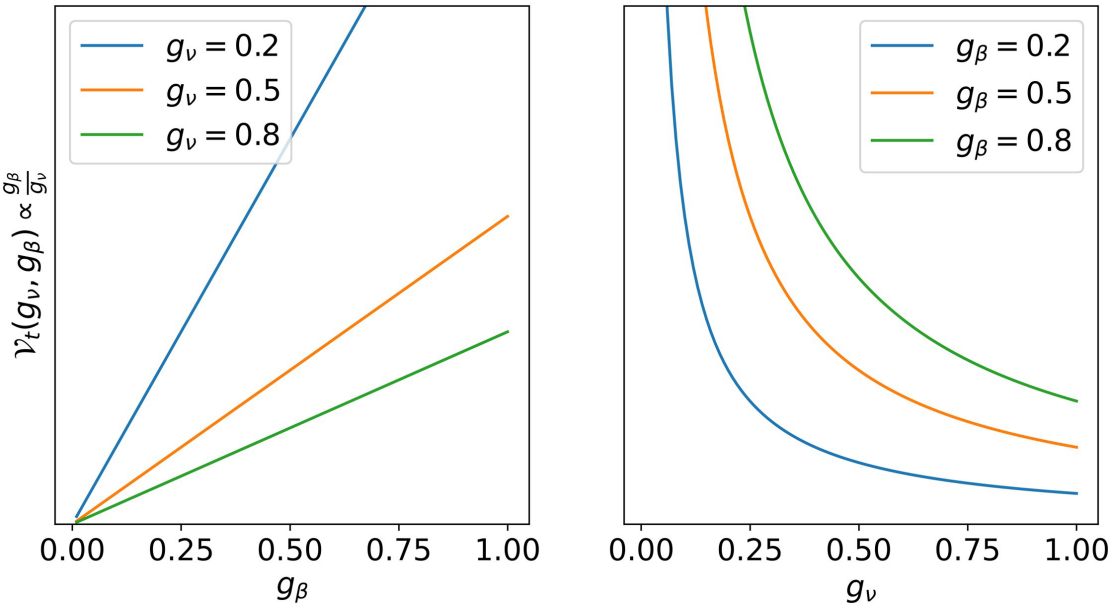

Fig 2. Trade-off based virulence function $\mathcal{V}_t$. The left panel shows how $\mathcal{V}_t$ varies with g_β for fixed values of g_ν; $\mathcal{V}_t$ is high for high values of g_β and low otherwise. The right panel shows how $\mathcal{V}_t$ varies with g_ν for fixed values of g_β; $\mathcal{V}_t$ is high for low values of g_ν and low otherwise.

https://doi.org/10.1371/journal.pcbi.1010228.g002

remains the same as that of the parent. The virus v_i cannot infect any more hosts. It is removed from the virus population **V** and the copies of the virus are added to the population.

The behavior of the model is investigated for different parameter values and interaction functions. Sensitivity analyses for virus to host ratios (VHR), limiting resource concentration, and dilution rates are carried out to study the effects of environmental conditions on virus-host dynamics. A range of host and virus mutation probabilities as well as standard deviation for the mutations are considered to see how the arms-race dynamics are influenced by host- and virus-specific cellular constraints. Finally, genotypic and random compatibility/virulence functions are explored in order to analyze the sensitivity of arms-race dynamics to trade-off based virus-host interactions. Additional investigations of the effects of various physiological parameters on virus-host population dynamics are summarized in the supplementary material. In all cases, the effects of different parameters and interaction functions are ascertained from an ensemble average of 100 independent simulations.

Laboratory experiment

To characterize virus-host infection dynamics in a biological system, as well as to validate the general dynamics emerging from our IBM, we performed an infection experiment with the bacteria *Escherichia coli* E28 (DSM 103246) and a T-4 like virus (DSM 103876, hereby called B28) at five different VHRs (0.01, 0.15, 0.73, 1.90, 3.30). The experiment was conducted in a 96-well flat-bottomed microplate using the 2300 EnSpire Multilabel Plate Reader (PerkinElmer), allowing the entire experiment including multiple replicates to be run simultaneously under one assay. The growth of the host was monitored through automated measurement of

optical density at 600 nm (OD600) every 15 mins. All cultures were grown in the minimal medium M9 containing 2 mM $MgSO_4 \cdot 7H_2O$, 0.1 mM $CaCl_2 \cdot 2H_2O$, 6 mM glucose [27]. All dilutions were also done using M9 medium as diluent.

An outline of the steps involved is as follows: an overnight culture of *E. coli* was prepared, adjusted to OD600 = $\sim$0.2 using a Cell Density Meter (Fisher Scientific), and further diluted by factor 1:25. A sterile microplate was filled with the host culture, as well as M9 medium as blank solution, final volume of 200 μL per well. The assay was then run at 37˚C, 150 rpm (linear mode, 3 mm diameter) inside the plate reader. The growth of the host culture was monitored and once the host had entered the exponential growth phase, and its OD600 had increased by 0.04 ($\sim$3.5 hr), the assay was paused to retrieve the plate. A sample of the host culture was withdrawn and flash-frozen in 20% glycerol for host enumeration at B28 infection timepoint. B28 lysate ($\sim 10^8$ PFU mL^{-1}) was then added to the host culture to final volumes of 200 μL and concentrations of 0.1, 1, 5, 12.5, and 20% v/v. A sample of the lysate was also flash-frozen in 20% glycerol for phage enumeration. The assay was then resumed under the same culture conditions for another $\sim$37 hr. Host and phage enumeration was later done using a Calibur flow cytometer (Becton Dickinson) following a standard protocol [28], in order to calculate the exact VHRs. The experimental data (`experimental_data.csv`) are available as supporting information.

Results

In this section, we present host-virus infection dynamics from our growth experiments in the lab (Fig 3), along with results from our IBM (Figs 4–6). The latter are based on an ensemble average of 100 simulations. First we present the effects of environmental conditions on the outcome of the virus-host interaction dynamics in the first 1.5 days after virus infection (Fig 4), then we show the effects of evolution at the cellular level—specifically, mutation probability and mutation variance—(Fig 5), and finally we show the effects of trade-offs in host-virus interactions, considering a longer time-scale of 30 days (Fig 6). All parameter values except those being tested were held constant as shown in Table 1. Parameter values being tested (Figs 4 and 5) are shown in the figure legends. In all figures, host and virus population dynamics are reported in the first and second row, respectively. Note that in each figure, for ease of comparison, we use the same scale for the *y*-axes for hosts and viruses.

Growth experiments with different VHR over the course of 1.5 days reveal that the host population crashes fastest for highest VHR, thereby also reaching a lower maximum population size at the initial population peak. At the same time, the host population recovers fastest for high VHR, resulting in a pronounced second population peak after one day of incubation (yellow, pink and green curves vs black and blue curves in Fig 3). This has the practical consequence that high VHR allows us to observe a full virus-host infection cycle with subsequent recovery of the host within the timeframe of our experiment.

Our IBM captures these dynamics (Figs 4 and 5). Specifically, analogous to the laboratory experiment, high VHR results in earliest crash but also fastest recovery and emergence of potentially resistant hosts in the infected population within the first 36 hours of our in-silico experiments. This manifests as a second peak in host populations reaching between 800 and 1,100 cells μL^{-1} roughly 20 hours into the infection cycle (Fig 4a).

Virus numbers increase as they are released from infected hosts and the host population starts collapsing, roughly 10 to 20 hours into the infection cycle. They keep increasing after recovery of the host population, reaching up to 70,000 cells μL^{-1}. Highest VHR at the start of infection cycle consistently results in higher virus population numbers throughout the simulated time frame (Fig 4d).

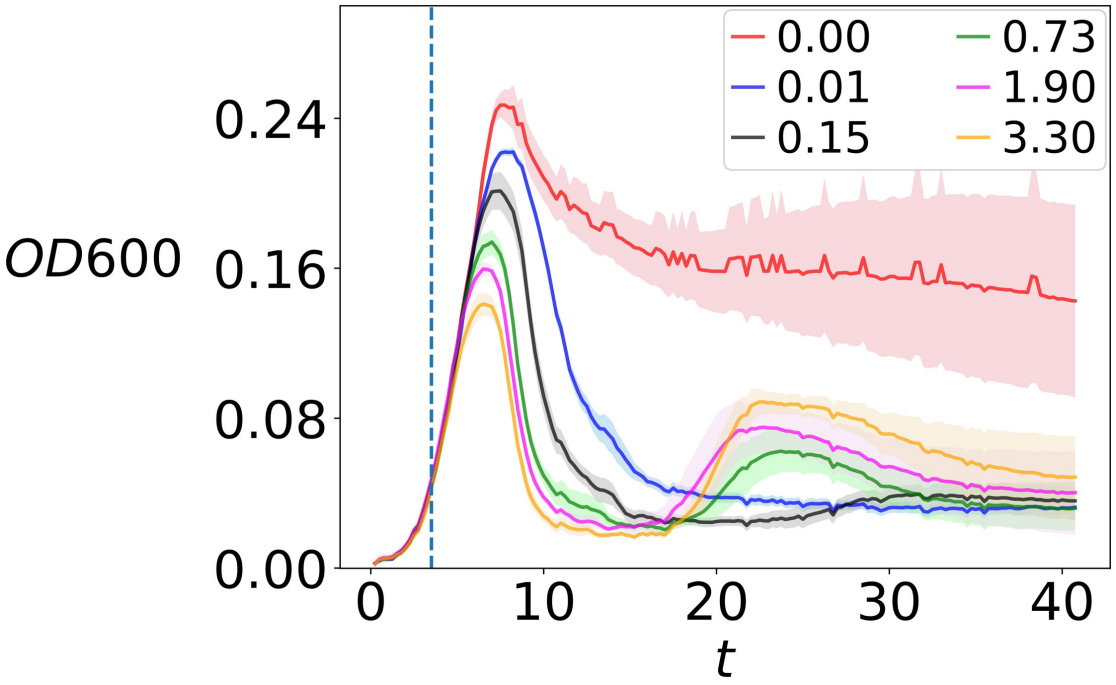

Fig 3. Infection dynamics of B28 virus and *E. coli*. Infection experiments performed as plate reader assays for different virus to host ratios (VHR). Optical density at 600 nm (OD600) was monitored to serve as a proxy for the host abundance. The growth curve of *E. coli* without virus infection (control) is shown in red. Plotted curves: mean values ($n = 8$ and $n_{control} = 11$) shown as solid lines and standard deviaitons shown as shading, with the vertical dashed line denoting the time ($t = 3.5$ hr) for viral infection.

https://doi.org/10.1371/journal.pcbi.1010228.g003

Nutrient concentration also influences population dynamics; our model indicates that high availability of nutrients leads to a more pronounced boom and bust scenario in the host population, with hosts reaching higher maximum population numbers in their first peak before they crash (up to 16,000 cells μL^{-1}) and growing back to high population numbers (around 1,000 cells μL^{-1}) due to potentially resistant hosts emerging (Fig 4b). Higher limiting nutrient availability is also reflected in highest virus population numbers, which exceeds 80,000 viruses μL^{-1} after 36 hours (Fig 4e).

Washout also has a strong effect on population dynamics. A crash in the host population with recovery half-way through the simulated time is most pronounced at low washout rates, reaching numbers down to 300 cells μL^{-1} around 18 hours into the infection cycle. Highest washout rates yield no reduction in host population after viral addition, resulting in steady host population numbers of around 1,200 cells μL^{-1} from about 12 hours into the infection cycle (Fig 4c). Virus population numbers are highest for low washout rates (Fig 4f). Interestingly, a saturation of the medium with hosts and absence of viruses occurs when the washout value exceeds 0.3 h^{-1} (Fig 4c and 4f).

Besides the effects of environmental parameters (Fig 4), our model shows clear dependence of the virus-host dynamics on the organism-specific evolution of traits, namely mutation probability π and standard deviation σ of mutations (Fig 5). In particular, increasing the values for

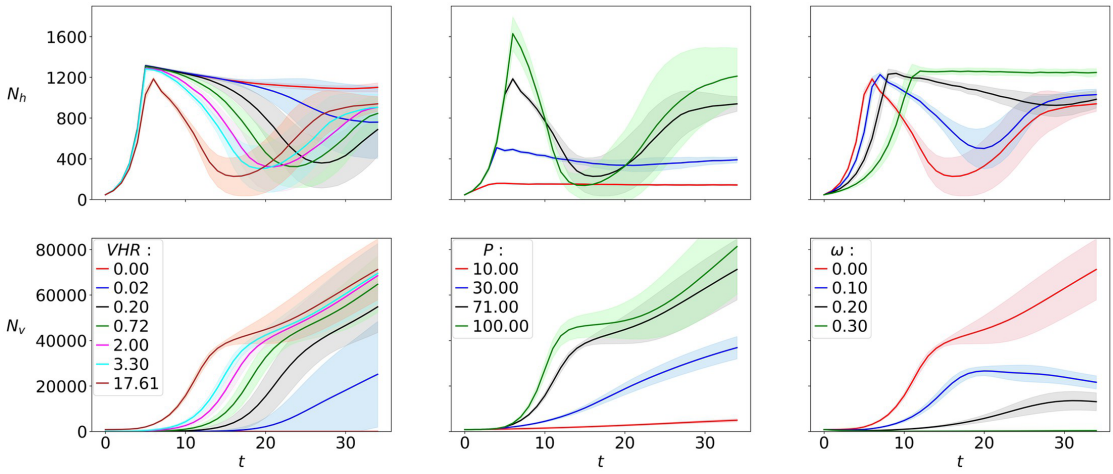

Fig 4. Model's sensitivity to environmental parameters. Population dynamics for hosts (a-c) and viruses (d-f) for varying virus to host ratios (VHR), total phosphorous content (P, μmol-P L^{-1}) and washout rate (ω, h^{-1}). Plotted curves: ensemble averages from 100 runs lasting $T = 36$ h, with standard deviations shown as shading.

https://doi.org/10.1371/journal.pcbi.1010228.g004

the host (π_h and σ_h, respectively) leads to a reduced crash and earlier recovery of potentially resistant hosts, with the host population growing back to high densities up to 900 cells μL^{-1} within the simulated time (Fig 5a and 5c).

For the lowest tested π_h, hosts struggle to recover within the simulated time, whereas they collapse entirely for the two lowest tested values σ_h (Fig 5a & 5c). Virus population numbers reach high values of up to 80,000 viruses μL^{-1} in the simulated time for high π_h and σ_h,

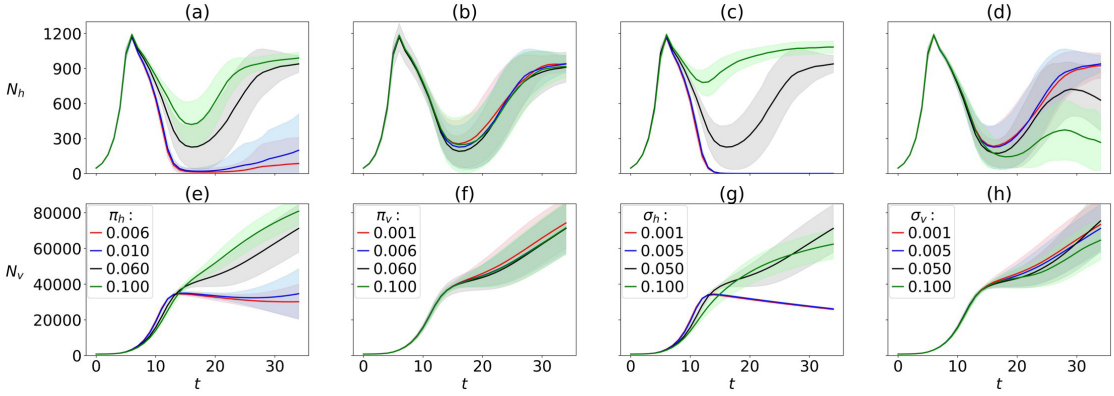

Fig 5. Model's sensitivity to evolution in organism traits. Sensitivity of host (a-d) and virus dynamics (e-h) to mutation probability in host traits (π_h), virus traits (π_v), standard deviation in mutation for host traits (σ_h) and standard deviation in mutation for virus traits (σ_v). Plotted curves: ensemble averages from 100 runs lasting $T = 36$ h, with standard deviations shown as shading.

https://doi.org/10.1371/journal.pcbi.1010228.g005

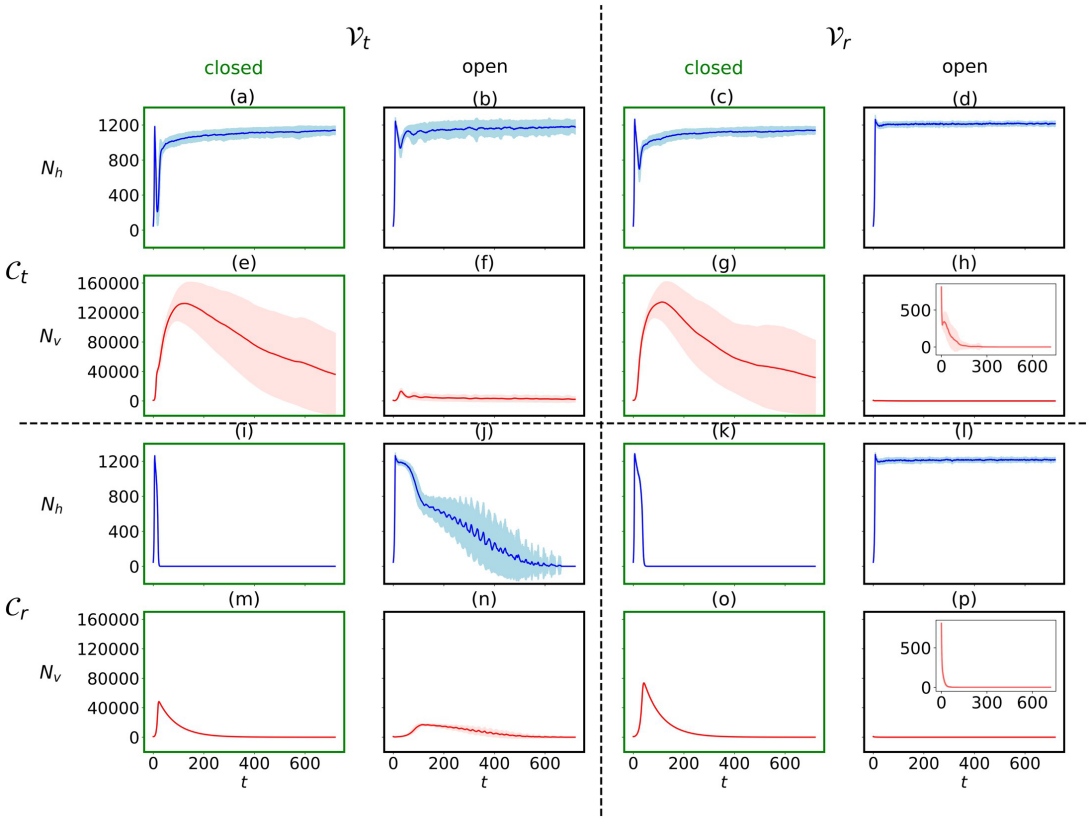

Fig 6. Model's sensitivity to trade-off-based vs random infection processes. Host (a-d, i-l) and virus population dynamics (e-h, m-p) shown for closed systems and open systems with washout rate 0.2 h^{-1} for genotypic compatibility and genotypic virulence ($\mathcal{C}_t$, $\mathcal{V}_t$, upper left), genotypic compatibility and random virulence ($\mathcal{C}_t$, $\mathcal{V}_r$, upper right), random compatibility and genotyipc virulence ($\mathcal{C}_r$, $\mathcal{V}_t$, lower left) and random compatibility and random virulence ($\mathcal{C}_r$, $\mathcal{V}_r$, lower right). Ensemble averages of 100 simulations (lines) with standard deviation (shaded areas) lasting for $T = 720$ h are shown. Sub-panels show virus dynamics on adjusted y-axis scales.

https://doi.org/10.1371/journal.pcbi.1010228.g006

increasing readily as the host population recovers from the first crash, whereas low π_h and σ_h result in stagnant or declining virus population numbers from about 12 hours into infection cycle, never exceeding 40,000 viruses μL^{-1} (Fig 5e and 5g).

In contrast to host mutation probabilities, changing the mutation probability for the virus π_v over two orders of magnitude does not show any effect on the host-virus dynamics (Fig 5b and 5f). Similarly, increasing the standard deviation for virus mutations σ_v does not show a clear effect on virus population dynamics within the simulated time, but the host population recovery after the first crash is dampened with higher σ_v, reducing the size of the second peak in the host population reaching moderate numbers of 300 cells μL^{-1} roughly 28 hours into infection cycle and also allowing for a second crash of the host population within the simulated time of 36 hours (Fig 5d and 5h).

Long-term simulations of 30 days (720 h) reveals marked differences of trade-off based vs random interaction function for virus-host compatibility and virulence (Fig 6). Recall that a trade-off based compatibility function ($\mathcal{C}_t$) in our simulations implies that infection success is mediated by a trade-off between the host's nutrient affinity and the virus' adsorpiton coefficient (Fig 1), whereas a trade-off based virulence function ($\mathcal{V}_t$) implies that the infection success is dictated by a trade-off between the virus host range and the virus adsorption coefficient (Fig 2).

In all long-term simulations (Fig 6), the system tends towards an equilibrium after the first fluctuations of host crash and typical re-growth thereof that is also visible in the short-term simulations (Figs 4 and 5). The initial crash in host population is most pronounced in closed systems, and hosts as well as viruses die out completely in closed systems under random compatibility modes (Fig 6i, 6m, 6k and 6o).

In simulations with compatibility trade-offs (Fig 6a–6h), hosts reach a high population size at equilibrium after initial drops both in closed and open systems. As in case of random compatibility mode, the first crash of host population is most pronounced in closed systems (Fig 6a and 6c). Viruses reach very high population size at first, independently of whether its virulence is trade-off based or random, but they experience a steady decline over the course of the simulation. Note that the spread in virus population size over the 100 simulation runs is large in closed systems with trade-off based compatibility compared to all other scenarios. In contrast to closed systems, open systems (washout 0.2 h^{-1}) suppress the emergence of large viral population all together, keeping them at low numbers after an initial spike when simulations are driven by trade-off based virulence (Fig 6f). For open systems with random virulence, virus population size drop right from the start of the simulation (Fig 6h).

In case of random compatibility (Fig 6i–6p), the host population typically collapses to extinction with the consequence that also viruses eventually die out. The only exception is in open systems where virulence is random. In this case, the viruses disappear early on in the simulation and the hosts persist with high population numbers (Fig 6l). With random compatibility and trade-off based virulence in an open system, host population decreases more slowly and undergoes fluctuations while doing so (Fig 6j). Highest viral population numbers before decline are reached in closed systems. As in open systems with trade-off based compatibility but random virulence (Fig 6h), virus population numbers drop from the beginning of the simulation for open systems and random virulence (Fig 6p).

Discussion

We have developed a simple individual-based virus-host interaction model to i) study the effects of environmental and organism-specific parameters on population dynamics and ii) evaluate the importance of trade-offs between competitive and defensive host traits on population dynamics and long-term evolutionary change. The model is highly idealized, focusing on specific trait-based mechanisms. Whereas experimental support for trade-offs between competition and defense in diverse biological systems exists [14, 15, 18], other mechanisms such as environmental disturbance and resource specialization also promote diversity. The model is validated with laboratory data from a short-term infection experiment. Some quantitative discrepancy appears between dynamics in the laboratory experiment and our simulations for low VHR, possibly because all viruses in our model are infectious, whereas a fraction of viruses is non-infections in the laboratory. This implies that higher VHR in the laboratory functionally correpsond with lower VHR in our simulations. Regardless of this, the qualitative match between laboratory data and simulation results for host dynamics provides confidence in basic mechanisms underlying virus—host dynamics. Besides, the model produces plausible results

in terms of compatibility trade-offs promoting long-term co-existence of hosts and viruses. However, further validation of the model is needed, in particular for viral population dynamics, which are not as straight forward to measure in laboratory experiments. In the following we discuss details of our findings.

Our model suggests that high VHR results in earliest crash but also fastest recovery of the host population, such that a full infection cycle is complete within the first 36 hours of our simulation experiments. This agrees qualitatively with infection cycles observed in our *E. coli*-B28 experimental model system (Fig 3) where highest VHR also led to fastest regrowth. Interestingly, similar dynamics have been observed previously in marine algal host-virus systems, namely *Emiliania huxleyi* and EhV-99B1, *Pyramimonas orientalis* and PoV-01B, and *Phaeocystis pouchetii* and PpV-01 [29]. Considering selection pressure to be the highest under strong viral control, it is reasonable to assume that re-growth of host populations after the first crash is given by resistant mutants, which readily establish in high VHR conditions. Virus numbers increase simultaneously with the first crash in host populations as they are set free from infected hosts, and keep increasing after recovery of the host population. This suggests that regrowth of the host population is either not exculsively caused by resistant types, but that it is instead diversifying into resistant and susceptible hosts, or that viruses undergo evolutionary change establishing strains that are able to re-infect the originally resistant hosts. The two alternatives not being mutually exclusive, genomic studies will be needed to decipher the cause.

Analogous to microbial blooms under favorable growth conditions, high availability of limiting nutrient gives a boom-and-bust scenario in our simulations with host population reaching very high peaks before crashing to values below those of more stable host population numbers at lower nutrient concentrations (Fig 4b).

Washout rate is also an important parameter for virus-host population dynamics, especially in shorter time-scales, where washout seems to prevent the accumulation of high viral numbers, keeping viral pressure relatively low in open systems (Fig 6, closed vs open system runs). A possible explanation for low viral pressure in open systems could be a combination of washout of viruses and favorable growth conditions for hosts with inflow of fresh medium.

Evolution of organism-specific traits also affects virus-host population dynamics. Our results suggest that variation in host traits may have stronger effects on virus-host population dynamics than variations in virus traits (ie, different host mutation probabilities and standard deviations give more distinct results compared to different viral mutation probabilities and standard deviations, Fig 5). Noticeably, the host population recovery after the first crash is dampened the most with higher standard deviation in mutation for viruses (σ_v), reducing the size of the second peak in the host population and also allowing for a second crash of the host population within the simulated time (Fig 5d). In other words, high σ_v and thus higher flexibility in adjustments of infectious traits as adaptation to acquired host immunity seems to impose a strong selection pressure on hosts, speeding up evolutionary time-scales. Additionally, high σ_v should have facilitated the emergence of broader virus host-range, which in nature has been shown to associate with longer interaction periods with hosts [30], potentially making these viruses strong limiting factors for their hosts. Emerging diversity within host and virus specific traits, such as host-range evolution in our model is a subject for a follow-up study. Preliminary results of diversity based on Shannon entropy in distributions of nutrient affinity, virus adsorption coefficient, and memory gene shown in the Supporting Information section indicate increasing diversity over the course of the simulations.

Overall, population dynamics are remarkably different for trade-off based vs random interaction functions. Long-term coexistence of both hosts and viruses is facilitated when the compatibility function is trade-off based (Fig 6a–6h), in which case the viruses persist the longest in closed systems (Fig 6e and 6g). Spatial sturcture has been discussed as mechanism

facilitating long-term co-existence of bacteria and viruses [31], for example by rendering low virulent viruses higher fitness [32]. These findings might explain why eventually, even with compatibility trade-offs, virus populations die out in our well-mixed setting.

The dominance of variation in host traits over virus traits in regulating virus-host population dynamics described in the previous paragraph aligns with the observation that trade-offs involving host traits (ie, compatibility trade-off, which links host traits to virus traits, rather than virulence trade-off that is purely based on viral traits) appeared to have the most pronounced effects effects on the virus-host population dynamics. Indeed, further support for this is provided by our long-term simulations with and without compatibility trade-offs (Fig 6, top half vs bottom half), where trade-off based vs random compatiblity functions result in most distinct long-term dynamics, contrasting trade-off based vs random virulence runs in which difference are only pronounced in open systems (Fig 6, left half vs right half). Interestingly, long-term co-existence also most easily emerge when compatibility trade-offs are expressed. This is true even when viral pressure is high early on in the infection cycle in closed systems. We thus postulate that compatibility trade-offs facilitate virus-host coexistence observed in nature. Interestingly, observations of narrow host range viruses interacting with their hosts at lower total host abundance compared to broad-host range viruses [30] suggest that low host-range interactions are more efficient than those of high host-range viruses, which could be an expression of such a compatibility trade-off playing out in nature. Ranking traits and trade-offs involved in virus-host interaction according to their impacts on evolutionary outcomes is, however, challenging and remains to be studied further.

Our analysis on co-existence of host and viruses supports the hypothesis that trade-offs associated with competitive abilities of hosts and traits influencing the efficiency of viral infection are critical to shaping realistic long-term population dynamics and co-existence in virus-host systems. Competition and defense trade-off being a fundamental phenomenon in nature [33–35], we conjecture that findings from this study might be useful in understanding long-term perseverence of parasites in epidemiological context. Besides, in terms of conditions for high virus population numbers, results might also be useful in pharmaceutical applications, in particular large scale phage production for phage therapy. As a next step, we intend to shed light on host- and virus-population internal trait diversification as a consequence of this trade-off, touching upon the phenomenon of microdiversity in natural microbial communities.

Supporting information

S1 Data. Experimental data. Data on bacteria—phage co-infection experiments rendered in Fig 3 of the main text. The data file inlcudes timeseries of optical density measured at 600 nm, showing number of replicates, mean and standard deviation with 15 minutes interval for different initial virus to host ratios used.
(CSV)

S1 Pseudocode. Model structures and algorithmic procedures. The pseudocode describes details of initialization, interactions, budgets and evolutionary dynamics implemented in the model, step by step.
(PDF)

S1 Fig. Model's sensitivity to physiological parameters. Host (a-h) and virus dynamics for various resource affinities for hosts (α), adsorption coefficients for viruses (β), maximum growth rates for hosts (μ_h) and burst size for viruses (κ). Plotted curves: ensemble averages from 100 runs for $T = 36$ h, with standard deviations shown as shading.
(TIFF)

S2 Fig. Evolutionary diversification of host and virus genotypes. Diversity time-series based on Shannon entropy of ensemble averages from 100 runs in a trade-off based compatibiltiy and virulence scenario shown for a) nutrient affinity of host (g_α), b) adsorption coefficient of virus (g_β), and c) memory gene of virus (g_ν). Small subpanels show abundance distribution for the genotypes at three distinct time points over the course of $T = 720$ h.
(TIFF)

Author Contributions

Conceptualization: Selina Våge.

Data curation: Jesslyn Tjendra.

Formal analysis: Fateme Pourhasanzade, Swami Iyer.

Funding acquisition: Selina Våge.

Investigation: Selina Våge.

Methodology: Swami Iyer.

Project administration: Selina Våge.

Software: Fateme Pourhasanzade, Swami Iyer.

Supervision: Selina Våge.

Validation: Jesslyn Tjendra.

Visualization: Fateme Pourhasanzade, Swami Iyer.

Writing – original draft: Fateme Pourhasanzade, Swami Iyer, Selina Våge.

Writing – review & editing: Fateme Pourhasanzade, Swami Iyer, Jesslyn Tjendra, Lotta Landor, Selina Våge.

References

1. Rohwer F, Thurber RV. Viruses manipulate the marine environment. Nature. 2009; 459(7244):207–212. https://doi.org/10.1038/nature08060 PMID: 19444207
2. Suttle CA. Environmental microbiology: Viral diversity on the global stage. Nature microbiology. 2016; 1(11):1–2. https://doi.org/10.1038/nmicrobiol.2016.205
3. Middelboe M, Brussaard CP. Marine viruses: key players in marine ecosystems; 2017. https://doi.org/10.3390/v9100302
4. French RK, Holmes EC. An ecosystems perspective on virus evolution and emergence. Trends in microbiology. 2020; 28(3):165–175. https://doi.org/10.1016/j.tim.2019.10.010 PMID: 31744665
5. Peters MA, Jandrić P, McLaren P. Viral modernity? Epidemics, infodemics, and the 'bioinformational'-paradigm; 2020.
6. Stano M, Beke G, Klucar L. viruSITE—integrated database for viral genomics. Database. 2016; 2016. https://doi.org/10.1093/database/baw162 PMID: 28025349
7. Hurwitz BL, U'Ren JM, Youens-Clark K. Computational prospecting the great viral unknown. FEMS microbiology letters. 2016; 363(10). https://doi.org/10.1093/femsle/fnw077 PMID: 27030726
8. Messier J, McGill BJ, Lechowicz MJ. How do traits vary across ecological scales? A case for trait-based ecology. Ecology letters. 2010; 13(7):838–848. https://doi.org/10.1111/j.1461-0248.2010.01476.x PMID: 20482582
9. Wong MK, Guénard B, Lewis OT. Trait-based ecology of terrestrial arthropods. Biological Reviews. 2019; 94(3):999–1022. https://doi.org/10.1111/brv.12488 PMID: 30548743
10. Kiørboe T, Visser A, Andersen KH. A trait-based approach to ocean ecology. ICES Journal of Marine Science. 2018; 75(6):1849–1863. https://doi.org/10.1093/icesjms/fsy090

11. Follows MJ, Dutkiewicz S, Grant S, Chisholm SW. Emergent biogeography of microbial communities in a model ocean. science. 2007; 315(5820):1843–1846. https://doi.org/10.1126/science.1138544
12. Litchman E, Klausmeier CA. Trait-based community ecology of phytoplankton. Annual review of ecology, evolution, and systematics. 2008; 39:615–639. https://doi.org/10.1146/annurev.ecolsys.39.110707.173549
13. Allison S. A trait-based approach for modelling microbial litter decomposition. Ecology letters. 2012; 15(9):1058–1070. https://doi.org/10.1111/j.1461-0248.2012.01807.x PMID: 22642621
14. Bohannan BJ, Kerr B, Jessup CM, Hughes JB, Sandvik G. Trade-offs and coexistence in microbial microcosms. Antonie Van Leeuwenhoek. 2002; 81(1):107–115. https://doi.org/10.1023/A:1020585711378
15. Wright SJ, Kitajima K, Kraft NJ, Reich PB, Wright IJ, Bunker DE, et al. Functional traits and the growth–mortality trade-off in tropical trees. Ecology. 2010; 91(12):3664–3674. https://doi.org/10.1890/09-2335.1 PMID: 21302837
16. Grubb PJ. Trade-offs in interspecific comparisons in plant ecology and how plants overcome proposed constraints. Plant Ecology & Diversity. 2016; 9(1):3–33. https://doi.org/10.1080/17550874.2015.1048761
17. Ferenci T. Trade-off mechanisms shaping the diversity of bacteria. Trends in microbiology. 2016; 24(3):209–223. https://doi.org/10.1016/j.tim.2015.11.009 PMID: 26705697
18. Hodge JR, Alim C, Bertrand NG, Lee W, Price SA, Tran B, et al. Ecology shapes the evolutionary trade-off between predator avoidance and defence in coral reef butterflyfishes. Ecology letters. 2018; 21(7):1033–1042. https://doi.org/10.1111/ele.12969 PMID: 29744987
19. Våge S, Bratbak G, Egge J, Heldal M, Larsen A, Norland S, et al. Simple models combining competition, defence and resource availability have broad implications in pelagic microbial food webs. Ecology letters. 2018; 21(9):1440–1452. https://doi.org/10.1111/ele.13122 PMID: 30014593
20. Record NR, Talmy D, Våge S. Quantifying tradeoffs for marine viruses. Frontiers in Marine Science. 2016; 3:251. https://doi.org/10.3389/fmars.2016.00251
21. Williams HT. Coevolving parasites improve host evolutionary search on structured fitness landscapes. In: Artificial Life Conference Proceedings 12. MIT Press; 2012. p. 129–136.
22. DeAngelis DL, Grimm V. Individual-based models in ecology after four decades. F1000prime reports. 2014; 6. https://doi.org/10.12703/P6-39 PMID: 24991416
23. Bonabeau E. Agent-based modeling: Methods and techniques for simulating human systems. Proceedings of the National Academy of Sciences. 2002; 99(3):7280–7287. https://doi.org/10.1073/pnas.082080899
24. Iyer S, Pourhasanzade F, Våge S. Microbial Evolution: An Individual-based Model in Python; 2022. https://github.com/swamiiyer/microbial_evolution.
25. Thingstad TF. Elements of a theory for the mechanisms controlling abundance, diversity, and biogeochemical role of lytic bacterial viruses in aquatic systems. Limnology and Oceanography. 2000; 45(6):1320–1328. https://doi.org/10.4319/lo.2000.45.6.1320
26. Våge S, Castellani M, Giske J, Thingstad TF. Successful strategies in size structured mixotrophic food webs. Aquatic Ecology. 2013; 47(3):329–347. https://doi.org/10.1007/s10452-013-9447-y
27. Anonymous. M9 minimal medium (standard). Cold Spring Harbor Protocols. 2010; 2010:pdb–rec12295.
28. Brussaard CP. Viral control of phytoplankton populations—a review 1. Journal of Eukaryotic Microbiology. 2004; 51(2):125–138. https://doi.org/10.1111/j.1550-7408.2004.tb00537.x PMID: 15134247
29. Thyrhaug R, Larsen A, Thingstad TF, Bratbak G. Stable coexistence in marine algal host-virus systems. Marine Ecology Progress Series. 2003; 254:27–35. https://doi.org/10.3354/meps254027
30. Sakowski EG, Arora-Williams K, Tian F, Zayed AA, Zablocki O, Sullivan MB, et al. Interaction dynamics and virus–host range for estuarine actinophages captured by epicPCR. Nature Microbiology. 2021; 6(5):630–642. https://doi.org/10.1038/s41564-021-00873-4 PMID: 33633401
31. Heilmann S, Sneppen K, Krishna S. Coexistence of phage and bacteria on the boundary of self-organized refuges. Proceedings of the National Academy of Sciences. 2012; 109(31):12828–12833. https://doi.org/10.1073/pnas.1200771109 PMID: 22807479
32. Roychoudhury P, Shrestha N, Wiss VR, Krone SM. Fitness benefits of low infectivity in a spatially structured population of bacteriophages. Proceedings of the Royal Society B: Biological Sciences. 2014; 281(1774):20132563. https://doi.org/10.1098/rspb.2013.2563 PMID: 24225463
33. Jessup CM, Bohannan BJ. The shape of an ecological trade-off varies with environment. Ecology Letters. 2008; 11(9):947–959. https://doi.org/10.1111/j.1461-0248.2008.01205.x PMID: 18557986

34. Petry WK, Kandlikar GS, Kraft NJ, Godoy O, Levine JM. A competition–defence trade-off both promotes and weakens coexistence in an annual plant community. Journal of Ecology. 2018; 106(5):1806–1818. https://doi.org/10.1111/1365-2745.13028

35. Winter C, Bouvier T, Weinbauer MG, Thingstad TF. Trade-offs between competition and defense specialists among unicellular planktonic organisms: the "killing the winner" hypothesis revisited. Microbiology and Molecular Biology Reviews. 2010; 74(1):42–57. https://doi.org/10.1128/MMBR.00034-09

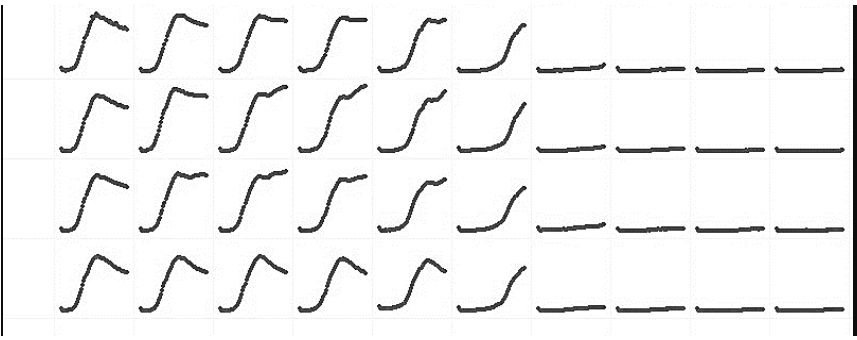

Paper 2

Journal of Microbiological Methods 206 (2023) 106679

Contents lists available at ScienceDirect

Journal of Microbiological Methods

journal homepage: www.elsevier.com/locate/jmicmeth

Differential toxicity of bioorthogonal non-canonical amino acids (BONCAT) in *Escherichia coli*

Lotta A.I. Landor [a], Gunnar Bratbak [a], Aud Larsen [b], Jesslyn Tjendra [a], Selina Våge [a,*]

[a] Department of Biological Sciences, University of Bergen, Norway
[b] NORCE Environment and Climate, Bergen, Norway

ARTICLE INFO

Keywords:
BONCAT
Non-canonical amino acids
AHA
HPG
Toxicity

ABSTRACT

Single-cell methods allow studying the activity of single bacterial cells, potentially shedding light on regulatory mechanisms involved in services like biochemical cycling. Bioorthogonal non-canonical amino acid tagging (BONCAT) is a promising method for studying bacterial activity in natural communities, using the methionine analogues L-azidohomoalanine (AHA) and L-homopropargylglycine (HPG) to track protein production in single cells. Both AHA and HPG have been deemed non-toxic, but recent findings suggest that HPG affects bacterial metabolism. In this study we examined the effect of AHA and HPG on *Escherichia coli* with respect to acute toxicity and growth. *E. coli* exposed to 5.6–90 μM HPG showed no growth, and the growth rate was significantly reduced at >0.35 μM HPG, compared to the HPG-free control. In contrast, *E. coli* showed growth at concentrations up to 9 mM AHA. In assays where AHA or HPG were added during the exponential growth phase, the growth sustained but the growth rate was immediately reduced at the highest concentrations (90 μM HPG and 10 mM AHA). Prolonged incubations (20*h*) with apparently non-toxic concentrations suggest that the cells incorporating NCAAs fail to divide and do not contribute to the next generation resulting in the relative abundance of labelled cells to decrease over time. These results show that HPG and AHA have different impact on the growth of *E. coli*. Both concentration and incubation time affect the results and need to be considered when designing BONCAT experiments and evaluating results. Time course incubations are suggested as a possible way to obtain more reliable results.

1. Introduction

Bacterial activity in natural communities is crucial for biochemical cycling and ecosystem services. Resolving the bacterial activity to the single bacterial cell provides an opportunity to explore the mechanisms regulating activity in bacteria. Bioorthogonal non-canonical amino acid tagging (BONCAT) has shown promise as a fast and relatively inexpensive method to study bacterial in situ protein synthesis at a single-cell level. BONCAT has been applied to study bacterial activity distributions in soil (Couradeau et al., 2019), anaerobic (Hatzenpichler et al., 2014) and marine environments (Leizeaga et al., 2017; Samo et al., 2014) as well as in pulmonary bacteria (Valentini et al., 2020). One general principle of BONCAT is that the non-canonical amino acids (NCAA) are incorporated into proteins by translational activity, supposedly without disrupting the physiology or metabolism of the cell (Steward et al., 2020). "Bioorthogonal" is hence referring to non-interacting with cellular functions (Hatzenpichler et al., 2016).

The most used NCAAs in microbial studies are the methionine analogues L-azidohomoalanine (AHA) and L-homopropargylglycine (HPG) (Hatzenpichler et al., 2020). Currently, several protocols are used for BONCAT experiments (e.g. Leizeaga et al., 2017; Hatzenpichler and Orphan, 2015; Samo et al., 2014). Despite adjustments between protocols, the general procedure of BONCAT in microbial studies is the same: A sample containing living bacterial cells is incubated with a certain concentration of NCAA which are taken up by the cells' metabolic machinery and incorporated into polypeptides through translational activity. After incubation, the cells are fixed and then labelled with a fluorescent dye having azide or alkyne moieties that complement and react with the alkyne or azide moieties of the NCAA in a "click" reaction (Hatzenpichler et al., 2016). The labelling is specific, and the cells may be observed and enumerated using fluorescence microscopy (Hatzenpichler et al., 2014) or flow cytometry (Lindivat et al., 2020).

Although several studies have attempted to develop optimized protocols for the BONCAT method for microbial systems, the

* Corresponding author.
E-mail address: selina.vage@uib.no (S. Våge).

https://doi.org/10.1016/j.mimet.2023.106679
Received 30 November 2022; Received in revised form 24 January 2023; Accepted 25 January 2023
Available online 30 January 2023

recommendation is to optimize procedures for each system (Samo et al., 2014). During optimization of the BONCAT protocol for an experiment involving *E. coli*, we observed unexpected metabolic effects of the NCAAs used. While incubations with high concentrations (≥ 100 μM) of NCAAs for more than a few generations has been thought to affect bacterial growth rate (Hatzenpichler et al., 2020; Hatzenpichler et al., 2014), we found effects on bacterial growth at concentrations lower than previously reported (Valentini et al., 2020; Hatzenpichler et al., 2016). To scrutinize these findings, we studied the effects of a wide range of concentrations of AHA and HPG on growth of *E. coli*. In addition to acute effects, we also studied the consequences of prolonged incubations.

2. Materials and methods

2.1. Media and reagents

Minimal M9 liquid media (M9) was made from an autoclaved M9 salt solution (48 mM $Na_2HPO_4{\cdot}2H_2O$; 22 mM KH_2PO_4; 19 mM NH_4Cl; 8.6 mM NaCl) by adding 5.6 mM glucose, 2 mM $MgSO_4{\cdot}8\ H_2O$ and 0.1 mM $CaCl_2$ from sterile stocks solutions. The final pH of the M9 medium was 7.0 at room temperature. M9 agar media (M9 agar) was prepared with 11.2 mM glucose and 1.5% agar. Phosphate-buffered saline (PBS; 2.7 mM KCl, 1.8 mM KH_2PO_4, 10.1 mM $Na_2HPO_4{\cdot}2H_2O$, 137 mM NaCl, pH 7.4) was prepared in deionized water and sterile filtered (0.2 μm). All ingredients above, except $MgSO_4{\cdot}8\ H_2O$ (Merck, Darmstadt, Germany), were acquired from Sigma-Aldrich (Saint-Louis, Missouri, USA).

L-azidohomoalanine (AHA) (Cat# 1066) and L-homopropargylglycine (HPG) (Cat# 1067) were acquired from Click Chemistry Tools (Arizona, USA), and methionine (Met; J61904) was acquired from Alfa Aesar (Massachusetts, USA). Stock solutions (100 mM) of AHA, HPG and Met were prepared in milli-Q water and sterile filtered (0.2 μm).

2.2. Bacterial strain and glycerol stock production

The *E. coli* strain DSM 103246 was acquired from the German Collection of Microorganisms and Cell Cultures. Glycerol stocks were produced from one colony grown in M9 media at 37 °C to a cell density of approximately 8.0×10^8 CFU mL^{-1}, determined by plate counts. Autoclave-sterilized glycerol was added to a final concentration of 20% and mixed completely with the culture. The glycerol-culture mix was frozen at −80 °C in 500 μL aliquots. For each experiment, one aliquot was used and then discarded.

2.3. Growth inhibition experiments

Overnight *E. coli* cultures (10 mL M9 inoculated with 100 μL thawed glycerol stock) were diluted 1:10 in pre-warmed M9 and grown until mid-exponential phase, $OD_{600} = 0.2 \pm 0.01$, i.e. when the culture reached half the maximum OD they typically obtain in the M9 medium used. The cultures were then diluted 1:10 in M9 and used as inoculum (20 μL). For the assays we used flat-bottomed, non-treated 96-well plates (VWR European Art. No. 734–2781) filled with 180 μL of M9 supplemented with either AHA, HPG or methionine (Met). In AHA and HPG assays, the wells contained final concentrations of 0.2, 0.4, 0.7, 1.4, 2.8, 5.6, 11, 23, 45 and 90 μM. AHA assays were in addition performed with 35, 70, 140, 280, 560 μM and 1.1, 2.3, 4.5, 9 and 18 mM. Met was used as substrate control in all assays and in the same concentration as the NCAAs. All assays were run with four parallel wells. Growth controls were inoculated as above but in M9 medium without AHA, HPG and Met. In negative controls the inoculum was replaced by 20 μL sterile M9 medium. The two latter controls were run with eight parallels each. Each assay was run three times.

The initial cell density in the assays was about 1.6×10^6 CFU mL^{-1}. The plates were incubated at 37 °C in a Perkin Elmer Enspire™ 2300 Multilabel plate reader programmed to measure OD_{600} every 20 min for 18 h.

Before use, the microwell plate lids were made hydrophobic with 0.05% Triton X-100 to avoid condensation (Brewster, 2003). As triton X-100 is a potential cell lysing agent (Cornett and Shockman, 1978), control plates without this treatment were incubated in parallel, but no negative effects were observed after 18 h.

2.4. Acute inhibition experiments

Exponentially growing *E. coli* cultures were prepared as above, diluted 1:100 in pre-warmed M9 medium and pipetted into 96-well flat-bottomed microwell plates (180 μL per well). One row of 8 wells was filled with sterile M9 as a control. The plates were incubated in the plate reader until OD_{600} reached 0.104 ± 0.001 (approx. 300 min) which is equivalent to about 3.9×10^7 CFU mL^{-1}. HPG and Met were then added to final concentrations of 2.8, 5.6 and 90 μM; or AHA and Met to final concentrations of 2.8 and 90 μM and 10 mM to designated rows in the plate. Three parallel wells were used for each substrate and concentration. To keep the well volume constant, the same volume was removed as was added. Incubation in the plate was then resumed and continued for at least 18 h.

2.5. BONCAT staining and flow cytometry

Overnight *E. coli* cultures were diluted 1:10 in prewarmed M9 and incubated at 37 °C until $OD_{600} = 0.2$. The cultures were then diluted 1:100 in prewarmed M9 supplemented with 0.2–90 μM AHA or HPG and incubated at 37 °C for 30 min or overnight (20 h) and preserved with 0.9% formaldehyde solution (Sigma-Aldrich 47,608).

For BONCAT staining and flow cytometry, we used the protocol outlined earlier (Lindivat et al., 2020) with minor modifications. In short, the samples were centrifuged at 14000 ×*g* for 10 min in 2 mL tubes, supernatants were removed and replaced by PBS (pH 7.4).Freshly made sodium ascorbate (Merck A4034) and aminoguanidine hydrochloride (Sigma-Aldrich 396,494) was then added to final concentrations of 5 mM, followed by addition of a freshly made dye premix giving final concentrations of 120 μM $CuSO_4$, 570 μM THPTA (Sigma-Aldrich 762,342) and 5.7 μM AlexaFluor™ 647 alkyne or piconyl azide dye (Click Chemistry tools Catalog no 1301 and 1300). The samples were then incubated for 1 h in the dark before they were centrifuged at 14000 ×*g* for 10 min. Supernatants were removed and the cells resuspended in 700 μL 0.02% Tween Tris-EDTA buffer. Prior to flow cytometric analysis, the samples were diluted 1:10–1:1000 in Tris-EDTA buffer and stained for 10 min in the dark with 10 μL/mL SYBR green I (10^{-4} final dilution of stock) (Thermo Fisher Scientific). The samples were analyzed using the Attune NxT Flow Cytometer (Thermo Fisher Scientific) using a blue laser (488 nm, 50 mW) and a red laser (638 nm, 100 mW) at dye-specific excitation/emission wavelengths: 590/30 nm for SYBR Green I and 670/14 for AlexaFluor™ 647 (AF647). The flow rate was set at 100 μL/min. Bacteria were detected through gating of SYBR green-stained cells and BONCAT-positive cells were detected based on AF647-fluorescence.

2.6. Data analysis

The plate reader output data file (.csv) was processed using a Python script, where OD_{600} values and plate maps were organized into Excel data sheets. Both types of experiments were repeated three times and the results are reported as the mean. Data analysis was performed in Excel and growth rate was estimated from the early exponential growth phase (i.e. from when $OD_{600} > 0.025$ and the following 100 min) by linear regression of natural logarithm (ln) transformed growth curves. The effect of the different NCAA-treatments was tested using two-tailed Student's *t*-test in Excel.

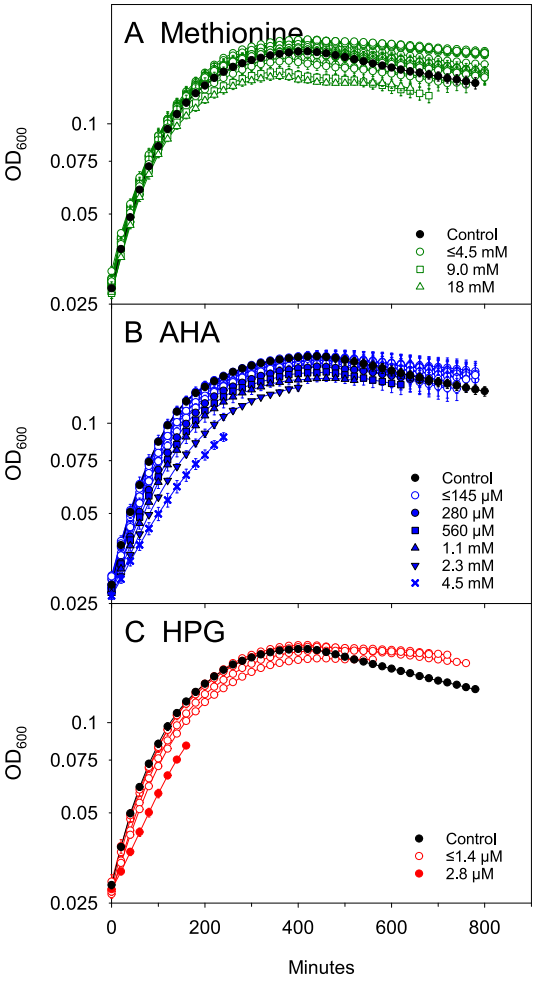

Fig. 1. Growth curves of *E. coli* in media containing different concentrations of methionine (A), L-azidohomoalanine (AHA, B), or L-homopropargylglycine (HPG, C). Each data point is the average of 3 independent experiments and error bars indicate standard error.

3. Results and discussion

Growth of *E. coli* at increasing concentrations of methionine, AHA and HPG compared to the respective control cultures (0 μM) is shown in Fig. 1. For Met we found no decrease in growth rate with increasing concentration (consider slope at origin), but the growth yield appeared to be lower at the two highest concentrations (Fig. 1 A). The growth rate decreased gradually at AHA concentrations between 280 μM and 4.5 mM (Fig. 1B). Lower concentrations (≤145 μM) had no significant effect (t-test, $p < 0.01$) while at the higher concentrations tested (9 and 18 mM) the cultures never exceeded $OD_{600} = 0.01$. We found significantly (*t*-test, $p < 0.01$) reduced growth rate at 2.8 μM HPG (Fig. 1C). At higher concentrations (5.6–90 μM), the cultures never exceeded $OD_{600} = 0.01$. Maximum growth rates (μ_{max}) in the non-inhibited cultures were 0.63 ± 0.02 h^{-1} (mean ± SD).

To investigate the acute effects, NCAAs and methionine were added in different concentrations to exponentially growing *E. coli* cultures

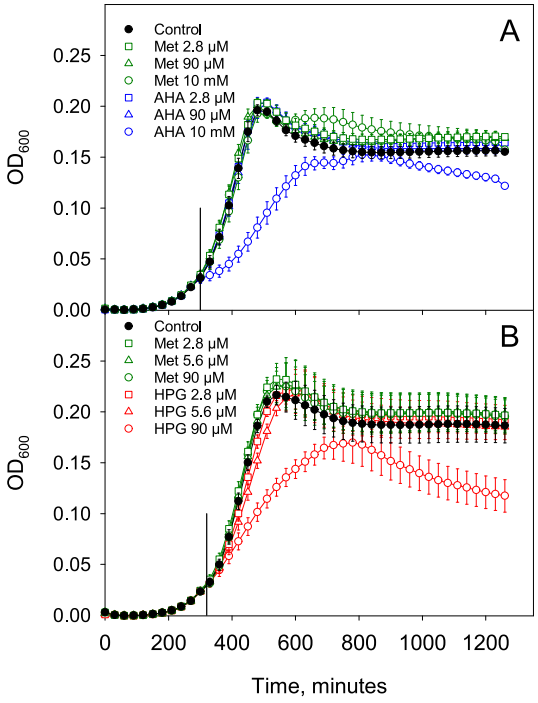

Fig. 2. Growth curves of *E. coli* in acute inhibition experiments where (A) HPG or Met and (B) AHA or Met were added in different concentrations during exponential growth. Addition of sterile M9 medium only served as control. Vertical lines indicates when AHA, HPG, Met or M9 (control) were added. Each data point is the average optical density (OD_{600}) from three independent experiments. Error bars represent the standard error. For clarity, only every third datapoint is plotted.

(Fig. 2). None of the tested HPG and AHA concentrations inhibited growth, but at the highest concentrations (90 μM HPG and 10 mM AHA) the growth rate was reduced immediately (0–90 min post addition, Student's t-test (two-tailed), $p < 0.02$ and $p < 0.001$ respectively) (Fig. 2). Met did not affect growth compared to the control culture at any concentration.

In summary, *E. coli* showed reduced growth when incubated with HPG concentrations >2.8 μM, but 90 μM was necessary to demonstrate an immediate effect on growth. AHA appeared to be less toxic, with reduced growth from >280 μM and > 9–10 mM for immediate impact on growth.

Previous studies have reported that AHA and HPG do not affect cell growth when low concentrations (≤ 50 μM) and short incubation times (≤1–2 generations) are used, but also that higher concentrations and/or longer incubation do have negative effects (Hatzenpichler et al., 2014; Pasulka et al., 2018). The concentrations of HPG we found toxic is lower than the 50 μM concentration frequently used and recommended in the literature (e.g. Hatzenpichler et al., 2016; Couradeau et al., 2019; Reichart et al., 2020; Steward et al., 2020) while the AHA concentrations used (50 μM – 6 mM; Wang et al., 2008; Steward et al., 2020; Valentini et al., 2020) are in the non-toxic range.

The negative effect of NCAA on cell growth and metabolism has been related to higher concentrations and longer incubation times, but as shown in the present study, the impact of both concentration and time is not straightforward. HPG appeared to have a negative effect on *E. coli* at a lower concentration than AHA. Wang et al. (2008) found only minor

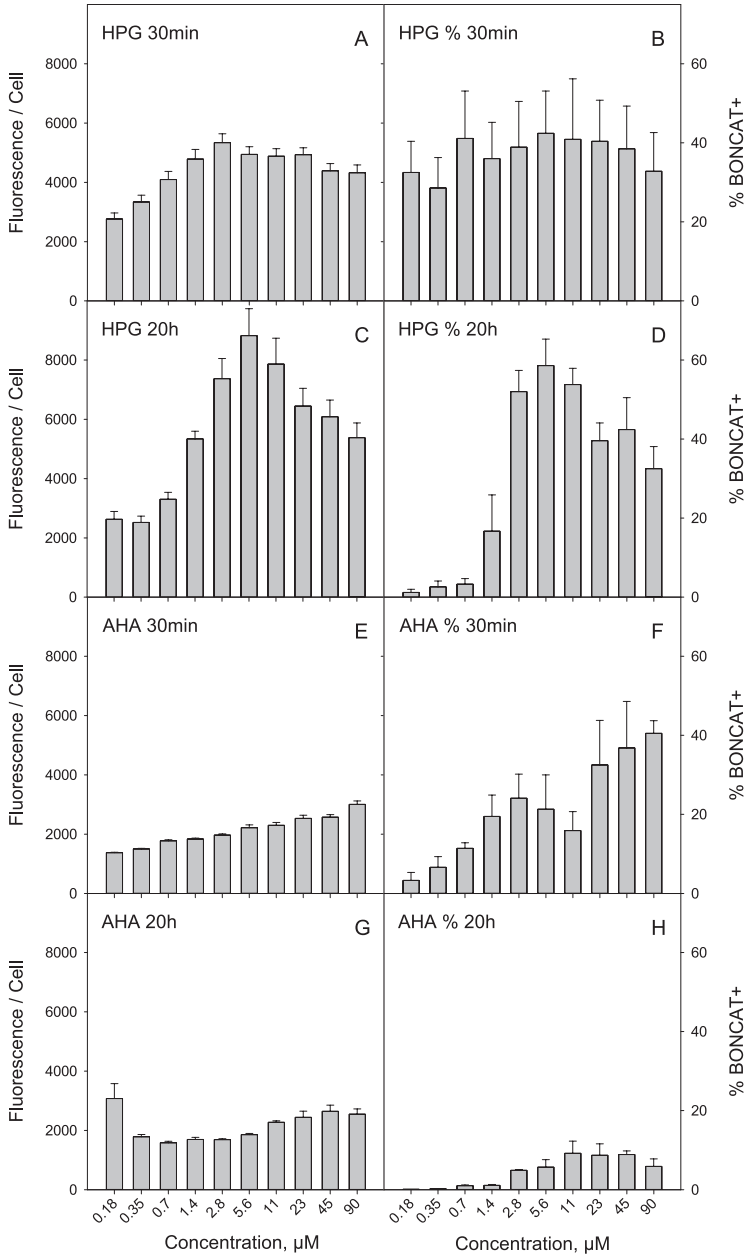

Fig. 3. Flow cytometric BONCAT data expressed as fluorescence/cell (left) and per cent BONCAT positive cells (% BONCAT +, right) for HPG (top half) and AHA (bottom half) with 30 min (A, B, E, F) and 20 h incubation times (C, D, G, H). X-axes show increasing concentrations of NCAA. Each bar is based on three replicate experiments with error bars showing standard error.

differences in metabolism of AHA and HPG in *E. coli*; both were efficient substrates for methionyl-tRNA synthetase and were efficiently incorporated into recombinant proteins with expression levels equivalent to those obtained with methionine. Nevertheless, differences in the NCAA uptake mechanism, which at present is unknown (Hatzenpichler et al., 2020), as well as differences related to misfolding and accumulation of non-functional NCAA labelled proteins (Hatzenpichler et al., 2014; Hatzenpichler et al., 2020) may at least to some extent contribute to explain the observed difference between HPG and AHA. In plants (e.g. *Arabidopsis thaliana*) AHA has been found to have a greater negative

impact on growth than HPG (Tivendale et al., 2021) and assessments of metabolic implications of NCAA should thus be considered for any target system as the effect appear inconsistent.

The flow cytometric BONCAT data show that *E. coli* take up HPG in increasing amounts up to growth inhibiting concentrations ($\geq$ 2.8 μM HPG) when incubated for 30 min, but also that the fraction of labelled cells was relatively even (37 ± 4%, mean ± SD) at all tested concentrations (Fig. 3A, B). When incubated for 20 h, however, both the amount of label per cell (Fig. 3 C) and the fraction of labelled cells (Fig. 3D) was reduced in the non-toxic range ($<$ 2.8 μM) while they remained high or increased in the toxic range ($\geq$ 2.8 μM HPG). In the same concentration range, where AHA appears to be non-toxic, both the uptake and the fraction of labelled cells increase with increasing AHA concentration (Fig 3 E, F). After 20 h incubation, the fraction of AHA labelled cells was reduced (Fig. 3 H), while the amount of label per cell remained unchanged or was slightly reduced (Fluorescence / Cell 30 min: 2110 ± 150; 20 h: 2160 ± 150 (mean ± SE, $n = 10$)) (Fig. 3 G), as was the case for HPG in the non-toxic range. This may suggest that the cells that incorporate NCAAs fail to divide and hence do not contribute to the next generation so that the relative abundance of labelled cells decrease. This implies that some cells, even in a single species population, grow but do not incorporate NCAAs, a hypothesis supported by increasing total cell counts in cultures with non-toxic HPG concentrations during the 20 h incubation. Alternatively, cells that remains metabolically active may after prolonged incubation somehow render the incorporated NCAAs unavailable for click reaction, while cells that are intoxicated by NCAAs remain unchanged and maintain the labelling obtained after short term incubation.

The growth inhibition and negative effects of NCAAs on cell metabolism may not be important for BONCAT studies as long as the initial rate of incorporation is related to growth and activity at the moment of NCAA addition and maintained long enough to be detectable. Care is nevertheless called for when interpreting uptake reported as fluorescence per cell or fraction of labelled (i.e. active) cells when based on a single, fixed incubation time. Results obtained from incubations lasting several generations (Fig. 3) appear to be upset by NCAA metabolism and such protocols need further testing and considerations for reliable interpretation.

Diversity in metabolism and potential species-specific response to NCAA amendments is another challenge that make the interpretations difficult when the BONCAT method is applied to mixed natural microbial communities (e.g., Hatzenpichler et al., 2016; Samo et al., 2014). Nonetheless, even for mixed communities, BONCAT provides an estimate of the number of protein-synthesizing cells and the signal intensity has been demonstrated to correlate with the rate of protein synthesis and is also used to assess the range of activity at the single-cell level (Samo et al., 2014; Leizeaga et al., 2017; Valentini et al., 2020). Flow cytometric fluorescence per cell data contains information both on the number of active cells and single cell activity (i.e., the intensity of the fluorescence signal is a proxy for single cell activity), whereas the fraction of active cells only carries the cell number signal. The fraction of active cells has the potential advantage that it only requires the synthesis rate in a cell to be maintained until the signal has reached detection level and may therefore be less sensitive to toxicity problems. The fluorescence per cell data should however provide more information on the underlying activity distribution and as a function of incubation time these data may be used to assess both growth rate and growth rate distribution. For incubations lasting several generations, assuming that non-functional proteins are not an issue, we may expect a decrease in per cell labelling rate because cells divide. The rate of cell labeling should decrease exponentially over time and fluorescence per cell at time t can be expressed with the logarithmic equation $R_t = R_0(1 - 2^{-t/t_g})$; where R_t = fluorescence per cell at time t, R_0 = fluorescence per cell in fully labelled cells, t = incubation time, and t_g = generation time. This equation implies that the growth rate may be estimated from time course incubations, providing a possible theoretical framework for interpretation of BONCAT data. Hence, when the basic limitations related to toxicity and inhibition vs incubation time are worked out and considered, we propose the BONCAT method may be more applicable than anticipated.

Further application and systematic experimentation on a range of different microbial systems, careful interpretation of results and data accumulation is the only way forward. In the meantime, we adhere to the general recommendation of keeping the NCAA concentrations low and incubation time to a minimum.

Author contributions

SV provided funding. LL conceptualized the study with support of GB and SV. LL acquired data and performed analyses with support of GB and SV. JT produced software for data curation and analysis. GB created the figs. LL wrote the original draft and all authors contributed to reviewing and editing the paper.

Declaration of Competing Interest

There are no competing interests.

Data availability

Data will be made available on request.

Acknowledgements

We thank T. Frede Thingstad for valuable insight regarding data interpretation, and Tatiana Tsagaraki for valuable input in the finalizing of this text. We also thank Elzbieta Petelenz for helpful discussions and assistance with FCM analyses. The work was supported by the Trond Mohn Research Foundation (TMS2018REK02).

References

Brewster, J.D., 2003. A simple micro-growth assay for enumerating bacteria. J. Microbiol. Methods 53, 77–86. https://doi.org/10.1016/s0167-7012(02)00226-9.

Cornett, J.B., Shockman, G.D., 1978. Cellular lysis of *Streptococcus faecalis* with triton x-100. J. Bacteriol. 135 (1), 153–160. https://doi.org/10.1128/jb.135.1.153-160.1978.

Couradeau, E., Sasse, J., Goudeau, D., Nath, N., Hazen, T.C., Bowen, B.P., et al., 2019. Probing the active fraction of soil microbiomes using BONCAT-FACS. Nat. Commun. 10, 2770. https://doi.org/10.1038/s41467-019-10542-0.

Hatzenpichler, R., Orphan, V.J., 2015. Detection of protein-synthesizing microorganisms in the environment via biorthogonal noncanonical amino acid tagging (BONCAT). In: McGenity, et al. (Eds.), Hydrocarbon and Lipid Microbiology Protocols, Springer Protocols Handbooks. Springer-Verlag, Berlin Heidelberg. https://doi.org/10.1007/8623_2015_61.

Hatzenpichler, R., Scheller, S., Tavormina, P.L., Babin, B.M., Tirrell, D.A., Orphan, V.J., 2014. *In situ* visualization of newly synthesized protein in environmental microbes using amino acid tagging and click chemistry. Environ. Microbiol. 16 (8), 2568–2590. https://doi.org/10.1111/1462-2920.12436.

Hatzenpichler, R., Connon, S.A., Goudeau, D., Malmstrom, R.R., Woyke, R., Orphan, V., 2016. Visualizing in situ translational activity for identifying and sorting slow-growing archaeal–bacterial consortia. PNAS 113 (28), E4069–E4078. https://doi.org/10.1073/pnas.1603757113.

Hatzenpichler, R., Kruckenberg, V., Spietz, R.L., Jay, Z.J., 2020. Next-generation physiology approaches at single cell level. Nat Rev Microbiol 18 (4), 241–256. https://doi.org/10.1038/s41579-020-0323-1.

Leizeaga, A., Estrany, M., Forn, I., Sebastián, M., 2017. Using click-chemistry for visualizing *in situ* changes of translational activity in planktonic marine bacteria. Front. Microbiol. 8, 2360. https://doi.org/10.3389/fmicb.2017.02360.

Lindivat, M., Larsen, A., Hess-Erga, O.K., Bratbak, G., Hoell, I.A., 2020. Bioorthogonal non-canonical amino acid tagging combined with flow cytometry for determination of activity in aquatic microorganisms. Front. Microbiol. 11, 1929. https://doi.org/10.3389/fmicb.2020.01929.

Pasulka, A.L., Thamatrakoln, K., Kopf, S.H., Guan, Y., Poulos, B., Moradian, A., et al., 2018. Interrogating marine virus-host interactions and elemental transfer with BONCAT and nanoSIMS-based methods. Environ. Microbiol. 20 (2), 671–692. https://doi.org/10.1111/1462-2920.13996.

Reichart, N.J., Jay, Z.J., Kruckenberg, V., Parker, A.E., Spietz, R.L., Hatzenpichler, R., 2020. Activity-based cell sorting reveals responses of uncultured archaea and bacteria to substrate enrichment. ISME J 14, 2851–2861. https://doi.org/10.1038/s41396-020-00749-1.

Samo, T.J., Smriga, S., Malfatti, F., Sherwood, F., Azam, F., 2014. Broad distribution and high proportion of protein synthesis active marine bacteria revealed by click chemistry at the single cell level. Front. Mar. Sci. 1, 48. https://doi.org/10.3389/fmars.2014.00048.

Steward, K.F., Eilers, B., Tripet, B., Fuchs, A., Dorle, M., Rawle, R., et al., 2020. Metabolic implications of using biorthogonal non-canonical amino acid tagging (BONCAT) for tracking protein synthesis. Front. Microbiol. 11, 197. https://doi.org/10.3389/fmicb.2020.00197.

Tivendale, N.D., Fenske, R., Duncan, O., Millar, A.H., 2021. *In vivo* homopropargylglycine incorporation enables nascent protein tagging, isolation and characterisation from *Arabidopsis thaliana*. Plant J. 107, 1260–1276. https://doi.org/10.1111/tpj.15376.

Valentini, T.D., Lucas, S.K., Binder, K.A., Cameron, L.C., Moti, J.A., Dunitz, J.M., et al., 2020. Bioorthogonal non-canonical amino acid tagging reveals translationally active subpopulations of the cystic fibrosis lung microbiota. Nat. Commun. 11, 2287. https://doi.org/10.1038/s41467-020-16163-2.

Wang, A., Nairn, N.W., Johnson, R.S., Tirrell, D., Grabstein, K., 2008. Processing of N-terminal unnatural amino acids in recombinant human interferon-β in *Escherichia coli*. Chembiochem 9, 324–330. https://doi.org/10.1002/cbic.200700379.

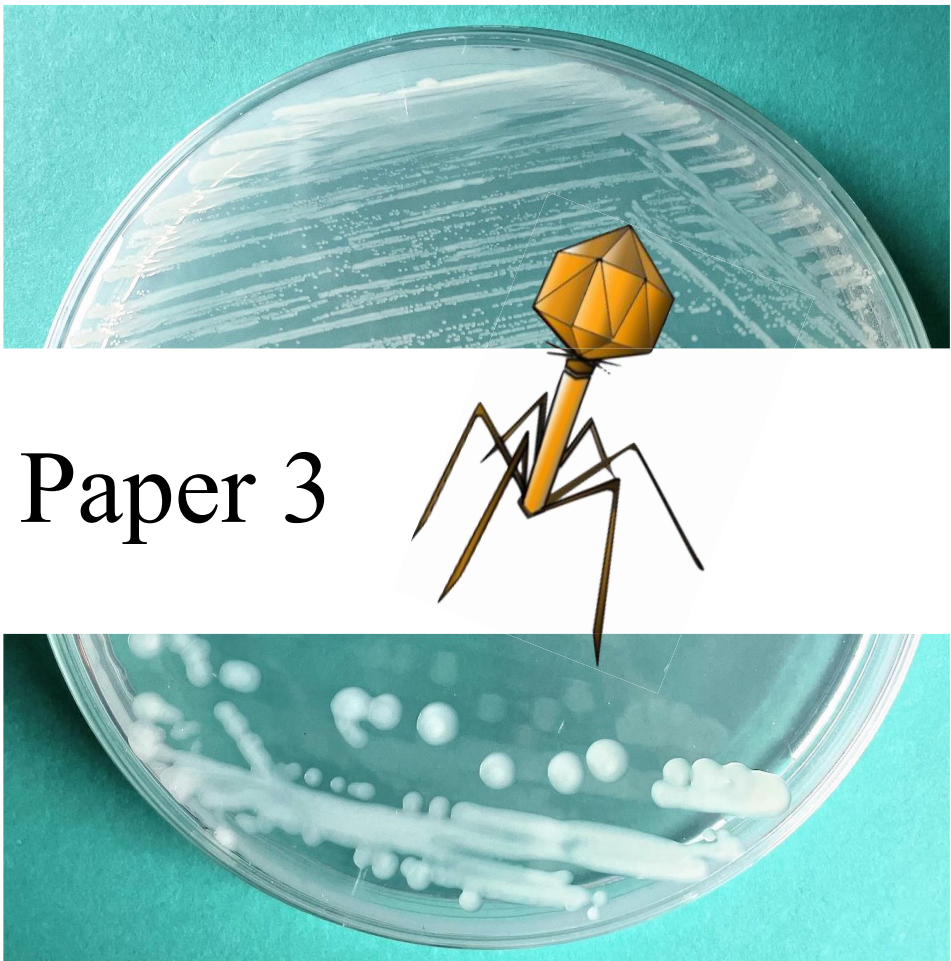

Paper 3

APPENDIX I

Media

1. **2 M Glucose**

D-Glucose	360 g
RO-H_2O	to 1000 mL

Dissolve ingredient and sterile-filter (0.2 μm) the solution once the powder has completely dissolved.

2. **0.2 M $MgSO_4$**

$MgSO_4 \cdot 7$ H2O	50 g
RO-H_2O	to 1000 mL

Dissolve ingredient in RO-H_2O. Autoclave.

3. **0.001 M $CaCl_2$**

$CaCl_2 \cdot 2$ H_2O	1.5 g
RO-H_2O	to 1000 mL

Dissolve ingredient in RO-H_2O and autoclave.

4. **M9 salts, × 4 concentrate** (adapted from [1])

$Na_2HPO_4 \cdot 2$ H_2O	34 g
KH_2PO_4	12 g
NaCl	2 g
NH_4Cl	4 g
RO-H_2O	to 1000 mL

Dissolve salts in RO-H_2O. Autoclave. Dilute to × 1 for use.

5. **M9 medium*** (adapted from [2])

M9 salts × 4 (4)	250 mL
2 M Glucose (1)	2.8 mL
0.2 M $MgSO_4$ (2)	10 mL
0.001 M $CaCl_2$ (3)	10 mL
Sterile RO-H_2O	to 1000 mL

All ingredients are autoclaved separately and mixed immediately before use. pH = 7.1

6. **Water agar**

a) ***3 % water agar***

Used as solidifying agent for M9 solid media (7)

Agar, powder	30 g
RO-H_2O	to 1000 mL

b) ***4 % water agar***

Used as solidifying agent for LB medium (8)

Agar, powder	40 g
dH_2O	to 1000 ml

c) ***1 % water agar***

Agar, powder	10 g
RO-H_2O	to 1000 mL

a – c: Dissolve agar powder completely in water by heating at 100 °C. Dispense into desired volumes and autoclave. Cool down agar to < 60 °C before use, or store at 4 °C.

7. M9 solid medium (M9 agar)

M9 salts × 4 (4)	250 mL
Sterile RO-H_2O	250 mL
3 % water agar (6a)	500 mL
2 M Glucose (1)	5.5 mL
0.2 M $MgSO_4$ (2)	10 mL
0.001 M $CaCl_2$ (3)	10 mL

All ingredients are to be prepared and autoclaved separately. Melt agar by autoclaving or by heating at 100 °C. Dilute M9 salts in the RO-H_2O. Unless hot from the autoclave, warm salts dilution and glucose to 45 – 50 °C. Allow the melted agar to cool to < 60 °C before adding warmed, sterile salts and glucose while stirring. Dispense media into plates.

For antimicrobial supplemented plates, 10 µg/ml chloramphenicol is added and properly mixed into the media before pouring the plates.

8. Overlay agar (M9 soft agar)

Used as overlay-layer for plaque assays.

M9 salts × 4 (4)	250 mL
Sterile RO-H_2O	250 mL
2 M Glucose (1)	5.5 mL
0.2 M $MgSO_4$ (2)	10 mL
0.001 M $CaCl_2$ (3)	10 mL
1 % water agar (6c)	500 mL

All ingredients are to be prepared and autoclaved separately. Melt agar by autoclaving or by heating at 100 °C. Dilute the M9 salts in the RO-H_2O. Unless hot from the autoclave, warm salts and glucose to 45 – 50 °C. Allow the melted agar to cool to < 60 °C before adding warmed, sterile salts and glucose while stirring.

Aliquot 4 mL of melted mixture into sterile tubes and cool to 45 – 50 °C without the agar to solidifying. Add 3 ml of overnight bacterial culture adjusted to OD_{600} = 0.2 in M9 medium (5). Promptly vortex the overlay solution and immediately pour over dry underlay agar plates, made with M9 solid medium (7). Placed poured plates to cool in 4 °C and use within 3 h

9. LB (Luria-Bertani) medium [3]

Tryptone	10 g
Yeast extract	5 g
NaCl	10 g
RO-H_2O	to 500 mL
4 % water agar (6b)	500 mL

Dissolve dry ingredients in RO-H_2O and adjust pH to 7.0 and autoclave. Melt water agar by autoclaving or by heating at 100 °C. Let both mixtures cool to < 60 °C before combining them while stirring. Dispense into plates.

For antimicrobial supplemented plates, 10 µg/mL chloramphenicol is added and properly mixed into the media before pouring the plates.

10. LB broth

Tryptone	10 g
Yeast extract	5 g
NaCl	10 g
RO-H_2O	to 1000 mL

Dissolve ingredients in RO-H_2O. Adjust pH to 7.0. Autoclave.

11. Tris-EDTA (TE) buffer

Tris, pH 8.0 (autoclaved)	5 mL
EDTA, 0.5 M (autoclaved)	2 mL
RO-H2O	to 1000 mL

Sterile-filter (0.2 μm) before use.

12. Nutrient broth (adapted from [4])

Peptone	5 g
Meat extract	3 g
$NaCl_2$	0.5 g
0.2 M $MgSO_4$ (2)	10 mL
0.001 M $CaCl_2$ (3)	10 mL
RO-H_2O	to 1000 mL

Dissolve dry ingredients in RO-H_2O. Autoclave. After autoclavation add $MgSO_4$ and $CaCl_2$ solutions.

13. PBS (phosphate buffered saline, × 10)

KCl	2 g
KH_2PO_4	2.4 g
Na_2HPO_4	18 g
NaCl	80 g
RO-H_2O*	to 1000 mL

Dissolve ingredients in 800 mL of RO-H_2O while stirring. Once dissolved, add RO-H_2O to 1000 mL. Autoclave. When diluted to × 1 in sterile RO-H_2O, the pH will adjust itself to pH = 7.4

*prepared immediately before use/plate pouring

References:

[1] Cold Spring Harbor Protocols, 2009. doi:10.1101/pdb.rec11973; [2] Cold Spring Harbor Protocols, 2010. doi:10.1101/pdb.rec12295; [3] DSMZ, 2007. https://www.dsmz.de/microorganisms/medium/pdf/DSMZ_Medium381.pdf (accessed 09.10.23); [4] DSMZ, 2010. https://www.dsmz.de/microorganisms/medium/pdf/DSMZ_Medium101.pdf (accessed 09.10.23)

APPENDIX II

Protocols

a. Glycerol stock production
b. Lysate production
c. Spot assay
d. Isolation of phage-resistant *E. coli*
e. Cleaning phage-resistant isolates from contaminant phage
f. General BONCAT-FCM protocol
g. Validation experiment: Temperature-BONCAT
h. Conjugation experiment

a. Glycerol stock production

Glycerol stocks were produced from all bacterial strains in the studies, to reduce mutation accumulation and preserve resistance characteristics over time.

1. Prepare an overnight culture by inoculating a single colony in sterile media (e.g., M9 media, Appendix 1.5) and incubate at the optimal temperature (37 °C for *Escherichia coli* strains) for the bacterium
2. Adjust the optical density (OD) of the culture at 600 nm to 0.2
3. After incubation, add autoclave-sterilized glycerol to the culture to a final concentration of 20 % glycerol
4. Aliquot the glycerol-culture mix into sterile cryotubes, make at least two replicate tubes per strain
5. Streak a drop of the glycerol-culture mix onto an agar plate (M9 or LB agar plate, Appendix 1.7 or 1.10), incubate for several days at the optimal temperature for the bacterium (37 °C for *E. coli* strains) and periodically inspect the plates for signs of contamination

6. Flash freeze the cryotubes in liquid nitrogen, OR freeze them step-wise by freezing them in –20 °C for an hour, before transferring them without thawing into –80 °C

When using glycerol stocks, avoid numerous freeze-thaw cycles. If repeated use of one strain is necessary, make many glycerol stocks, use one stock per experiment and discard thereafter.

b. Lysate production

A "starter lysate" of phage DSM 103876 (phage G28) was produced according to the collection's instructions for "liquid lysis" (DSMZ, 2013).

This protocol was developed for the reliable production of high titer phage lysate, adapted DSMZ (2013):

1. Prepare an overnight culture of *E. coli* DSM 103246 by inoculating in M9 media (Appendix 1.5) at 37 °C
2. Melt autoclave-sterilized soft water agar (1 % agar, Appendix 1.6.c) completely, and let cool to ca. 60 °C
3. To one part melted agar, mix one part double-strength M9 salts (final agar concentration 0.5 %), add salts and glucose (Appendix 1.8) and let cool to 45 – 50 °C
4. Dilute the starting lysate in M9 media up to $1{:}10^8$
5. To each dilution, add an equal volume of overnight culture (OD-adjusted to 0.3)
6. To 4-mL melted soft agar, pipette 300 µL of culture-lysate mix
7. Vortex the agar mix briefly and promptly pour it over a room temperature M9 agar plate (Appendix 1.7), prepare one plate for each dilution of lysate
8. Incubate the plates at 37 °C overnight. Prepare another overnight host culture (step 1.)
9. After incubation, inspect the double-layer plates for plaques (round clearings in the bacterial lawn), pick a plate with clear, round, well-separated plaques

10. With a sterile pipette tip, transfer single plaques into tubes containing 200 µL sterile glucose-free M9 media. One plaque per tube. *Optional:* Each tube is briefly (< 1 sec.) vortexed to suspend the phage
11. Make one double-layer agar plate for each suspended plaque + 2 control plates (repeat steps 2, 3, and 5, but skip addition of lysate dilution into the host culture)
12. Except for the 2 control plates, without disrupting the thin soft-agar upper-layer, gently pipette the plaque suspension onto the newly prepared double-layer agar plates. Rotate the plate to spread the lysate onto a larger surface area, but leave some area free from lysate to confirm bacterial growth
13. Incubate the plates at 37 °C overnight. Prepare another overnight host culture (step 1.)
14. Following incubation, inspect the plates for a large clearance in the bacterial lawn in the double-layer plates. Check the control plates for an even, plaque-free bacterial lawn
15. Carefully, without disrupting the thin top-layer, pipette 8 – 12 mL (depending on the thickness of the bottom-layer agar) of sterile glucose-free M9 media onto each plate surface (also control plates)
16. Slowly turn the plates on a horizontal rotating block at room temperature, preferably in the dark, for at least 4 h
17. Harvest the lysate (and the phage-free control) by transferring the liquid on the plates' surface into a sterile centrifuge tube
18. Centrifuge at 5 000 × g for 5 min
19. Transfer the supernatant into a sterile centrifuge tube. Repeat step 18
20. Filter the supernatant through a 0.45 µm filter. The resulting lysate should be clear liquid
21. Do a spot assay (Appendix 2.c.) to estimate phage concentration (3 replicate plates per lysate)
22. Freeze some of the lysate in 20 % glycerol at –80 ºC
23. Store the lysate at 4 ºC in the dark

Use the lysate within a few days for an expected concentration of 10^9 – 10^{10} PFU/mL; 10^{10} total virions/mL. After this, a drop in titer is expected. However, the lysate remains active for > 12 months when stored according to step 23.

When using the lysate, practice aseptic techniques to prevent bacterial contamination that can destroy the lysate. Before using the lysate, ensure that the lysate is clear and free from microbial growth.

c. Spot assay

The spot assay is a method to measure the concentration of active phage in a lysate using a susceptible bacterium. It can also be used to test phage-susceptibility in phage-resistant mutants. The spot assay is adapted from Symonds (1968) and Stenholm et al. (2008).

1. Prepare an overnight culture of a phage susceptible strain (and a non-susceptible, if phage-susceptibility is tested; always include a susceptible strain as control)
2. The next day, melt autoclave-sterilized soft water agar (1 % agar) completely, and let cool to ca. 60 °C
3. To one part melted agar, mix one part double-strength M9 salts (final agar concentration 0.5 %), add salts and glucose (Appendix 1.8) and let cool to 45 – 50 °C
4. OD-adjust the overnight culture(s) to OD = 0.2 in M9 media (Appendix 1.5)
5. Perform a dilution series of phage lysate (1:1 – 1:10^8) in glucose-free M9 media. Mark M9 agar plates with designated areas for each dilution. Consider replicates
6. To 4 mL of molten soft agar, pipette 300 µL of OD-adjusted culture. Vortex the culture-agar mix briefly and promptly pour it over a room temperature underlay agar plate. One strain per plate, include at least one phage-susceptible control strain

7. Once the top layer has solidified and cooled to room temperature, drop 5 µL of each lysate dilution on the agar surface. Make sure to replicate the drops, either on individual plates or several drops of same dilution per plate, or both
8. Let the drops air-dry. Once dry, place the plates lid-side up in an incubator and incubate overnight at 37 °C
9. After incubation, inspect the plates. Count plaques for drops showing separate and countable plaques. Estimate the plaque-forming units (PFU) per volume unit for each strain tested

d. Isolation of phage-resistant *E. coli*

This protocol is adapted for the *E. coli* strain DSM 102346 and the lytic phage DSM 103878. The success of this protocol varies, and it is expected that some bacteria isolated using this protocol are susceptible to phage. The protocol is adapted from the Lysate production protocol (Appendix 2.b.), as bacterial colonies were observed to grow on double-layer plates of with high level of lysis.

1. Prepare an overnight culture of *E. coli* DSM 103246 by inoculating in M9 media (Appendix 1.5) at 37 °C
2. Melt autoclave-sterilized soft water agar (1 % agar) completely, and let cool to ca. 60 °C
3. To one part melted agar, mix one part double-strength M9 salts (final agar concentration 0.5 %), add salts and glucose (Appendix 1.8) and let cool to 45 – 50 °C
4. Dilute the starting lysate in M9 media (1:1 – 1:1000), prepare replicates of each dilution
5. To each lysate dilution, add an equal volume of overnight culture (OD ca. 0.3)
6. To 4 mL of molten soft agar, add 300 µL of lysate-culture mix. Briefly vortex the mixture and promptly pour it over a room temperature M9 agar plate (Appendix 1.7). One plate per dilution
7. Once the top layer has solidified, place the plates in an incubator and incubate overnight at 37 °C

8. The next day, inspect the plates for colonies growing on the surface of the agar. Carefully isolate single colonies, and streak onto a phage-free M9 agar plate using a sterile loop. One colony per plate
9. Incubate the single-colony plates overnight at 37 °C
10. Following incubation, inspect the plates for signs of different colony types. Isolate different colony types onto separate plates, repeat steps 9 and 10
11. Prepare glycerol stocks (Appendix 2.a.) from single colony type cultures and test the phage susceptibility of each culture through spot assays (Appendix 2.c.). Keep the passage of isolated colonies to a minimum to avoid loss of phage-resistant properties; Prepare glycerol stocks as soon as the isolates are single-colony-type cultures, before phage-susceptibility testing
12. Once phage resistance is confirmed, check the isolates for phage-contamination (Appendix 2.e.)

For *E. coli* DSM 103246, three different colony types have been observed using this protocol: smooth, white/grey colonies like those of the wildtype; mucoid, large, white/grey colonies; and translucent grey colonies. The first two colony types are relatively easy to isolate and subculture, but the translucent colonies are difficult to subculture without reverting to a different colony morphology (similar to the wildtype) and often show phage susceptibility.

e. Cleaning phage-resistant isolates from contaminant phage

Make sure to have made a glycerol stock from the isolate before the clean-up process, as the passage of the isolate can cause the loss of phage resistance traits.

1. Prepare an overnight culture of the phage-resistant isolate (Alternatively, use the same culture used for the glycerol stock production). Also prepare a culture of the wildtype that has not been exposed to phage. Prepare the cultures in M9 media (Appendix 1.5) and incubate at 37 °C
2. Streak the overnight culture and control culture onto one phage-free M9 agar plate (Appendix 1.7) each, incubate the plates at 37 °C overnight

3. From the remaining culture, transfer a volume into separate sterile tube. Fix one part of the culture with 25 µL/mL 37 % formaldehyde solution (Sigma-Aldrich)
4. From the unfixed culture, perform a spot assay (Appendix 2.c.). Also perform a spot assay on the supernatant from the resistant isolate, by spinning down the cells for 5 min at 5 000 × g
5. Prepare a dilution series of the fixed culture in sterile-filtered TE buffer (Appendix 1.11) and stain each dilution with SYBR Green I nucleic acid stain (Thermo Fisher Scientific). Incubate the dilutions in the dark for 10 minutes
6. Analyse the dilutions at a flow cytometer using dye-specific excitation/emission wavelenghts at a flow rate of 50 – 200 cells/minutes
7. Compare the phage-free control isolate with the phage-resistant isolate and look for any signs of populations of small particles in the resistant isolate
8. If a population of small particles is observed, prepare an overnight culture from a single culture of the isolate growing on phage-free M9 agar (from step 2.)
9. Repeat steps 2 – 8 until the resistant isolate is comparable to the phage-free control in terms of small particles
10. Once the isolate is free from phage contamination, produce a glycerol stock (Appendix 2.a.) from the isolate and confirm phage resistance with a spot assay (Appendix 2.c.). Confirm that the supernatant of the phage-resistant isolate does not produce plaques in the wildtype

f. General BONCAT-FCM protocol

This protocol is for the labelling of bacterial cells that have been incubated with non-canonical amino acids L-azidohomoalanine (AHA) or L-homopropargylglycine (HPG). Cells should be fixed after before labelling (I used 25 µL/mL 37 % formaldehyde solution, Thermo Fisher Scientific). The protocol is adapted from Hatzepichler & Orphan (2015), Leizeaga et al. (2017) and Lindivat et al. (2020).

Reagents:

- 20 mM $CuSO_4$ (Sigma-Aldrich) prepared in mQ-water, sterile-filtered (0.2 µm), stored at 4 °C
- 50 mM THPTA (tris[(1-hydroxypropyl-1H-1,2,3-triazol-4-yl)methyl]amine, Click Chemistry Tools) prepared in mQ-water, sterile-filtered (0.2 µm) and stored at – 20 °C
- 2 mM AlexaFluor 647 picolyl azide (Click Chemistry Tools) prepared in sterile-filtered (0.2 µm) PBS (Appendix 1.13), stored at – 20 °C
- 2 mM AlexaFluor 647 alkyne (Click Chemistry Tools) prepared in sterile-filtered (0.2 µm) PBS, stored at – 20 °C
- Sodium ascorbate (Sigma-Aldrich), undissolved powder
- Aminoguanidine hydrochloride (Sigma-Aldrich), undissolved powder
- 0.02 % Tween-20-Tris-EDTA buffer, prepared from 9 parts TE buffer and 1 part 0.2 % Tween-20 (Sigma-Aldrich) prepared in mQ-water and sterile-filtered (0.2 µm), stored at 4 °C

BONCAT-staining through the click reaction:

1. Remove AHA/HPG and fixative from samples by centrifugation at 16 000 × g for 5 min. Replace supernatant with sterile-filtered (0.2 µm) PBS. Include control samples without AHA/HPG
2. Prepare a dye premix per 1 mL sample: 5.85 µL 20 mM $CuSO_4$; 11.3 µL 50 mM THPTA; 2.85 µL 2 mM AlexaFluor 647 picolyl azide (for HPG)/alkyne (for AHA). Incubate the dye premix for 3 min in the dark
3. Prepare 100 mM solutions of sodium ascorbate and aminoguanidine hydrochloride, respectively, in sterile-filtered mQ-water. Avoid getting oxygen in the solutions
4. To each 1 mL sample, add 57 µL of 100 mM sodium ascorbate; 57 µL 100 mM aminoguanidine hydrochloride; and 20 µL dye premix. Gently pipette to mix the samples, avoid air bubbles
5. Incubate the samples for 1 h in the dark at room temperature

6. After incubation, centrifuge the samples at 16 000 × g for 5 min
7. Remove the supernatant and resuspend the pellet in 0.02 % Tween-20-Tris-EDTA buffer
8. Store the samples at 4 °C in the dark until flow cytometric analysis. Analyze the samples within 24 h of staining

Flow cytometric analysis:

1. Dilute samples in sterile-filtered (0.2 µm) TE buffer, if necessary
2. To 1 mL sample, add 10 µL 100-times concentrated SYBR Green I nucleic acid stain (Thermo Fisher Scientific), include a bacteria-free TE buffer control
3. Incubate samples in the dark for at least 10 min
4. Analyze the samples using a flow cytometer equipped with lasers set at dye-specific excitation/emission wavelengths at an appropriate flow rate (e.g., 50 – 200 cells/min)
5. Use gating to separate the BONCAT-positive and BONCAT-negative cells. Use negative control samples that were not incubated with AHA/HPG before BONCAT-staining to establish the expected fluorescence of BONCAT-negative cells

g. Validation experiment: Temperature-BONCAT

1. The day before the experiment, an overnight culture of *E. coli* DSM 103246 was prepared in M9 media (Appendix 1.5) at 37 °C.
2. The day of the experiment, the overnight culture was diluted 1:10 in prewarmed M9 media and incubated at 37 °C until OD = 0.2 was reached.
3. *For optical growth curves*, dilute the 1:100 in M9 media into wells of 96-well flat-bottomed microwell plate (200 µL/well) and place the plate in a 2300 EnSpire™ Multilabel reader.
    a. In 37 ºC growth curves, set the reader to 37 ºC with reads every 20 minutes at wavelength 600 nm.

b. In 28 ºC growth curves, set the reader to 28 ºC with reads every 30 minutes at 600 nm.
c. Due to the lack of cooling function in the plate reader, for the 15 ºC growth curves, incubate the culture at 15 ºC and perform optical measurements, using a cuvette-based FisherBrand™ Cell Density meter, at appropriate intervals.

4. Extract the plate reader data and organize it appropriately in Excel to calculate mean maximum growth rates according to Kurokawa & Ying (2017).
5. *BONCAT incubations at different temperatures* are performed by diluting the starting culture 1:100 in prewarmed/precooled M9 media supplemented with AHA at 100 µM, 50 µM, 2.8 µM or 1.4 µM, respectively.
6. Incubate the AHA exposed cultures at 37 ºC, 28 ºC or 15 ºC for 30 min. In addition, incubate control cultures without AHA, corresponding concentrations of methionine, as well as killed controls (25 µL/mL 37 % formaldehyde), respectively, at similar conditions.
7. After incubation fix all samples, except killed controls, using 25 µL/mL 37 % formaldehyde, and proceed to BONCAT-labelling according to Appendix 2.f.

h. Conjugation experiment

This protocol is adapted from McIntosh et al. (2008). It requires a plasmid donor unable to grow at the highest incubation temperature (37 °C) and a recipient unable to grow exposed to the selective antimicrobial for the plasmid (chloramphenicol in this case).

1. Incubate both donor and recipient strains in LB broth (Appendix 1.10) at room temperature for 24 h before the experiment
2. Following incubation, OD-adjust both cultures to 0.8 in LB media
3. Add equal part plasmid donor and recipient into one sterile tube
4. Incubate the co-culture for 24 h at room temperature under 150 rpm agitation
5. The next day, dilute the co-culture 1:10 through 1:1000 in LB media

6. Pipette 150 µL of each dilution, including the undiluted control, onto designated LB agar plates containing 10 µg/mL chloramphenicol (Appendix 1.9).
7. Incubate the plates at 37 °C overnight
8. The following day, inspect the plates for colonies. Isolate single colonies onto LB agar plates containing 10 µg/mL chloramphenicol and incubate at 37 °C

Note on the experiment presented in Chapter 4:
Wildtype *E. coli* DSM 103246 cannot grow if exposed to 10 µg/mL chloramphenicol (this was confirmed before the experiment) and the plasmid donor *A. salmonicida* subsp. *salmonicida* P20-1A/17 cannot grow at temperatures as high as 37 °C. The colonies growing on the antimicrobial-containing plates after step 7 should therefore be *E. coli* that had received the plasmid encoding chloramphenicol resistance. However, species identity was also inferred by the lack of the distinctive dark pigment that *A. salmonicida* subsp. *salmonicida* produces on agar (Figure A1). When cultured in liquid media, the chloramphenicol resistant isolates were observed to grow suspended in the media, which further indicating that they were *E. coli*; *A. salmonicida* subsp. *salminicida* is a non-motile bacterium and sediments to the bottom in liquid culture.

Once chloramphenicol resistant isolates of *E. coli* had been produced, optical growth curves were produced to observe any change in growth rate from the received plasmid. Overnight cultures of both wildtype *E. coli* DSM 103246 and a chloramphenicol resistant isolate in M9 media (Appendix 1.5) at 37 °C. The cultures were OD-adjusted to 0.2 and diluted 1:100 in M9 media. Each culture dilution was divided into two tubes, and to one tube per strain, 10 µg/mL chloramphenicol was added. The content of each tube was pipetted into 21 wells of a flat-bottomed 96-well microwell plate, 200 µL per well. The remaining 12 wells were filled with chloramphenicol-free M9 media (6 wells) and M9 media with 10 µg/mL chloramphenicol (6 wells), as negative controls. The microwell plate was place in a 2300 EnSpire™ Multilabel reader, and incubated at 37 °C overnight, reading the plate every 20 minutes.

Figure A1. *Aeromonas salmonicida* subsp. *salmonicida* strain P20-1A/17 grown on tryptic soy agar. The dark brown pigment is an indicative characteristic for the species. Photograph taken with iPhone SE by Lotta Landor.

References

DSMZ (2013) 'Supply, storage, propagation and purification of phages' ed. Rohde, C. Leibniz Institute, The German Collection of Microorganisms and Cell Cultures, https://www.dsmz.de/fileadmin/Bereiche/Microbiology/Dateien/Kultivierungshinweise/PDF_Internet_Propagation_of_Phages13.pdf (23.07.23)

Hatzenpichler, R. and Orphan., V. (2015) 'Detection of protein-synthesizing microorganisms in the environment via bioorthogonal noncanonical amino acid tagging (BONCAT)' In: McGenity, T.J., et al. (eds.), *Hydrocarbon and Lipid Microbiology*, Springer Protocols Handbooks, Springer-Verlag, Berlin

Korf, I.H.E., Kittler, S., Bierbrodt, A., Mengden, R, Rohde, C., Rohde, M., Kroj, A., Lehnherr, T., Fruth, A., Flieger, A., Lehnherr, H. and Wittmann, J. (2020) 'In vitro evaluation of phage cocktail controlling infections with *Escherichia coli*' *Viruses* 12, 1470

Kurokawa, M. and Ying, B-W. (2017) 'Precise, high-throughput analysis of bacterial growth' *Journal of Visual Experiments* 127, e56197

Leizeaga, A., Estrany, M., Forn, I. and Sebastián, M. (2017) 'Using click-chemistry for visualizing *in situ* changes of translational activity in planktonic marine bacteria' *Frontiers in Microbiology* 8, 2360

Lindivat, M., Larsen, A., Hess-Erga, O.K., Bratbak, G. and Hoell, I.A. (2020) 'Bioorthogonal non-canonical amino acid tagging combined with flow cytometry for determination of activity in aquatic microorganisms' *Frontiers in* Microbiology 11, 1929

McIntosh, D., Cunningham, M., Ji, B., Fekete, F.A., Parry, E.M., Clark, S.E., Zalinger, Z.B., Glig, I.C., Danner, G.R., Johnson, K.A., Beattie, M. and Ritchie, R. (2008) 'Transferable, multiple antibiotic and mercury resistance in Atlantic Canadian isolates of Aeromonas salmonicida subsp. salmonicida is associated with carriage of an IncA/C plasmid similar to the Salmonella enterica plasmid pSN254' The Journal of Antimicrobial Chemotherapy 61(6), 1221 – 1228Stenholm, A.R., Dalsgaard, I. and Middelboe, M. (2008) 'Isolation and characterization of bacteriophages infecting the fish pathogen *Flavobacterium psychrophilum*' Applied Environmental Biology 74(13), 4070 – 4078

Symonds, N.D. (1968) 'Experiments with virulent bacteriophages' In: Clowes, R.C. and Hayes, W. (eds) *Experiments in Microbial Genetics*, pp. 68 – 89, Blackwell Scientific Publications, Oxford

Graphic design: Communication Division, UiB / Print: Skipnes Kommunikasjon AS

uib.no

ISBN: 9788230852521 (print)
9788230869307 (PDF)